MECHANISMS OF NEURODEGENERATION IN A MOUSE MODEL OF SANDHOFF DISEASE

MECHANISMS OF NEURODEGENERATION IN A MOUSE MODEL OF SANDHOFF DISEASE: ROLES OF INFLAMMATION, EXCITOTOXICITY, AND APOPTOSIS

By ALEXANDER WM HOOPER, B.SC.

A Thesis Submitted to the School of Graduate Studies in Partial Fulfilment of the Requirements for the Degree Doctor of Philosophy

DOCTOR OF PHILOSOPHY (Biology, 2016)
McMaster University Hamilton, Ontario, Canada

TITLE: Mechanisms of Neurodegeneration in GM2 Gangliosidoses: Roles of Inflammation, Apoptosis, and Synaptic Proteins
AUTHOR: Alexander WM Hooper, B.Sc. (University of Western Ontario)
SUPERVISOR: Dr. Suleiman A. Igdoura
NUMBER OF PAGES: xiv, 148

LAY ABSTRACT

Lysosomal storage disorders are a group of neurological diseases that are debilitating, and often fatal at a young age. Two diseases of this group- Tay-Sachs disease and Sandhoff disease – are similar in their causes and symptoms. Current treatments for these diseases only slow or stall an inevitable decline in health. New targets for treatment are required, and we provide data suggesting several proteins that may fit this criterion. We also provide evidence of the discovery of a new form of one of these proteins, which is found in high levels in the disease, indicating it may be important in these and other neurodegenerative diseases. Finally, we provide findings indicating that a certain cell type, which is largely ignored in current research for these diseases, may be important in the disease progress. These findings increase our knowledge of Tay-Sachs disease and Sandhoff disease, and open new avenues for medicinal intervention.

ABSTRACT

Lysosomal storage disorders are a group of rare neurodegenerative diseases that are collectively common, sharing many aspects with other neurodegenerative disorders, including substrate build-up and neuroinflammation. The GM2 Gangliosidoses, Tay-Sachs disease and Sandhoff disease, are pathologically overlapping lysosomal storage disorders, with high prevalence within specific ethnicities. Their effects are neurologically devastating and often fatal at young ages. Current treatments only slow or stall an inevitable decline in health. Novel treatment targets are needed for these disorders, and others with similar pathologies. In these works we demonstrate the negative effect the inflammatory cytokine tumour necrosis factor-alpha has on survival of a model of Sandhoff disease. We demonstrate its role in the upregulation of astrogliosis, and apoptosis, and we present evidence that this effect on astrogliosis occurs through an upregulation of the JAK-2/STAT3 pathway. Though fruitful, a singular focus on inflammation/gliosis in these diseases has left a vacuum in the research into neuron specific molecular processes. We observe the development of inflammation, astrogliosis and neuronal processes in our model, and demonstrate a bi-phasic disease progression, in which early onset microgliosis precedes terminal astrogliosis, apoptosis, and a decline in excitatory glutamate receptors, suggesting neuron-specific malfunction. Furthermore, we show that knockout of the synaptic protein neuronal pentraxin 1 retards neurodegeneration and extends the lifespan of Sandhoff disease mice, independent of inflammation or astrogliosis. Through electrophysiology, we provide

evidence of dysregulation of glutamate receptors in Sandhoff disease, and show that knockout of neuronal pentraxin 1 provides rescue from this dysregulation. This work expands on research into gliosis in GM2 gangliosidoses, presents the finding of a novel protein isoform, and presents a new focus on non-glial disease mechanisms and treatments for these and other neurodegenerative disorders.

ACKNOWLEDGMENTS

I would like to thank Dr. Suleiman Igdoura for his guidance and support through the years. I have learned so much under his supervision, and am grateful for the encouragement he gave me during difficult times.

I would like to thank Dr. Geoff Werstuck and Dr. Rama Singh for their advice, guidance and dedication to my education. I would like to thank Dr. Deda Gillespie and Dr. Javier Alamilla for their collaborative work and for allowing me the time to learn from them.

I owe a debt of gratitude to Dr. Elizabeth White, Dr. Gabriel Gyulay for their invaluable technical expertise, and personal support- I could not have done this without their help. I would like to thank Rosemarie Venier for her collaborative findings, her perfectionism, and for sharing a certain kind of madness. I would like to thank Dr. Hatem Abo-Ouf, with whom I worked closest, and from who I learned many things, about both science and life. I would like to thank Melissa Lambourne who has saved my skin on many occasions, and who was instrumental in bringing our lab together- not just as coworkers, but as good friends. I would like to thank Erin Montgomery, Dave Egier, Kal Mungovan and Ellen Janse Van Rensburg for their friendship, and for all the great laughs. I wish all my previous labmates the best in the future.

I would especially like to thank Dani for her patience and support, and for staying by my side, all these years. And I would finally like to thank my parents and family- without their support and belief in me, I could not have accomplished anything. I owe them everything.

TABLE OF CONTENTS

LIST OF FIGURES AND TABLES

ABBREVIATIONS AND SYMBOLS

AAV: Adeno-associated virus
AAVrh: Rhesus monkey isolated adeno-associated virus
aCSF: Artificial cerebro-spinal fluid
AUP: Animal utilization protocol
AD: Alzheimer's disease
AMPA: α-amino-3-hydroxy-5-methyl-4-isoxazolepropionic acid
AMPAR: AMPA Receptor
BAX: BCL2 associated X protein
BMT: Bone marrow transplant
C1q: Complement component 1, q
CCAC: Council on Animal Care
CCR2: C-C chemokine receptor type 2
CNS: Central nervous system
EAAC1: Excitatory amino-acid carrier 1
EAAT1: Excitatory amino acid transporter
ERAD: Endoplasmic reticulum associated protein degradation
FcRγ: Fc receptor common-gamma chain
GABA: Gamma-aminobutyric acid
GFAP: Glial fibrillary acidic protein
GluR1-4: AMPA Receptor subunit 1-4
HexA: Beta-hexosaminidase A
HexB: Beta-hexosaminidase B
LOTS: Late-Onset Tay-Sachs disease
IL-1α: Interleukin-1 alpha
IL-1β:Interleukin-1 beta
IL-6: Interleukin-6
iPSC: Induced pluripotent stem cells
JAK2: Janus kinase 2
KCNK2: Potassium channel, subfamily K, member 2
M6P: Mannose-6-phosphate
M6PR: Mannose-6-phosphate receptor
MAC3: Macrophage-3 antigen, CD107 antigen-like family member B
MIP-1α: Macrophage inflammatory protein-1-alpha
MMP: Matrix metalloprotease
NARP: Neuronal pentraxin 2, Neuronal activity regulated pentraxin
*N*B-DGJ: *N*-butyldeoxygalactonojirimycin
*N*B-DNJ: *N*-butyldeoxynojirimycin
NF-L: Neurofilament-Light, Neurofilament-Low
NMDA: *N*-methyl-D-aspartate
NMDAR: *N*-methyl-D-aspartate receptor

NP1: Neuronal pentraxin 1
NP1-38: Neuronal pentraxin 1-38
NPR: Neuronal pentraxin receptor
NR2A: *N*-methyl-D-aspartate receptor subunit 2A
NR2B: *N*-methyl-D-aspartate receptor subunit 2B
NSAID: Nonsteroidal anti-inflammatory drug
PBMC: Peripheral blood mononuclear cell
PCR: Polymerase chain reaction
PD: Parkinson's disease
PhTx-74: Philanthotoxin-7,4
PSD-95: Postsynaptic density protein-95
PYR: Pyrimethamine
qRT-PCR: Quantitative real-time PCR, qRT, qPCR
rAAV: Recombinant adeno-associated virus
SD: Sandhoff disease
SPHK1: Sphingosine kinase 1
STAT3: Signal transducer and activator of transcription 3
TACE: Tumor necrosis factor-alpha converting enzyme
TNFα: tumor necrosis factor-alpha
TSD: Tay-Sachs disease
TUNEL: Terminal deoxynucleotidyl transferase dUTP nick end labeling
WT: Wild-type

DECLARATION OF ACADEMIC ACHIEVEMENT

All work was performed by Alexander Hooper except the following:

Chapter 2: Figure 2.1, Figure 2.2, Figure 2.3, Figure 2.4, Figure 2.5a-b, Figure 2.6, Figure 2.9, Table 2.1. Hatem Abo-Ouf performed the behaviour testing (Figure 2.1), Ganglioside assays (Figure 2.2, 2.3), qPCR (Figure 2.4), and bone marrow transplant experiments (Table 1). Hatem Abo-Ouf and Helena Janse Van Rensburg worked together on the western blots (Figure 2.5A-B, 2.6A-E, 2.9A-D). Elizabeth White performed the immunofluorescence experiment (Figure 2.6F).

Chapter 4: Figure 4.1, Figure 4.6. Rosemarie Venier performed the qRT-PCR experiment (Figure 4.1A). Javier Alamilla performed the electrophysiology experiments (Figure 4.6).

CHAPTER 1: Introduction

1.1 Neurodegenerative Diseases

As the average age of the global population grows, neurodegenerative diseases are progressively more common, and the costs- both financial and personal- are also increasing. In Canada, the percentage of Canadians aged 65 years or higher is expected to shift from 15% to 23% during the period of 2011- 2031 (The Government of Canada and Neurological Health Charities Canada, 2011). According to a report by the World Health Organization in 2004, Alzheimer's disease (AD) and other dementias cost the world population approximately 11.16 million disability-adjusted life years (DALY, a measure of the cumulative number of years lost due to poor health and death) (The World Health Organization, 2004). More than 340,000 Canadians currently suffer from Alzheimer's disease, and 84,700 Canadians suffer from Parkinson's disease (PD). By 2031, these numbers are expected to grow to 674,000 and 163,700, respectively (The Government of Canada and Neurological Health Charities Canada, 2011). The burden of neurological conditions extends beyond the patient. According to data published by the Government of Canada and Neurological Health Charities Canada in 2011, 28% of informal caregivers to people with neurological conditions in Canada reported distress, versus 13% for caregivers to people without neurological conditions. In 2011, 39.6% of Canadians with a neurological condition received informal assistance. Aside from quality of life costs, there are also financial costs; for British Columbia alone during the period of 2010-2011, the cost of direct care for patients with Alzheimer's and other dementias

totalled approximately $527,494,000, and Parkinson's totalled $120,358,000. It is critical that our understanding of neurological disorders remains on par with advances in medicine which result in increased longevity, in order to maintain quality of life for patients, families, and caretakers.

1.2 Lysosomal Storage Disorders

The lysosome is a subcellular organelle responsible for the degradation of biomolecules. In a normally functioning cell, lysosomal enzymes are translated through translocons into the lumen of the rough endoplasmic reticulum (RER) as either a soluble or membrane bound protein. Here, they receive a mannose-containing *N*-linked oligosaccharide. The hydrolases then move to the Golgi apparatus where the mannose is phosphorylated in a reaction with uridine diphosphate-*N*-acetylglucosamine, *N*-acetylglucosamine-1-phosphotransferase, and an α-N-acetylglucosaminyl phosphodiesterase (Reitman and Kornfeld, 1981). In the *trans*-Gogli network the M6P is recognized by a M6P receptor (M6PR). Clathrin coated vesicles form, carrying the hydrolases to endosomes. Proton-pump ATPases then reduce the pH of the lysosomal lumen to pH 4.6-5.0, which activates the low pH-dependent hydrolases which are then able to degrade their target substrates (Kornfeld and Mellman, 1989; Saftig and Klumperman, 2009). Lysosomal storage disorders (LSD) are a group of neurodegenerative diseases including, Neimann-Pick, type C, Gaucher disease, Fabry disease, Tay-Sachs disease, and Sandhoff disease, all characterized by the inability of the lysosome to properly degrade substrates, leading to their build up within the cell. This

generally occurs due to a reduction or lack in specific hydrolase enzyme function, due to genetic defects. Individually, these diseases are rare- with specific LSDs rates in an Australian study ranging from 1 in 57,000 live births to 1 in 4.2 million live births- but collectively, they occur at a rate of up to 1 in 7,700 live births (Meikle et al., 1999). Tay-Sachs disease occurs at a high rate in certain populations (a carrier frequency of 1 in 31 North American Jews) (Petersen et al., 1983). Since these diseases often share characteristics, such as substrate buildup, hindrance of the protein synthesis pathways, and neurological symptoms, research into one disease may also be beneficial to our understanding of others. Due to the buildup of substrates within the CNS, LSDs are in some ways similar to more prevalent diseases such as Alzheimer's disease. In fact, in mouse models for a subset of LSDs- GM2 gangliosidoses- intraneuronal amyloid-β (Aβ), and ganglioside-bound Aβ (GAβ) were found to accumulate (Keilani et al., 2012). Both of these accumulations are characteristic of Alzheimer's disease, suggesting similarities in their pathogeneses (Yanagisawa et al., 1995). GAβ was also found to have accumulated in the frontal cortex of the brains of human GM2 gangliosidosis patients.

1.3 GM2 Gangliosidoses

GM2 gangliosidoses are a group of similar LSDs related by the inability to degrade the ganglioside GM2 to GM3. This substrate accumulates in the cell, leading to a plethora of detrimental effects. These diseases occur through malfunction of the enzyme β-hexosaminidase, which is composed of a dimer of two possible subunits (α- found on the human chromosome 15/mouse chromosome 9, and β- found on human

chromosome 5/mouse chromosome 13). The α-subunit contains a GM2 activator protein binding site, which presents GM2 and allows for its hydrolyzation to GM3. The αβ isozyme is known as β-hexosaminidase A (HEXA), and is responsible for cleavage of N-acetylglucosamine and N-acetylgalactosamine residues from the ganglioside GM2. The ββ isozyme is called β-hexosaminidase B (HEXB); the enzyme responsible for cleavage of N-acetylgalactosamine residues from the ganglioside GA2, and from globoside. The αα isozyme (β-hexosaminidase S), has no currently known function.

1.3.1 Tay-Sachs Disease

Tay-Sachs disease (TSD) is caused by a mutation of the gene *HEXA*, the product of which is the α-subunit of β-hexosaminidase A. There are four forms of Tay-Sachs disease, characterized by the period of onset. In the infantile form, patients are unaffected at birth, but develop a slew of symptoms at 3-6 months, including mild motor weakness, hypotonia, poor head control, decreasing attentiveness and a cherry red spot around the fovea. Motor, mental and visual abilities decline after 10 months and patients suffer from seizures and macroencephaly by year 2. Within 4 years, patients fall to a vegetative state and expire. In the Juvenile form, sufferers develop motor symptoms with 2-6 years, loss of speech, seizure, loss of vision, dementia and spasticity by year 10. The vegetative state and death occur within 10-15 years. Chronic onset patients adopt an abnormal gait and posture within 5 years, and live to approximately 40, with neurological symptoms, although intelligence remains intact. Adult onset sufferers begin mimicking neurological disorders in their 20s, but – like those with

chronic onset- intelligence is not affected (Kolter and Sandhoff, 2006). Diagnosis of the disease can be performed via enzymatic assays. HEXA is heat labile at 50C, while HEXB is not. By measuring the difference in enzyme activity on a common substrate, 4-methylumbelliferyl β-*N*-acetyl-glucosaminide (4-MUG), before and after exposure to heat, it is possible to estimate the enzymatic contribution of each enzyme (Narkis et al., 1997). Genetic testing for common mutations is also an efficient way to identify disease carriers and sufferers. The most common allele for TSD is a 4-bp TATC insertion in exon 11 of the *HEXA* gene, which produces a premature stop codon (Boles and Proia, 1995). This mutation represents approximately 79% of TSD alleles in Ashkenazi Jewish carriers- a particularily at-risk group- but as low as 16% percent of TSD alleles in non-Jewish carriers (Paw et al., 1990; Triggs-Raine et al., 1990). French Canadians are also commonly affected, and the most common mutation in the French Canadian population is a 7.6-kb genomic deletion involving the HEXA promoter and exon 1; no mRNA is produced by this allele (Myerowitz and Hogikyan, 1986).

1.3.2 Sandhoff Disease

Sandhoff disease (SD) is caused by a mutation of the gene *HEXB*, the product of which is a subunit of not only β-hexosaminidase A, but also β-hexosaminidase B. Patients with this disease suffer similar symptoms as those with Tay-Sachs, with the following caveats: infant sufferers have organomegaly and slight bone deformation; juvenile onset type is typified by slurred speech, cerebellar ataxia, psychomotor retardation, normal vision, spasticity and mental deterioration with 3-10 years of life;

adult sufferers have an build-up of uncharged enzyme substrates (Kolter and Sandhoff, 2006).

1.4 Animal Models

Mouse models have been developed on C57BL/6 backgrounds that mimic TSD and SD, through knockouts of the orthologous *Hexa* and *Hexb* genes respectively (Phaneuf et al., 1996). The *Hexa* gene was disrupted by insertion of a neomycin-resistance gene cassette in exon 11, and *Hexb* by insertion of a neomycin-resistance gene cassette in exon 2. *Hexa*$^{-/-}$ mice are largely asymptomatic however, due to an alternative metabolic pathway which allows conversion of GM2 to GA2 by the enzyme sialidase, which can then be metabolised to lactosylceramide (Sango et al., 1995). A similar effect has been produced in human neuroglia via upregulation of sialidase via an exogenous cDNA expression vector (Igdoura et al., 1999). Some *Hexa*$^{-/-}$ mice develop clinical symptoms, including tremors, within 1-2 years, in particular females who have bred, and this coincides with a reduction of HEXB expression (Jeyakumar et al., 2002). The *Hexb*$^{-/-}$ mice accumulate gangliosides in the CNS and other tissues including the testis and epididymis, and have symptoms involving slow movement, muscle weakness, ataxic gait, and inability to right selves, onset at 3-4 months. Death occurs within 6 weeks of onset, after development of tremors, myoclonus and spastic quadraparesis (Adamali et al., 1999; Phaneuf et al., 1996). *Hexb*$^{-/-}$ mice display cognitive dysfunction presenting as hypoactivity and increased thigmotaxis, considered a measure of anxiety in mice (Gulinello et al., 2008; Simon et al., 1994). These mice also presented with

memory deficits, presenting as a reduction in novel object recognition. SD mice respond to a calorie restricted diet, with improved survival and performance on behaviour tests, and reduced inflammation, despite no marked difference in brain lipids, suggesting an avenue for treatment (Denny et al., 2006). SD mice accumulate not only GM2 and GA2, but also α-synuclein and β-synuclein, presynaptic proteins related to the cytoskeleton (Suzuki et al., 2003). α-synuclein accumulates in neurons of many regions of the brain, including the cingulate gyrus, subiculum, striatum terminus, olfactory bulb, thalamus, the deep cerebral cortex, the dentate gyrus, and CA3-4 region of the hippocampus. β-synuclein shares many areas of expression with α-synuclein, but in particular accumulates in the cingulum, pontine gyrus, and granule cell layer of the cerebellum. As previously mentioned, SD mice also accumulate amyloid-β, and ganglioside-bound Aβ, both typical of other neurodegenerative diseases including Alzheimer's disease (Keilani et al., 2012; Yanagisawa et al., 1995). A reduction in phospholipid metabolism is seen in *Hexb*$^{-/-}$ mice, which is consistent with observation in human SD patients (Buccoliero et al., 2004; Sandhoff et al., 1971). SD mice show heavy involvement of inflammation in the progression of the disease. *Hexb*$^{-/-}$ mice present with infiltration of peripheral blood mononuclear cells (PBMC) into the CNS (Kyrkanides et al., 2008). They also suffer from thymic involution (shrinking of the thymus), occurring at approximately 15 weeks of age, due to apoptosis, which correlates with an increase in corticosterone levels (Matsuoka et al., 2011b). Interestingly, induced pluripotent stem cells (iPSC) from *Hexb*$^{-/-}$ mice are impaired in their ability to differentiate to early neural precursors, and fewer neurons

develop from these precursors, relative to WT iPSCs (Ogawa et al., 2013). Hippocampal neurons from *Hexb*$^{-/-}$ mice also have reduced axonal and minor process growth in culture, and retinal ganglion cells of SD mice show reduced numbers of neurite outgrowths relative to WT cells (Pelled et al., 2003b; Sango et al., 2005). This could indicate that neurological issues in SD are not just due to neuronal death, but also a decreased ability to generate new neurons and processes.

1.5 Neuroinflammation, Neurodegeneration, and Sandhoff Disease

Neuroinflammation has been indicated in many neurodegenerative diseases, such as Alzheimer's disease (AD), and Parkinson's disease (PD) as not just a symptom, but also an exacerbating factor (Akiyama et al., 2000; Teismann and Schulz, 2004). Microglial activation has been shown to be an important element of Sandhoff disease progression in mouse models, with intense inflammation foregoing neurodegeneration- an effect suppressed via bone marrow transplantation from *Hexb*$^{+/+}$ mice, despite no changes in GM2 storage (Wada et al., 2000). As microglia take up GM2, they are unable to metabolise it due to their own deficiency of β-hexosaminidase B, leading to their demise, and the continuation of the inflammatory response (Fontaine et al., 2002; Skaper, 2007). CD45 positive cells are also shown to be increased in number in the brains of *Hexb*$^{-/-}$ mice relative to WT mice, suggesting an increase in the infiltration of peripheral blood mononuclear cells in the Sandhoff disease afflicted brain. Knockout of the CC-chemokine receptor CCR2 reduced the infiltration of PBMCs, and delayed the onset behavioural deficits in *Hexb*$^{-/-}$ *Ccr2*$^{-/-}$ mice relative to *Hexb*$^{-/-}$ mice (Kyrkanides et

al., 2008). Microglial activation can lead to the release of various cytokines, including interleukin-6 (IL6) and tumour necrosis factor-alpha (TNFα), which may induce an apoptotic pathway in neurons, thus proliferating the response (Fontaine et al., 2002; Shishodia and Aggarwal, 2002). Apoptosis has indeed been identified in the course of SD (Huang et al., 1997). Astrocytes appear to also play a role in neurodegeneration in Sandhoff disease. The number of glial fibrillary acidic protein (GFAP) positive cells- a marker for activated astrocytes- was shown to be increased in the brains of *Hexb*$^{-/-}$ mice relative to WT mice, suggesting an activation of astrocytes in the brains of mice with Sandhoff disease (Kyrkanides et al., 2008). Astrogliosis and development of astrocyte-based glial scars after neurodegeneration may inhibit the regeneration of neurite outgrowth, limiting recovery (Bovolenta et al., 1993). Knock-out of sphingosine kinase 1 (*Sphk1*) in *Hexb*$^{-/-}$ mice resulted in a reduction of astrocyte activation and improved survival, and increased body weight (Wu et al., 2008). There is evidence that these microglial and astroglial processes are increased through communication between the astrocytes and microglia/peripheral macrophages. It has been shown that macrophage infiltration into the brain from the periphery coincides with an increase in the expression of macrophage-inflammatory protein 1 alpha (MIP-1α) by astrocytes. Knockout of MIP-1α reduces the infiltration of macrophages, reduces expression of TNFα and increases the lifespan of *Hexb*$^{-/-}$ mice (Wu and Proia, 2004). Non-glial immune systems also appear to be involved in the Sandhoff disease. *Hexb*$^{-/-}$ mice produce anti-GM2 and anti-GA2 IgG antibodies in later stages of the disease, detectable in serum, and present on the

Perkinje cells of the cerebellum, and in the thalamus. Knockout of the antibody-binding Fc receptor common γ-chain (FcRγ) in SD mice improves lifespan and behaviour despite no change in GA2 or GM2 accumulations, verifying the involvement of adaptive immunity against gangliosides in the disease (Yamaguchi et al., 2004). Furthermore, *Hexb*$^{-/-}$*FcRγ*$^{+/+}$ mice have a decreased CD4^{+}/CD8^{+} ratio relative to CD4^{+}/CD8^{-} and CD4^{-} /CD8^{+} relative to *Hexb*$^{+/-}$*FcRγ*$^{+/+}$ and *Hexb*$^{-/-}$*FcRγ*$^{-/-}$ mice, indicating a shift towards mature populations of T-cells in SD mice, with rescue towards WT phenotype by knockout of FcRγ (Kanzaki et al., 2010). SD mice develop thymic involution at later ages due to apoptosis, and this is suggested to occur through autoimmunity against T cells that produce gangliosides, such as GA2. This autoimmunity may then lead to an immune response against neurons which also produce GA2 (Kanzaki et al., 2010; Matsuoka et al., 2011b). Due to the heavy involvement of inflammation in the disease, many inflammation related proteins have been suggested as biomarkers for gangliosidoses in human patients including ENA-78, MCP-1, MIP-1α, MIP-1β, and TNFR2 (Utz et al., 2015).

1.6 Glutamate as an Excitatory Transmitter and Involvement in Excitotoxicity

Glutamate acts in the CNS as an excitatory neurotransmitter by acting upon various glutamate receptors. Excitotoxicity is the process involving overstimulation of various glutamate receptors leading to a high influx of Ca^{+2} ions into the cytosol. Overstimulation of these receptors may have many detrimental effects, including production of free radicals and expression of pro-death transcription factors (Wang and Qin, 2010). Excitotoxic death appears to occur as a mixture of both necrosis and

apoptosis depending on the glutamate receptors involved and surrounding tissue conditions (Martin et al., 1998). It has been demonstrated that apoptosis is indeed increased in tissues across the CNS of SD mice relative to WT mice, adding clout to the hypothesis that this may be a pathway of neurodegeneration in SD (Huang et al., 1997). The four AMPA receptor subunits (GLUR1-4) that are sensitive to AMPA are permeable to Ca^{+} influx with the exception of the common GLUR2(R), which limits the permeability of the heterotetramers when in complex via a positively charged arginine. It has been shown that the ratio of GLUR1 to GLUR2 in a cell membrane affects the excitotoxic vulnerability of rat neurons through Ca^{+} influx, with higher GLUR1 levels being associated with higher excitotoxicity occurrence (Kim et al., 2001). Glutamate receptors have also been connected to neurodegeneration in AD, through the influx of Ca^{+} leading to excitotoxicity (Hynd et al., 2004). It has also been shown that TNFα may induce excitotoxicity in the rat hippocampus by inhibiting glutamate uptake by glutamate transporters, leading to overstimulation of *N*-methyl-D-aspartate receptors (NMDAR) which allows Na^{+} and Ca^{+2} ions to enter the cell, with the presence of NR2A or NR2B subunits being the determining factors in increased ion permeability. AMPARs do not appear to be a major factor for excitotoxicity in this case (Stanika et al., 2009; Zou and Crews, 2005). This may not always be the case however, as TNFα has been shown to cause localization of GLUR1 to at the cell membrane in dissociated rat hippocampal neurons, thereby increasing the risk of excitotoxicity (Ogoshi et al., 2005). It is unknown how this localization occurs, and this could occur through interaction with Np1.

1.7 Regulation of Glutamate Excitation via Neuronal Pentraxins

Neuronal pentraxins are a family of calcium-dependant lectins which can form heteromultimers, and together bind the snake venom taipoxin (Kirkpatrick et al., 2000; Xu et al., 2003). Neuronal pentraxins contain highly conserved structures between species, including a c-terminal 'pentraxin domain' that mediated binding to AMPA receptors, 2 coiled-coil domains, and 3 N-terminal cysteine residues, responsible for inter-pentraxin disulphide linkages (Omeis et al., 1996). Neuronal pentraxin 1 (NP1), neuronal pentraxin 2 (NARP) and the neuronal pentraxin receptor (NPR) have been shown to co-localize and cause the clustering of AMPA receptors (AMPAR)- responsible for binding glutamate and acting as an ion channel for Na^{+}, K^{+}, and Ca^{+2}- and are thus involved in postsynaptic shaping. Narp appears to be more efficient at clustering AMPARs, but is found in lower numbers in the CNS *in vivo*. Clustering appears to be more efficient when pentraxins are found on adjacent cells to those containing AMPARs (Xu et al., 2003). Both NP1 and Narp are expected to be soluble proteins, while NPR contains a transmembrane domain that may anchor the neuronal pentraxin heterocomplexes to the cellular membrane. It has been shown that cleavage of NPR by the metalloprotease TNF-alpha converting enzyme (TACE) can lead to colocalization of NPR with AMPAR within endosomes, resulting in depression of synapse excitability (Cho et al., 2008). Thus pentraxins may play a role in both increasing and decreasing synapse strength.

1.8 Roles of Neuronal Pentraxin 1 in Neuronal Death

Np1 has been shown as directly responsible for activation of apoptosis in rat cerebellar granule cells, and is implicated with excitotoxic neuronal death through GLUR1/AMPA during hypoxic-ischemic injury in neo-natal rats (DeGregorio-Rocasolano et al., 2001; Hossain, 2008; Yeste-Velasco et al., 2008). On the other hand, neuronal pentraxins could be protective against excitotoxicity, through endocytosis of AMPARs, and phagocytosis of synaptic contents by glia, through interaction with C1q complexes (Gasque et al., 2000; Kreutzberg et al., 1989; Stevens et al., 2007). These findings may suggest that NP1 is either positively or negatively acting in TSD and SD as a regulatory mechanism for AMPA induced excitotoxicity. A recent study has found a role for NP1 in relating low neuronal activity to the process of inducing BCL2 associated X protein (BAX)-dependant mitochondrial fragmentation and therefore apoptosis (Clayton et al., 2012). NP1 has also recently been shown to be expressed in astrocytes, where it may have any number of unexplored roles (Wang et al., 2012).

1.9 Available Treatments

Treatments for lysosomal storage disorders can generally be catagorized into six major groups; gene therapy, enzyme replacement, substrate reduction, bone marrow transplantation, pharmalogical chaperones, and treatment of secondary effects.

1.9.1 Gene Therapy

Gene therapies aim to correct the original cause of lysosomal storage disorders, which is a malfunctioning or non-functioning enzyme gene product. By introducing and expressing a functional version of the enzymes, the affected cells should be restored to a

relatively normal function. Recombinant adeno-associated viruses (rAAV) are the expression vector of choice for gene therapies due to their low immunogenicity, that they do not integrate into the genome, and they are able to infect postmitotic cells. Expression of HexA and HexB in mice via the recombinant adeno-associated virus rAAV2/1, has been shown to reduce the loss of neurons in the thalamus of SD mice, after injection into the striatum- a neighbouring brain structure (Sargeant et al., 2011). rAAV9 expressing HexB has also been used successfully in neonatal SD mice to increase lifespan and reduce GM2 in the brain, via intravenous injection (Walia et al., 2015). Another virus often used for this purpose- AAVrh8- is a vector isolated from rhesus monkeys, which is able to cross the blood brain barrier and displays reduced peripheral tropism, making it a good candidate for CNS specific gene-therapy (Giove et al., 2010; Yang et al., 2014). Use of AAVrh8 vectors and species-specific hexosaminidase enzymes produces a lessened (though measurable) immune reaction in the form of anti-vector antibodies, compared to AAV1 vectors expressing human hexosaminidase enzymes (Bradbury et al., 2013). AAVrh8 has been used to express feline HexA and HexB in cat models of SD via thalamic and intracerebroventricular injections, resulting in reduced GA2 and GM2 levels in the brain, reduced tremors at predetermined endpoint, and improved behaviour scores (McCurdy et al., 2015; Rockwell et al., 2015). This is a promising step from smaller organisms, such as mouse models, towards Tay-Sachs and Sandhoff disease patients. Although a promising technology for treatment, gene therapy has its caveats. Use of gene therapy appears to be most effective when administered

early in life, as evidenced by mouse models. After 12 weeks of life before treatment, there is no apparent difference in the survivability of mice treated with HexA and HexB expressing rAAV2/1 vectors and mice that were untreated. Myelination is also affected early on, and cannot be fully rescued, even with treatment administered at ages as early as 4 weeks (Cachon-Gonzalez et al., 2014). This means that treatment by this method may only be useful in those where the disease is detected as early as possible. Gene therapy is also a controversial technique with ethical considerations and mixed public opinion, which will not be expanded upon here.

1.9.2 Enzyme Replacement Therapy

By replacing the dysfunctional hexosaminidase enzymes with modified and/or functional equivalents, enzymatic activity can be restored, leading to a reduction of built-up GM2/GA2, and a lessening of symptoms. Recombinant β-hexosaminidase A has been produced in yeast, and bound with mannose-6-phosphate (M6P) to allow its transportation to the lysosomal through the cell. This recombinant enzyme was successfully taken up by TSD and SD patient-derived fibroblasts through surface M6P receptors, and reduced accumulated GM2 (Akeboshi et al., 2007). Introduction of replacement enzymes to the CNS can be difficult, due to the blood brain barrier, as well as immune responses to the introduced enzymes (Wang et al., 2008). Enzymes can be administered via intracerebroventricular injection to bypass the blood brain barrier, as has been performed on a SD mouse model (Matsuoka et al., 2011a).

1.9.3 Substrate Reduction Therapy

The primary result of the dysfunction of HexA and HexB, is the intralysosomal buildup of gangliosides in the cells of the CNS. By reducing the upstream metabolites that would later be converted to GM2 and GA2, the burden on the CNS can be relieved. This principle is validated by the increased lifespan of *Hexb*$^{-/-}$ *GalNAcT*$^{-/-}$ mice. These mice lack a functional β1,4-N-acetylgalactosaminyltransferase, essentially preventing the generation of the HexB target substrates (Liu et al., 1999). One inhibitor of the biosynthesis of gangliosides has been heavily studied, *N*-butyldeoxynojirimycin (*N*B-DNJ, Migulstat). *N*B-DNJ is an inhibitor of glucosylceramide synthase, a precursor of GM2 and GA2, and has been used in the treatment of patients with other lysosomal storage disorders, including adults with type I Gaucher disease and Niemann-Pick disease, types C. *N*B-DNJ has been used to treat several teenage patients with Sandhoff disease with at least some success, followed by stability of weight and slowing of disease progression(Tallaksen and Berg, 2009; Wortmann et al., 2009). A larger study 20 adults with late-onset Tay-Sachs disease treated with *N*B-DNJ found no difference between the treatment group and 10 control patients(Shapiro et al., 2009). *N*B-DNJ also has several side effects at high doses including weight loss, and bowel irritation (Andersson et al., 2004; Platt et al., 1997; Shapiro et al., 2009). Another iminosugar, *N*-butyldeoxygalactonojirimycin (*N*B-DGJ) has been shown to be effective in reducing the accumulation of GM2 in *Hexb*$^{-/-}$ mice via inhibition of glucosylceramide synthase with fewer adverse side effect, relative to *N*B-DNJ (Baek et al., 2008). Intraperitoneal injection with *N*B-DNJ was found to be more effective than intracranial transplantation of wild-

type neural stem cells at reducing GM2, with no additive effect between the two treatments (Arthur et al., 2012). These studies were conducted in early post-natal mice however (up to p5 and p15, respectively), and long term effects require further research.

1.9.4 Bone Marrow Transplantation

Since macrophages of TSD and SD patients are unable to metabolize GM2, and peripheral macrophages are able to infiltrate the brains of SD sufferers, bone marrow transplantation (BMT) of healthy cells may be a viable option for treatment (Wada et al., 2000). It has been shown that exposure to the bone marrow of *Hexb*$^{-/-}$*Tnf*$^{-/-}$ mice, can improve the lifespan of SD mice, suggesting the benefits are not entirely due to the improved metabolism of gangliosides, but also to an improved cytokine profile (Abo-Ouf et al., 2013). BMT has been performed as a treatment for several lysosomal storage disorders, including Gaucher disease and mucopolysaccharidoses, with encouraging results (Hoogerbrugge et al., 1995). Bone marrow transplantation between WT mouse donors and SD mouse recipients has been shown to increase the recipient's lifespan, though not to wild-type levels. In fact, co-treatment with the ceramide glucosyltransferase inhibitor *N*B-DNJ further increases the life span of the SD mice, indicating that the bone marrow transplant is not a complete treatment on its own (Jeyakumar et al., 2001). This is also a painful and potentially dangerous measure, and so may not be a suitable treatment for many patients.

1.9.5 Pharmacological Chaperones

HexA and HexB are produced in the ER and transported via the Golgi apparatus to the lysosome. When misfolding occurs, the enzymes are degraded by the endoplasmic reticulum associated protein degradation pathway (ERAD). Pharmacological chaperones are small molecules that can bind to misfolded proteins to either restore enzyme activity, or to aid in their transportation out the ER to their target destination, where any residual activity can be of benefit. Often, only partial return of enzyme function is required to increase prognosis. For HEXA, this level has been cited as low as 5-10% HEXA activity, with apparently healthy individuals observed in clinic with activity levels as low as 10% (Dreyfus et al., 1977). One such pharmacological chaperone that has been studied for use in GM2-ganglisidoses is pyrimethamine (PYR), which functions to increase HexA activity. This drug is orally administered and is able to cross the blood brain barrier to some extent (Weiss et al., 1988). Phase I/II clinical trials found increased HexA activity in TSD and SD patient at dosages below those that cause side effects, with varying levels of activity increase, depending on the mutation(Clarke et al., 2011). However, fibroblasts from several SD patients treated with PYR were able to hydrolyze artificial test substrates, but not natural GM2, indicating it is not a cure-all treatment (Chiricozzi et al., 2014). An issue with chaperones, including PYR, is that they need to be validated for each mutation, of which there are at least 86 known variants for TSD, and 22 for SD (Maegawa et al., 2007; Mahuran, 1999). Chaperones will also not work on nonsense mutations where functional regions of the enzyme are missing, or where no protein is produced.

1.9.6 Treatment of Secondary Effects

As inflammation is a major factor in the decline of patient health in those with TSD and SD, pathways involved in inflammation may be considered as therapeutic targets (Jeyakumar et al., 2003). Reduction of TNFα has been shown to increase the lifespan of SD mice, and there are many drugs that are active against TNFα, including thalidomide, and bupropion (Abo-Ouf et al., 2013)(Brustolim et al., 2006). Sandhoff disease mice also respond well to nonsteroidal anti-inflammatory drugs (NSAIDs), including indomethacin, ibuprofen and aspirin, showing approximately 12-15% increase in lifespan (Jeyakumar et al., 2004). One benefit of these treatments is that drugs for the reduction of inflammation are abundant and thoroughly tested, and many are approved by food and drug administrations, meaning they may be immediately prescribed for off – label use by physicians.

1.10 Rationale and Objectives

Since TSD and SD are relatively rare disorders, much less is known about them relative to other neurodegenerative diseases, such as Alzheimer's. The majority of research on TSD and SD involve the study of inflammatory processes and the treatment of these pathways. Other potential neurodegenerative pathways which are being investigated for other neurodegenerative diseases, including excitotoxicity, and apoptotic pathways have been ignored. There is a need for new treatment avenues, as current attempts are incomplete, intrusive, or have unwanted side-effects. By analyzing the order and mechanisms of neurodegenerative processes in mouse models of TSD and

SD, we may illuminate new areas for exploitation in the treatment of said diseases. As TNF is central to inflammatory, apoptotic and even survival pathways, its pluralistic role may make it a far-reaching target for therapies. Similarly, the dualistic roles of NP1 in both upregulation and downregulation of excitatory synapses, as well as its potential role in apoptosis, make it a completely unknown variable and an interesting potential candidate for treatment targeting. As several pathological pathways are involved in the disease (microgliosis, astrogliosis, and perhaps others), knowledge of the precise timing of the onset of these can be useful in designing treatment courses to take before critical events in the progression of the disease, and to avoid treatments before they are required.

1.10.1 Objectives:

1. To examine the effects of TNFα depletion on a SD mouse model in order to identify the interactive effects on microglia, astrocytes, and apoptosis. We will knockout TNFα from SD mice, and compare levels of microgliosis, and astrogliosis in various tissues of the brain and spine. We will measure the coinciding apoptosis at these sites to determine what effect any changes in glia have on the health of surrounding neuronal tissues.

2. To investigate the developmental progression of microgliosis and astrogliosis over the lifetime of SD mice. By measuring protein levels and activation of glia in the CNS of WT and SD mice, we intend to compare the onset of various inflammation markers, with neuronal and apoptotic markers at a greater resolution than measured in

the literature. We aim to identify the interaction between molecular pathways, as well as identifying critical stages of the disease, and the pathways responsible for each.

3. To establish a role for neuronal pentraxins and the regulation of excitatory synapses in the decline of neurons in SD. Knockout of the regulatory protein NP1 in an SD mouse model, will enable us to observe the effects on synaptic proteins such as GluR1, GluR2, and NMDAR1 in the CNS. We also intend to observe the effects on neurodegeneration by measuring apoptotic markers. An overall detrimental or beneficial effect on the mice will be quantified by behaviour, body mass and lifespan measurements.

CHAPTER 2: Deletion of tumor necrosis factor-α ameleriorates neurodegeneration in Sandhoff disease mice

This article was published in the journal Human Molecular Genetics and is cited as follows:

Abo-Ouf H, Hooper AW, White EJ, van Rensburg HJ, Trigatti BL, Igdoura SA. Deletion of tumor necrosis factor-α ameliorates neurodegeneration in Sandhoff disease mice. *Hum Mol Genet*. 2013 Oct 1;22(19):3960-75

Corresponding Author:
Dr. Suleiman Igdoura
McMaster University, 1280 Main St. W.
Hamilton, Ontario, Canada
L8S 4K1
Email: igdoura@Mcmaster.ca
(905) 525-9140 ex. 27729

2.1 Preface

Alexander Hooper performed the immunohistochemistry experiments (Figure 2.5, 2.7), the TUNEL experiments (Figure 2.8), prepared tissues for the slides used in the immunofluorescence experiments (Figure 2.6F), assisted with bone marrow isolation, and performed the statistical analysis of bone marrow transplantation results (Table 2.1), western blot results (Figure 2.9), behaviour (Figure 2.1), immunohistochemistry (Figure 2.5C-E, Figure 2.7A-C), and TUNEL experiments (Figure 2.8A-C).

Hatem Abo-Ouf performed the behaviour testing (Figure 2.1), Ganglioside assays (Figure 2.2, 2.3), qPCR (Figure 2.4), and bone marrow transplant experiments (Table 1). Hatem Abo-Ouf and Helena Janse Van Rensburg worked together on the western blots (Figure 2.5A-B, 2.6A-E, 2.9A-D). Elizabeth White performed the immunofluorescence experiment (Figure 2.6F).

Human Molecular Genetics, 2013, Vol. 22, No. 19 **3960–3975**
doi:10.1093/hmg/ddt250
Advance Access published on May 31, 2013

Deletion of tumor necrosis factor-α ameliorates neurodegeneration in Sandhoff disease mice

Hatem Abo-ouf[1], Alexander W.M. Hooper[1], Elizabeth J. White[1], Helena J. Janse van Rensburg[1], Bernardo L. Trigatti[2] and Suleiman A. Igdoura[1,3,*]

[1]Department of Biology, [2]Department of Biochemistry and Biomedical Sciences and [3]Department of Pathology and Molecular Medicine, McMaster University, Hamilton, Ontario, Canada

Received February 24, 2013; Revised May 1, 2013; Accepted May 28, 2013

Sandhoff disease (SD) is a lysosomal storage disorder caused by a lack of a functional β-subunit of the β-hexosaminidase A and B enzymes, leading to the accumulation of gangliosides in the central nervous system (CNS). The *Hexb*$^{-/-}$ mouse model of SD shows a progressive neurodegenerative phenotype similar to the human equivalent. Previous studies have revealed that *Hexb*$^{-/-}$ mice suffer from chronic neuroinflammation characterized by microglial activation and expansion. Tumor necrosis factor-α (TNFα), a key modulator of the CNS immune response in models of neurodegeneration, is a hallmark of this activation. In this study, we explore the role of TNFα in the development and progression of SD in mice, by creating a *Hexb*$^{-/-}$ *Tnfα*$^{-/-}$ double-knockout mouse. Our results revealed that the double-knockout mice have an ameliorated disease course, with an extended lifespan, enhanced sensorimotor coordination and improved neurological function. TNFα-deficient SD mice also show decreased levels of astrogliosis and reduced neuronal cell death, with no alterations in neuronal storage of gangliosides. Interestingly, temporal microglia activation appears similar between the *Hexb*$^{-/-}$ *Tnfα*$^{-/-}$ and SD mice. Evidence is provided for the TNFα activation of the JAK2/STAT3 pathway as a mechanism for astrocyte activation in the disease. Bone marrow transplantation experiments reveal that both CNS-derived and bone marrow-derived TNFα have a pathological effect in SD mouse models, with CNS-derived TNFα playing a larger role. This study reveals TNFα as a neurodegenerative cytokine mediating astrogliosis and neuronal cell death in SD and points to TNFα as a potential therapeutic target to attenuate neuropathogenesis.

INTRODUCTION

Lysosomal storage disorders are all characterized by the intralysosomal buildup of undegraded substrates due to the deficiency of one or more lysosomal enzymes and/or their cofactors (1). GM2 gangliosidoses are inherited storage diseases resulting from a functional deficiency in the lysosomal hydrolase β-hexosaminidase (2). β-Hexosaminidase removes terminal *N*-acetylgalactosamine from the GM2 ganglioside. The two major isoforms of β-hexosaminidase, HexA and HexB, are made up of distinct combinations of homologous α and β subunits. The heterodimer, HexA (αβ), is capable of cleaving terminal *N*-acetylgalactosamine from GM2, while the HexB homodimer (ββ) is not (1,3). Mutations in the *HEXA* gene encoding the α-subunit lead to a deficiency in HexA, clinically known as Tay–Sachs disease. Mutations in the *HEXB* gene encoding the β-subunit, on the other hand, give rise to a deficiency in both HexA and HexB isozymes, clinically known as Sandhoff disease (SD). Tay–Sachs and SD display similar clinical symptoms of neurodegeneration including motor function disturbances, spasticity, ataxia, seizures, visual loss and deafness. The high turnover of gangliosides in the central nervous system (CNS) accounts for the primarily neurological phenotype associated with these diseases. Both diseases are generally terminal in early childhood (2). The age of onset and severity of the diseases depends on residual enzyme activity, with null mutations giving rise to the more severe infantile phenotypes (1,4). Our understanding of the GM2 gangliosidoses has been greatly advanced by the development of authentic animal models. In keeping with the progressive neurodegenerative

*To whom correspondence should be addressed at: McMaster University, 1280 Main St. W. LSB 335, Hamilton, ON, Canada L8S 4K1. Tel: +1 9055259140; Fax: +1 9055226066; Email: igdoura@mcmaster.ca

course of SD, the *Hexb* $^{-/-}$ mice develop severe motor impairments by 3 months of age, with death usually ensuing 4–6 weeks after symptom onset (5). Unexpectedly, however, the *Hexa* $^{-/-}$ mice have a normal lifespan and show no obvious neurological impairments until at least 1 year of age (6). Currently, the *Hexb* knockouts are used as a model of the acute forms of both GM2 gangliosidoses, while the *Hexa* knockouts serve as a model for late onset variants of the diseases (7).

Several recent reports have implicated neuroinflammation as the driving force behind neurodegeneration in *Hexb* $^{-/-}$ mice (8,9). Neuroinflammation is an intricate process which involves the participation of various cellular types of the immune system (macrophages, neutrophils, mast cells, lymphocytes, platelets, dendritic cells), localized CNS cells (microglia, astrocytes, neurons) and cellular products (adhesion molecules, cytokines and chemokines) (10,11). Not only do neurons, astrocytes, microglia and oligodendrocytes generate inflammatory mediators but also they constitutively express cytokine receptors (12). Cytokines—including interleukin-1 alpha (IL-1α), IL-1β and IL-6 (12), transforming growth factor-β and tumor necrosis factor-α (TNFα)—are considered crucial players in the establishment of neuroinflammation (13,14). It is believed that activated microglia and astrocytes are the main sources of cytokines and chemokines. Activated microglia secrete multiple inflammatory factors including TNFα, IL-1β, IL-6, IL-12, chemokines, proteases, glutamate, free radicals and redox proteins via autocrine and paracrine mechanisms (15). In addition, glial cell-derived neurotrophic factor is released from activated glia cells and serves as a potent inflammatory factor that supports neuronal repair. An extensive expansion in the activated microglia in the brain of SD mice is observed prior to a wave of apoptosis, and neuronal apoptosis is also evident in patient brain samples (16,17). Although it is clear that the buildup of undegraded ganglioside substrates is the primary insult to neurons, the exact molecular sequence that converts this primary insult to neuronal apoptosis remains poorly understood (18). The bioactivity of TNFα has beneficial or deleterious consequences on neuronal tissues, and the expression of TNFα has been shown to increase sharply between 10 and 17 weeks of age in the brains of SD mouse models (19–21). To further explore the potential role of TNFα in the neurodegenerative process, we generated a *Hexb* $^{-/-}$ *Tnfα* $^{-/-}$ double knockout. Here, we present evidence that depletion of TNFα in SD mice results in improved neurological function, decreased levels of astrogliosis and reduced neural cell death. Bone marrow transplantation (BMT) experiments reveal that both CNS-derived as well as bone marrow-derived TNFα play a pathological role during SD progression. We also present evidence that the NF-kappa-B-inducing kinase (NIK)/non-canonical nuclear factor kappa-light-chain-enhancer of activated B cells (NF-κB) pathway is activated in SD and reduced in the absence of TNFα. Our findings demonstrate that neurological improvement through reduced neuro-inflammatory condition can be achieved without correction of neuronal ganglioside storage.

RESULTS

Deletion of TNFα improves the clinical course of SD in mice

Previous studies have established that SD mice exhibit an up-regulation in TNFα expression which coincides with neuronal apoptosis (16). To elucidate the importance of TNFα in the neurodegenerative course of SD mouse models, we generated *Hexb* $^{-/-}$ *Tnfα* $^{-/-}$ double-knockout mice. *Hexb* $^{-/-}$ *Tnfα* $^{-/-}$ mice show significantly higher body weights compared with *Hexb* $^{-/-}$ *Tnfα*$^{+/+}$ and *Hexb*$^{+/+}$ *Tnfα*$^{+/+}$ mice (Fig. 1A). While *Hexb* $^{-/-}$ *Tnfα*$^{+/+}$ mice exhibit disease phenotypes first at 85–90 days and reach a moribund endpoint state at a median of 124 days (Fig. 1B). *Hexb* $^{-/-}$ *Tnfα* $^{-/-}$ mice show longer lifespan, with a median endpoint of 143 days. The *Hexb* $^{-/-}$ *Tnfα*$^{+/-}$ mice followed a similar trend to *Hexb* $^{-/-}$ *Tnfα*$^{+/+}$ mice where the loss of a single copy of *Tnfα* only extended their life expectancy by several days (data not shown). To monitor motor function, three behavioral tests were performed, namely, righting reflex, rotorod and wire-hang experiments. The righting reflex was measured beginning at 12 weeks of age during acute neurodegeneration (Fig. 1F). The righting reflex times of *Hexb* $^{-/-}$ *Tnfα* $^{-/-}$ mice are comparable to the wild-type (WT) mouse times at 17 weeks of age. At this age, latency of *Hexb* $^{-/-}$ *Tnfα*$^{+/+}$ mice to right themselves is ∼3 times greater than *Hexb* $^{-/-}$ *Tnfα* $^{-/-}$ mice ($P < 0.03$).

In previous studies, *Hexb* $^{-/-}$ mice showed severe impairment in rotorod analysis indicating deterioration in sensorimotor coordination (5). In fact, the progressive loss in sensorimotor coordination started at 9 weeks of age. In this study, rotorod performance scores for *Hexb* $^{-/-}$ *Tnfα* $^{-/-}$ mice were higher than *Hexb* $^{-/-}$ *Tnfα*$^{+/+}$ mice after 90 days. In fact, *Hexb* $^{-/-}$ *Tnfα* $^{-/-}$ outperformed *Hexb* $^{-/-}$ *Tnfα*$^{+/+}$ mice in the rotorod test at 100 ($P < 0.005$) and 120 ($P < 0.03$) days old (Fig. 1C). Furthermore, wire hang scores of *Hexb* $^{-/-}$ *Tnfα* $^{-/-}$ mice were significantly higher at 100 ($P < 0.001$) and 116 ($P < 0.05$) days old in comparison with scores of *Hexb* $^{-/-}$ *Tnfα*$^{+/+}$mice, indicating that *Hexb* $^{-/-}$ *Tnfα* $^{-/-}$ mice show improved motor function relative to *Hexb* $^{-/-}$ *Tnfα*$^{+/+}$ mice. Performance on grip strength tests, which typically assess muscle strength, is similar between *Hexb* $^{-/-}$ *Tnfα*$^{+/+}$ and *Hexb* $^{-/-}$ *Tnfα* $^{-/-}$ mice but significantly lower than WT mice at 116 days ($P < 0.05$). There is however, a non-significant trend for *Hexb* $^{-/-}$ *Tnfα* $^{-/-}$ performing better at this age relative to *Hexb* $^{-/-}$ *Tnfα*$^{+/+}$ mice.

TNFα does not change glycolipid storage within the CNS of SD mice

The β-hexosamindase A and B deficiencies in SD produce significant accumulations in GM2 ganglioside and GA2 glycolipids in the CNS (16). In order to evaluate if the neurological improvement observed in double-knockout mice are attributed to reduced the storage of GM2 and GA2 glycolipids in the CNS, cerebrum and cerebellum from 17-week-old WT, SD and double-knockout mice were analyzed for glycosphingolipid content (22). In the cerebrum and cerebellum from SD mice, the GM2 and GA2 storage was higher than their WT controls, but the degree of accumulation did not differ significantly from that seen in *Hexb* $^{-/-}$ *Tnfα* $^{-/-}$ mice (Figs 2A–C and 3A–C). These results indicate that the neurological improvement observed in *Hexb* $^{-/-}$ *Tnfα* $^{-/-}$ mice is independent of ganglioside storage.

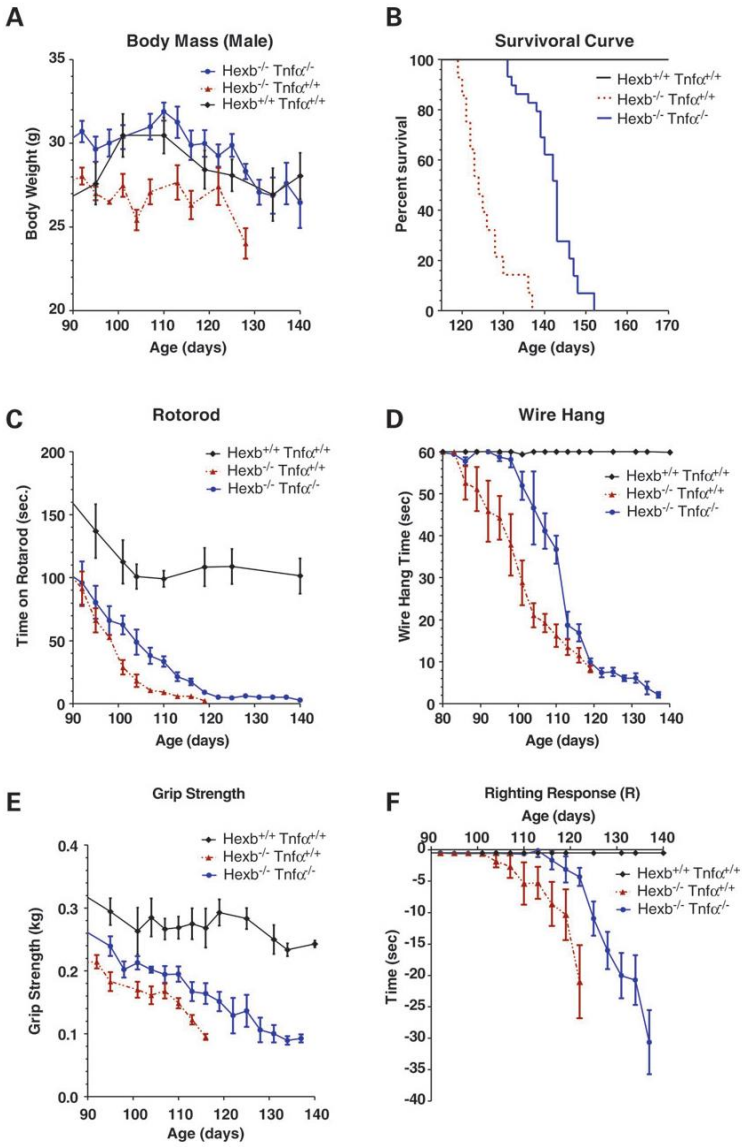

Figure 1. TNFα alters body weights, lifespan and motor behavior in SD mice. (**A**) *Hexb* $^{-/-}$ *Tnfα* $^{-/-}$ mice show significantly increased weights at 120 ($P = 0.02$) and 125 ($P = 0.0002$) days old, compared with *Hexb* $^{-/-}$ *Tnfα*$^{+/+}$ and *Hexb*$^{+/+}$*Tnfα*$^{+/+}$ mice ($n = 3–15$ mice per group). (**B**) Influence of TNFα on the survival of SD mice ($n = 11–31$ mice per group). The absence of TNFα in SD mice significantly extended their lifespan by 19 days ($P \leq 0.005$). (**C**) Rotorod test of WT, SD, and *Hexb* $^{-/-}$ *Tnfα* $^{-/-}$ mice. Means of latency to fall are presented ($n = 3–17$ mice per group). The rotorod times for *Hexb* $^{-/-}$ *Tnfα* $^{-/-}$ mice were longer than *Hexb* $^{-/-}$ *Tnfα*$^{+/+}$ mice at 101, 110, 119 days of age. (**D**) Wire hang times of *Hexb* $^{-/-}$ *Tnfα* $^{-/-}$ mice were compared to *Hexb* $^{-/-}$ *Tnfα*$^{+/+}$ mice. $n = 3–18$ mice per group. *Hexb* $^{-/-}$ *Tnfα* $^{-/-}$ had significantly better times at 100 and 116 days old, than *Hexb* $^{-/-}$ *Tnfα*$^{+/+}$. (**E**) Grip strength of *Hexb* $^{-/-}$ *Tnfα* $^{-/-}$ mice were compared to *Hexb* $^{-/-}$ *Tnfα*$^{+/+}$ mice. $n = 3–17$ mice per group. *Hexb* $^{-/-}$ *Tnfα* $^{-/-}$ had significantly better perfomance at 116 days old ($P < 0.05$, than *Hexb* $^{-/-}$ *Tnfα*$^{+/+}$. (**F**) Righting response of WT, SD, and *Hexb* $^{-/-}$ *Tnfα* $^{-/-}$ mice ($n = 6–12$). *Hexb* $^{-/-}$ *Tnfα* $^{-/-}$ mice show a significant improvement in righting reflex time as compared to the *Hexb* $^{-/-}$ *Tnfα*$^{+/+}$ mice ($P = 0.03$). Error bars = ± SE.

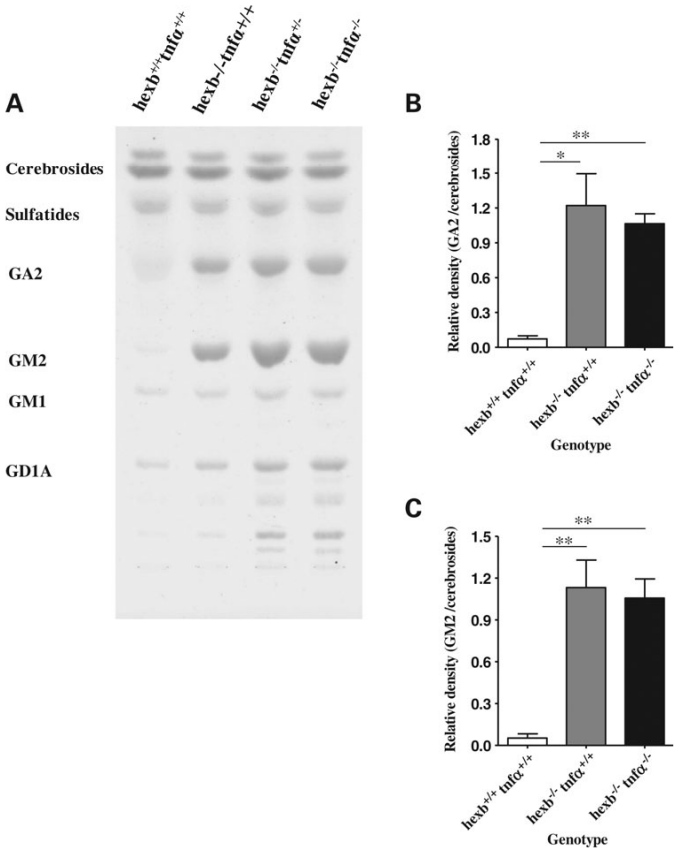

Figure 2. TNFα does not alter GM2 and GA2 gangliosidosis in the cerebrum of 17-week-old SD mice. Ganglioside fractions from cerebral lysates were analyzed by TLC. (**A**) Representative TLC distribution of ganglioside accumulation in the cerebrum ($n = 3$ experiments). The GM2 fraction was undetectable in WT mice. Sulfatides, cerebrosides and GM1 bands were not changed across the lanes. (**B**) Densitometric quantification of GA2 shows that it was significantly higher in SD and *Hexb*$^{-/-}$ *Tnfα*$^{-/-}$ genotypes, relative to their WT controls. (**C**) Densitometric quantification of GM2 faction shows significantly higher levels in SD and *Hexb*$^{-/-}$ *Tnfα*$^{-/-}$ genotypes ($n = 3$) when compared with control mice. $^{*}P \leq 0.05$, $^{**}P \leq 0.01$. Error bars, ± SE.

TNFα deletion attenuates the expression of markers of gliosis and oxidative stress

Utilizing mRNA isolated from the cerebella of *Hexb*$^{+/+}$ *Tnfα*$^{+/+}$, *Hexb*$^{-/-}$ *Tnfα*$^{+/+}$ and *Hexb*$^{-/-}$ *Tnfα*$^{-/-}$ mice, quantitative real-time reverse transcription polymerase chain reaction (qRT–PCR) was conducted to assess the expression level of the following genes: glial fibrillary acidic protein (*Gfap*), macrophage antigen alpha (*Mac-1α*), monocyte chemotactic protein-1 (*Mcp-1*), glutathione reductase (*Gsr*), nucleoredoxin (*Nxn*), peroxiredoxin 1 (*Prdx1*) and prostaglandin-endoperoxide synthase 1 (*Ptgs1*). Our data indicate that *Hexb*$^{-/-}$ *Tnfα*$^{+/+}$ mice show significant increases in the mRNA levels of *Gfap*, *Mac-1α* and *Mcp-1* genes, a significant decrease in *Gsr* expression and no change in the expression of *Nxn*, *Prdx1* and *Ptgs1* genes (Fig. 4). In comparison with *Hexb*$^{+/+}$ *Tnfα*$^{+/+}$ mice, *Hexb*$^{-/-}$ *Tnfα*$^{-/-}$ mice show significant increases in the mRNA levels of *Gfap* and *Mcp-1* genes, a significant decrease in Nxn expression and no significant change in the expression of *Mac-1α*, *Gsr*, *Prdx1* and *Ptgs1* genes (Fig. 4). The only gene product that appears to be affected by the absence of TNFα is *Nxn* which is significantly reduced in *Hexb*$^{-/-}$ *Tnfα*$^{-/-}$ mice in comparison with *Hexb*$^{-/-}$ *Tnfα*$^{+/+}$ mice.

TNFα deletion does not affect microgliosis in SD mice

In order to examine the molecular events leading to microglia activation, we examined the expression levels of MAC3 (CD107 antigen-like family member B) in the cerebellum of WT and *Hexb*$^{-/-}$ *Tnfα*$^{+/+}$ mice, relative to *Hexb*$^{-/-}$ *Tnfα*$^{-/-}$ mice (at 120 days of age). Our results indicate a significant up-regulation of cerebellar MAC3 expression levels in *Hexb*$^{-/-}$ *Tnfα*$^{+/+}$ and *Hexb*$^{-/-}$ *Tnfα*$^{-/-}$ in comparison with WT mice (Fig. 5A and B). To investigate the role of activated microglia as a possible pathogenetic mechanism that might be affected

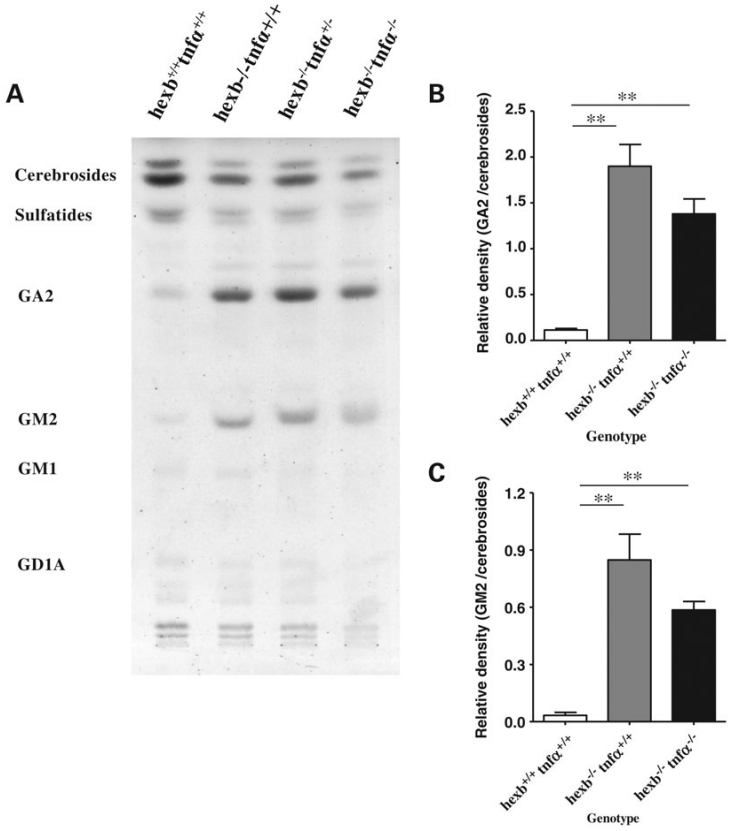

Figure 3. TNFα does not alter GM2 and GA2 gangliosidosis in the cerebella of 17-week-old SD mice. Ganglioside fractions from cerebellar lysates were analyzed by TLC. (**A**) Representative TLC photograph demonstrates the distribution of ganglioside accumulation in the cerebellum ($n = 3$ experiments). GM2 fraction was undetectable in WT mice. Sulfatides, cerebrosides and GM1 bands were not changed across the lanes. (**B**) Densitometric quantification of GA2 shows that it was significantly higher in SD and *Hexb*$^{-/-}$ *Tnfα*$^{-/-}$ genotypes, relative to their WT controls. (**C**) Densitometric quantification of GM2 faction shows significant increases in SD and *Hexb*$^{-/-}$ *Tnfα*$^{-/-}$ mice ($n = 3$ for each genotype) in comparison with WT control mice. $^{*}P \leq 0.05$, $^{**}P \leq 0.01$. Error bars, ± SE.

by TNFα deletion, we examined the frequency of activated microglia (MAC3-positive cells), in the cerebellum, cerebral cortex and spinal cord. Our results indicate that microglia/macrophage numbers are similar in the cerebella and cerebral cortices of *Hexb*$^{-/-}$*Tnfα*$^{+/+}$, and *Hexb*$^{-/-}$*Tnfα*$^{-/-}$ mice, despite a trend of lower levels in *Hexb*$^{-/-}$*Tnfα*$^{-/-}$ mice (Fig. 5C, D and F–H). This suggests that either there is no difference in the regulation of microglia in *Hexb*$^{-/-}$*Tnfα*$^{+/+}$ and *Hexb*$^{-/-}$*Tnfα*$^{-/-}$ mice or microgliosis occurs at a lower rate in *Hexb*$^{-/-}$*Tnfα*$^{-/-}$ mice relative to *Hexb*$^{-/-}$*Tnfα*$^{+/+}$ mice, but by 17 weeks a maximal level of microgliosis is reached in the brain tissues of *Hexb*$^{-/-}$*Tnfα*$^{+/+}$ mice and appears similar to levels observed in *Hexb*$^{-/-}$*Tnfα*$^{-/-}$ mice. In the spinal cord, microglia/macrophage numbers are not significantly different between *Hexb*$^{-/-}$*Tnfα*$^{+/+}$ and *Hexb*$^{-/-}$*Tnfα*$^{-/-}$ mice, although there again appears to be a trend in the three spinal regions toward elevated levels in *Hexb*$^{-/-}$*Tnfα*$^{+/+}$ mice (Fig. 5E and F). Our findings indicate that TNFα may not be a major player during the recruitment and/or activation of microglia/macrophages in the CNS to sites of neuroinflammation.

Astrogliosis is decreased with TNFα deletion in SD mice

To examine the level of GFAP expression as a measure of active astrogliosis in the SD pathology, we used western blot analysis of cerebellum lysates from 17-week-old *Hexb*$^{+/+}$*Tnfα*$^{+/+}$, *Hexb*$^{-/-}$*Tnfα*$^{+/+}$ and *Hexb*$^{-/-}$*Tnfα*$^{-/-}$ mice (Fig. 6A and E). GFAP expression in *Hexb*$^{-/-}$*Tnfα*$^{+/+}$ mice was significantly ($P < 0.01$) higher than *Hexb*$^{+/+}$*Tnfα*$^{+/+}$ mice. Notably, GFAP expression in the cerebellum of *Hexb*$^{-/-}$*Tnfα*$^{-/-}$ mice was significantly lower ($P < 0.05$) than the GFAP level in *Hexb*$^{-/-}$*Tnfα*$^{+/+}$ mice (Fig. 6A and E). Little is known about the signal transduction pathways that are involved in the activation/proliferation of astrocytes (23). However, the increased

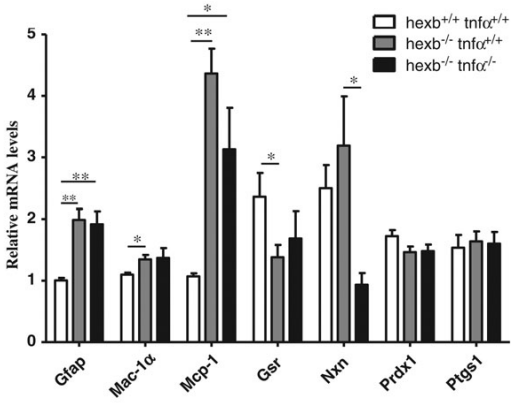

Figure 4. Expression levels of the genes involved in gliosis and oxidative stress pathways. mRNA isolated from the cerebella of 15-week-old $Hexb^{+/+}Tnf\alpha^{+/+}$, $Hexb^{-/-}Tnf\alpha^{+/+}$ and $Hexb^{-/-}Tnf\alpha^{-/-}$ mice was assessed using qPCR for the level of the expression of the following genes: *Gfap*, macrophage-a antigen (*Mac-1α*), monocyte chemoattractant protein-1 (*Mcp-1*), *Gsr*, *Nxn*, *Prdx1* and *Ptgs1*. The bar graph represents the mean expression measured in three independent quantitative real-time PCRs for each gene ± standard error bars. All plotted data represent gene expression levels relative to gene expression in the cerebella of age-matched $Hexb^{+/+}Tnf\alpha^{+/+}$ animals. The only gene that appears to be affected by the absence of TNFα in $Hexb^{-/-}Tnf\alpha^{-/-}$ mice is *Nxn*, which was significantly reduced in $Hexb^{-/-}Tnf\alpha^{-/-}$ mice in comparison with $Hexb^{-/-}Tnf\alpha^{+/+}$ mice. $^{*}P \leq 0.05$ and $^{**}P \leq 0.01$. Error bars, ± SE.

expression of GFAP in response to the activation of the IL-6/pSTAT3 pathway is considered the cardinal indication of reactive astrogliosis (23). To address the mechanisms underlying astrocyte activation, we examined the levels of IL-6 expression, JAK2 and STAT3 phosphorlyation and found no change in IL-6 or pJAK2 levels but a significant decrease in pSTAT3 in $Hexb^{-/-}Tnf\alpha^{-/-}$ compared with SD mice (Fig. 6A–D). To determine if STAT3 was present in the astrocytes of our mouse models, we double-labeled brains of 17-week-old $Hexb^{+/+}Tnf\alpha^{+/+}$, $Hexb^{-/-}Tnf\alpha^{+/+}$ and $Hexb^{-/-}Tnf\alpha^{-/-}$ mice with immunofluorescent antibodies for STAT3 and GFAP (Fig. 6F). Analysis of confocal optical slices reveals that STAT3 localizes within nuclei of GFAP-positive astrocytes in the cerebellum of these mice, adding credence to its role in astrocyte activation. Astrogliosis, in the CNS, has typically been identified morphologically by the presence of hypertrophic astrocytes with increased process ramifications and immunohistochemically by the presence of increased expression of GFAP (Fig. 7). The number of GFAP-positive astrocytes in the cerebellum was found to be significantly higher in $Hexb^{-/-}Tnf\alpha^{+/+}$ and $Hexb^{-/-}Tnf\alpha^{-/-}$ mice relative to WT (Fig. 7A). Notably, there were significantly fewer GFAP-positive astrocytes in the cerebella of $Hexb^{-/-}Tnf\alpha^{-/-}$ mice relative to $Hexb^{-/-}Tnf\alpha^{+/+}$ mice. In the cerebral cortex, there was a trend toward lower numbers of GFAP-positive astrocytes in $Hexb^{-/-}Tnf\alpha^{-/-}$ mice relative to $Hexb^{-/-}Tnf\alpha^{+/+}$ mice (Fig. 7B and D–F). These findings suggest that the onset of astrogliosis was delayed in $Hexb^{-/-}Tnf\alpha^{-/-}$ mice. Additionally, astrocyte proliferation may occur at an accelerated rate in $Hexb^{-/-}$ mice due to up-regulated TNFα expression. Furthermore, we examined the GFAP expression in the spinal cord using sections from the thoracic, cervical and lumbar regions from $Hexb^{+/+}Tnf\alpha^{+/+}$, $Hexb^{-/-}Tnf\alpha^{+/+}$ and $Hexb^{-/-}Tnf\alpha^{-/-}$ mice at 17 weeks of age (Fig. 7C and G–I). Our results reveal that astrocyte numbers were significantly higher in the thoracic and lumbar spinal cord of $Hexb^{-/-}Tnf\alpha^{+/+}$ mice compared with $Hexb^{-/-}Tnf\alpha^{-/-}$ mice, with a similar trend visible in the cervical region. This indicated that TNFα was involved in increasing the recruitment or differentiation of astrocyte precursors in the spinal cord of SD mice. Thus, the deletion of the *Tnfα* gene in $Hexb^{-/-}$ mice reduced the level of astrogliosis markers in the cerebellum and spinal cord. Our data indicate that the absence of TNFα activity in $Hexb^{-/-}$ mice results in a less severe neurodegenerative course that is associated with reduced astrogliosis.

Apoptotic neuronal death is decreased with deletion of TNFα in SD mice

We investigated if the deletion of TNFα could modulate neuronal apoptosis in $Hexb^{-/-}Tnf\alpha^{+/+}$ mice. There were significantly higher numbers of apoptotic cells in the cerebella of $Hexb^{-/-}Tnf\alpha^{+/+}$ mice relative to both $Hexb^{+/+}Tnf\alpha^{+/+}$ and $Hexb^{-/-}Tnf\alpha^{-/-}$ mice (Fig. 8A and D). This significant difference was also observed in the cervical region of the spine (Fig. 8C and F), with similar trends in the thoracic and lumbar regions of the spine, and in the cerebral cortex (Fig. 8B and E). These data suggest that apoptosis was reduced in the CNS of $Hexb^{-/-}Tnf\alpha^{-/-}$ mice relative to SD mice. In agreement with our previous result that GFAP immunoreactivity is significantly reduced in the cerebellum and spine of $Hexb^{-/-}Tnf\alpha^{-/-}$ mice in relation to $Hexb^{-/-}Tnf\alpha^{+/+}$ mice, we detected reduced neuronal cell death in the same regions of the CNS in the $Hexb^{-/-}Tnf\alpha^{-/-}$ mice (Fig. 8). Essentially, we found extensive apoptosis coincided with increased astrocyte activation. Our results raise the possibility that astrocytes residing in the spinal cord and cerebellum might play an important role in the apoptosis-mediated pathogenesis of SD.

It has been shown that NF-κB activation in microglia can be detrimental to neuronal cell survival via the release of excitotoxins and oxygen-free radicals (24). Nucleoredoxin, which we see to be down-regulated in $Hexb^{-/-}Tnf\alpha^{-/-}$ mice (Fig. 4), is shown to enhance TNFα- and NIK-induced activation of NF-κB pathways, suggesting that a reduction in the non-canonical NF-κB pathway in $Hexb^{-/-}Tnf\alpha^{-/-}$ mice may be a factor in their improved survival/behavioral performance (25,26). To explore this, the relative expression of TRAF3, NIK and RelB—components of the NIK/non-canonical NF-κB pathway—were determined by western blot (Fig. 9). The results revealed a significant decrease in TRAF3 expression ($P < 0.05$) in $Hexb^{-/-}Tnf\alpha^{-/-}$ mouse cerebella relative to SD mice (Fig. 9A and B). Furthermore, NIK expression was significantly reduced in both $Hexb^{+/+}Tnf\alpha^{+/+}$ and $Hexb^{-/-}Tnf\alpha^{-/-}$ *mice* relative to SD mice (Fig. 9A and C). The level of RelB was significantly lower in both $Hexb^{+/+}Tnf\alpha^{+/+}$ and $Hexb^{-/-}Tnf\alpha^{-/-}$ mice in comparison with SD mice (Fig. 9A and D; $P < 0.05$). These data suggest that the NIK/non-canonical NF-κB pathway is activated in SD and is limited by the deletion of *Tnfα*.

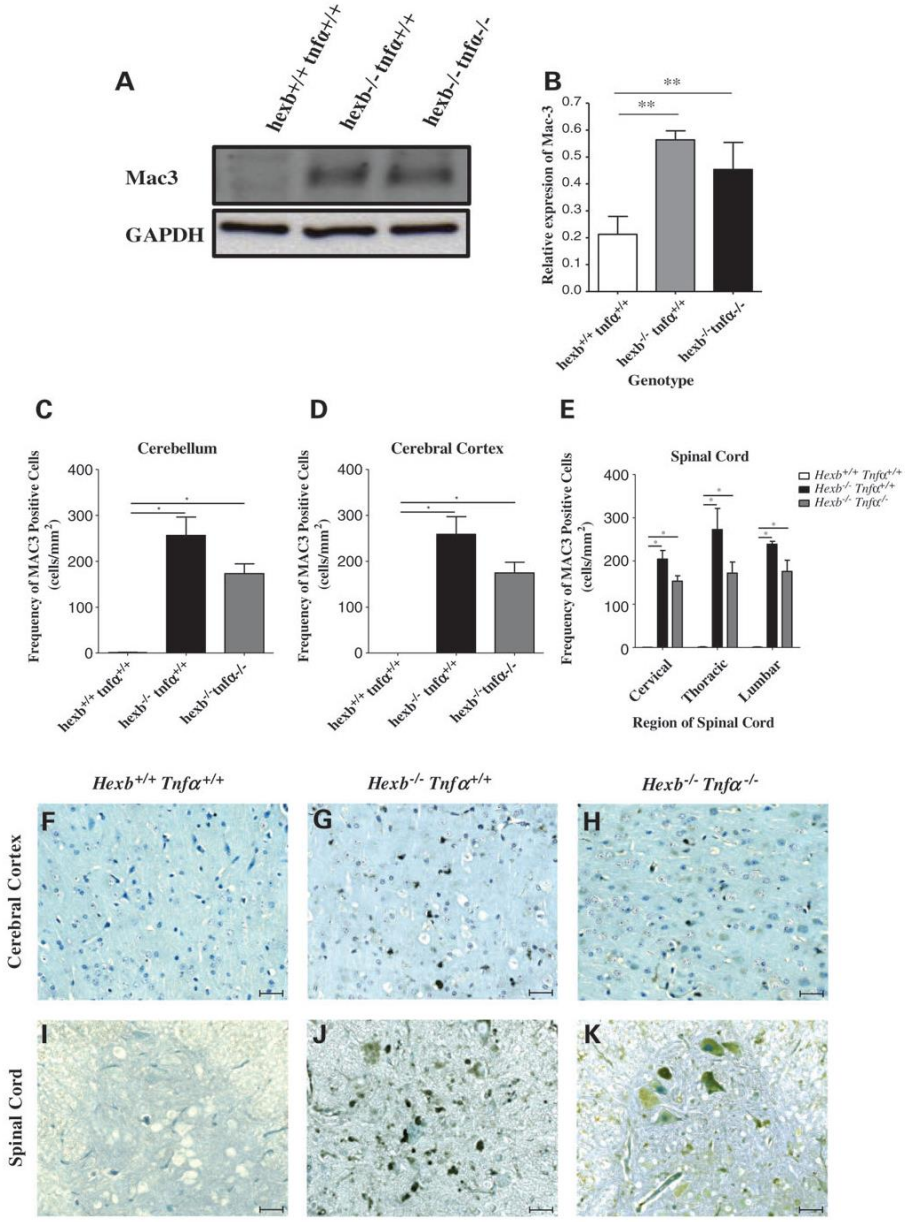

Figure 5. The effect of TNFα deletion on MAC3 expression in the CNS of SD mice. (**A**) MAC3 expression in the cerebellum was evaluated in 17-week-old $Hexb^{+/+}Tnf\alpha^{+/+}$, $Hexb^{-/-}Tnf\alpha^{+/+}$ and $Hexb^{-/-}Tnf\alpha^{-/-}$ mice by western blotting. An equal amount of sample protein was loaded in each lane. Glyceraldehyde-3-phosphate dehydrogenase (GAPDH) was used as a loading control. (**B**) Densitometric quantification of MAC3 expression in the cerebella of $Hexb^{-/-}Tnf\alpha^{+/+}$ mice show significantly higher expression relative to $Hexb^{+/+}Tnf\alpha^{+/+}$ mice. Decreased MAC3 expression in the double knockout mice is only a trend. (**C**–**E**) Quantification of MAC3-immunoreactive cells in the cerebellum, cerebral cortex and spine of $Hexb^{+/+}Tnf\alpha^{+/+}$, $Hexb^{-/-}Tnf\alpha^{+/+}$ and $Hexb^{-/-}Tnf\alpha^{-/-}$ mice. Macrophage numbers were similar in the cerebella, cerebral cortex and spines of $Hexb^{-/-}Tnf\alpha^{+/+}$ and $Hexb^{-/-}Tnf\alpha^{-/-}$ mice. (**F**–**K**) Images of the cerebral cortex illustrating differences in MAC3-immunoreactive microglia levels between $Hexb^{+/+}Tnf\alpha^{+/+}$, $Hexb^{-/-}Tnf\alpha^{+/+}$ and $Hexb^{-/-}Tnf\alpha^{-/-}$ mice. Images of spine sections illustrate MAC3 staining in the anterior horn. Scale bars indicate 20 μm. $n = 3-5$ mice per study. $^{*}P < 0.05$. Error bars, ± SE.

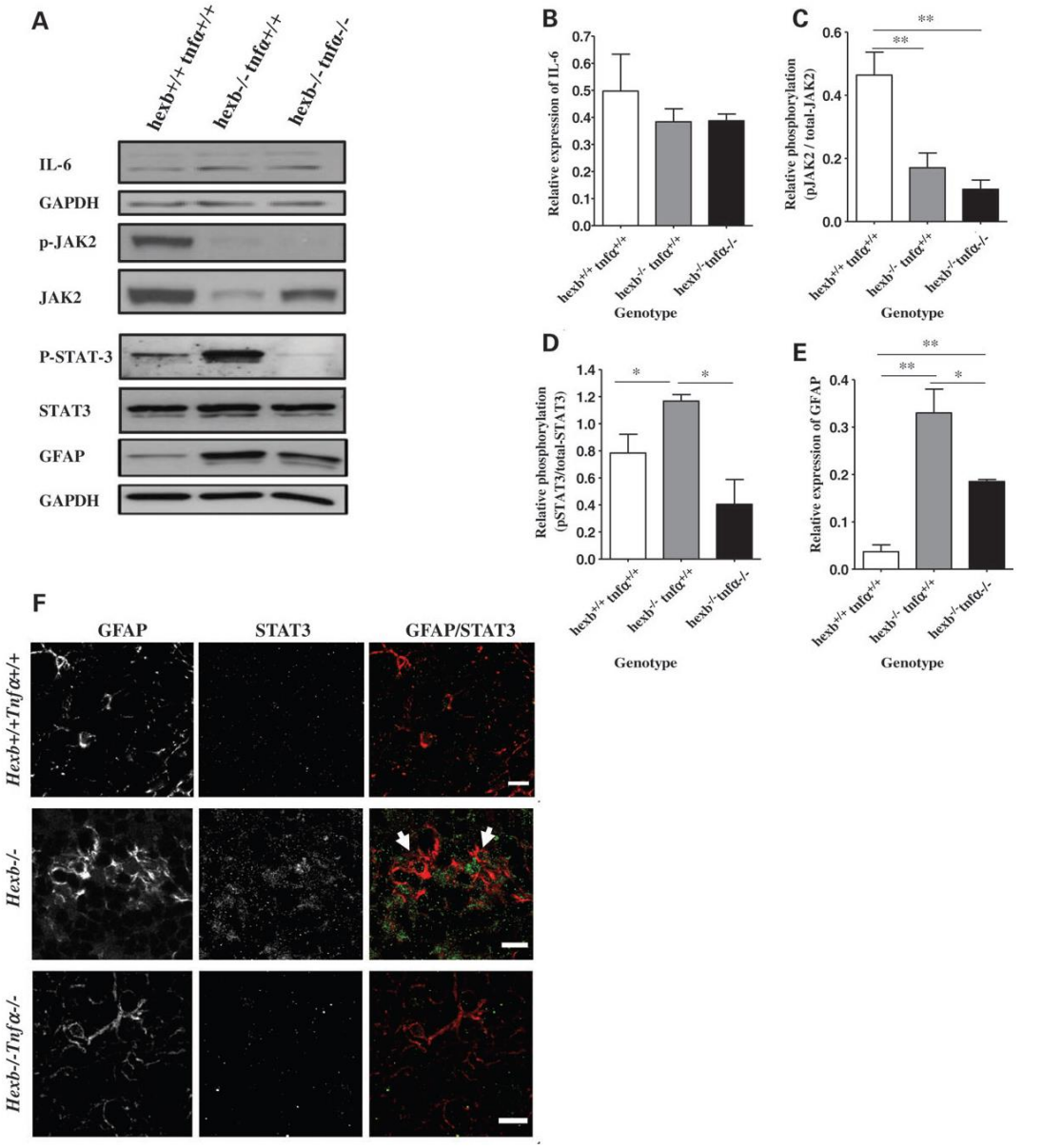

Figure 6. Effect of TNFα deletion on neuroinflammation markers and phospho-STAT3 signaling in SD cerebellum. (**A**) Expression of IL-6, JAK2, STAT3 and GFAP, as well as the phosphorylation of JAK2 and STAT3 in the cerebellum were evaluated in 17-week-old $Hexb^{+/+}Tnf\alpha^{+/+}$, $Hexb^{-/-}Tnf\alpha^{+/+}$ and $Hexb^{-/-}Tnf\alpha^{-/-}$ mice by western blot analysis. GAPDH was used as a loading control. (**B**) Densitometric quantification of IL-6 expression shows no significant difference among all three groups. (**C**). Densitometric quantification of pJAK2 in the cerebellum of $Hexb^{-/-}Tnf\alpha^{+/+}$ and $Hexb^{-/-}Tnf\alpha^{-/-}$ mice shows significantly lower phosphorylation relative to $Hexb^{+/+}Tnf\alpha^{+/+}$ mice. (**D**) Densitometric quantification of pSTAT3 in the cerebellum of $Hexb^{-/-}Tnf\alpha^{-/-}$ mice shows significantly higher phosphorylation relative to $Hexb^{+/+}Tnf\alpha^{+/+}$ and significantly lower phosphorylation relative to $Hexb^{-/-}Tnf\alpha^{+/+}$ mice. (**E**) GFAP expression was significantly increased in $Hexb^{-/-}Tnf\alpha^{+/+}$ and $Hexb^{-/-}Tnf\alpha^{-/-}$ mice relative to $Hexb^{+/+}Tnf\alpha^{+/+}$ mice; however, GFAP expression in the $Hexb^{-/-}Tnf\alpha^{-/-}$ mice was significantly lower than in $Hexb^{-/-}Tnf\alpha^{+/+}$ mice. The data represent the mean ± SEM of three animals per group. $^{*}P \leq 0.05$ and $^{**}P \leq 0.01$. (**F**) Confocal immunofluorencence optical slice in the cerebellum of $Hexb^{+/+}Tnf\alpha^{+/+}$, $Hexb^{-/-}Tnf\alpha^{+/+}$ and $Hexb^{-/-}Tnf\alpha^{-/-}$ mice, showing double staining for GFAP-positive astrocytes (red) and STAT3 (green). Note that STAT3 is present in astrocytes and, in some cases, localizes with nuclei (arrows). Bars represent 10 μm.

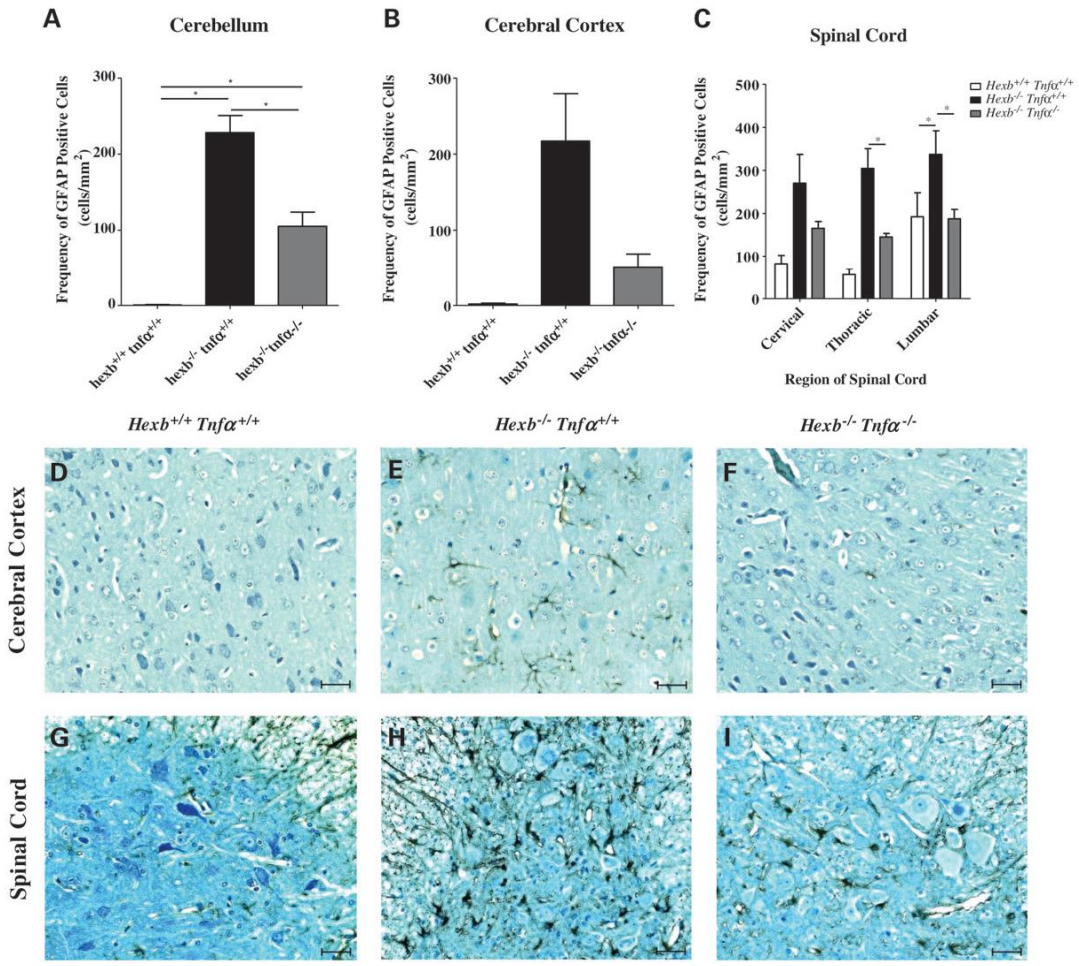

Figure 7. TNFα deletion in SD mice reduces CNS GFAP immunoreactivity. (**A**–**C**) Quantification of GFAP positive cells in the cerebellum, cerebral cortex and spine of $Hexb^{+/+}Tnf\alpha^{+/+}$, $Hexb^{-/-}Tnf\alpha^{+/+}$ and $Hexb^{-/-}Tnf\alpha^{-/-}$ mice. The number of GFAP positively cells is significantly lower in the cerebella and lumbar region of the spine in $Hexb^{-/-}Tnf\alpha^{-/-}$ mice relative to $Hexb^{-/-}Tnf\alpha^{+/+}$ mice. (**D**–**F**) Images of the cerebral cortex illustrating differences in GFAP-positive astrocyte levels between $Hexb^{+/+}Tnf\alpha^{+/+}$, $Hexb^{-/-}Tnf\alpha^{+/+}$ and $Hexb^{-/-}Tnf\alpha^{-/-}$ mice. (**G**–**I**) Spine images showing GFAP staining in the anterior horn. Intense GFAP expression is clearly visible in $Hexb^{-/-}Tnf\alpha^{+/+}$ mice and markedly reduced in $Hexb^{-/-}Tnf\alpha^{-/-}$ mice, indicating reduced astrogliosis. $Hexb^{+/+}Tnf\alpha^{+/+}$ mice show little to no GFAP staining across tissues of the CNS. Scale bars indicate 20 μm. $n = 3$–5 mice per study. $^{*}P \leq 0.05$. Error bars, ± SE.

Both CNS-derived and bone-marrow-derived TNFα play key roles in the pathogenesis of SD

In order to decipher the contribution of blood-derived versus CNS-derived TNFα in the neuroinflammatory cascade *in vivo*, we performed BMT of either $Hexb^{-/-}Tnf\alpha^{+/+}$ or $Hexb^{-/-}Tnf\alpha^{-/-}$ bone marrow into either $Hexb^{-/-}Tnf\alpha^{+/+}$ or $Hexb^{-/-}Tnf\alpha^{-/-}$ mice. Behavioral tests were performed as previously described above to assess neurological function as a measure of disease progression (Table 1). Tests were performed at 100 days, with the exception of righting reflex, which was measured at 120 days, near endpoint for $Hexb^{-/-}$ mice. Recipient mice who expressed neither endogenous nor transplanted TNFα ($Hexb^{-/-}Tnf\alpha^{-/-}$ into $Hexb^{-/-}Tnf\alpha^{-/-}$) performed the best of all groups, on all tests. Those expressing both blood-derived and CNS-derived TNFα ($Hexb^{-/-}Tnf\alpha^{+/+}$ into $Hexb^{-/-}Tnf\alpha^{+/+}$) had the worst performance on all tests, as expected if TNFα has a pathological effect. Interestingly, mice expressing only blood derived TNFα ($Hexb^{-/-}Tnf\alpha^{+/+}$ into $Hexb^{-/-}Tnf\alpha^{-/-}$) had slightly longer lifespans relative to those expressing only CNS-derived TNFα ($Hexb^{-/-}Tnf\alpha^{-/-}$ into $Hexb^{-/-}Tnf\alpha^{+/+}$), as well as significantly better performance on rotorod and wire hang tests. This suggests that CNS-resident microglia

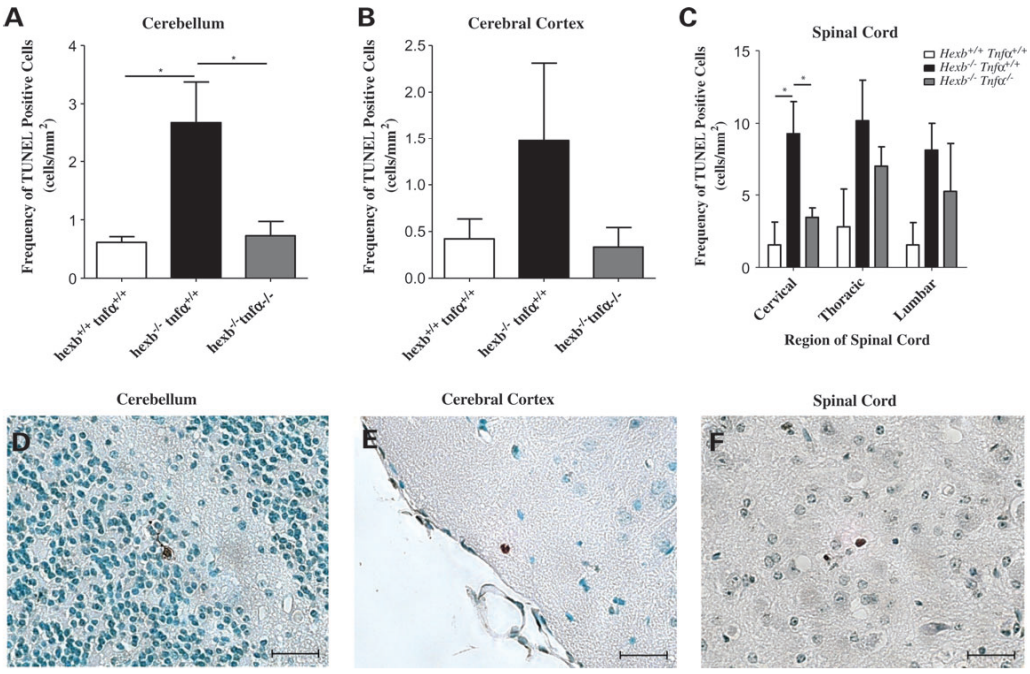

Figure 8. Apoptosis is reduced in the CNS of *Hexb* $^{-/-}$ *Tnfα* $^{-/-}$ mice. (**A**–**C**) Quantification of TUNEL positive cells in the cerebellum, cerebral cortex and spine of *Hexb*$^{+/+}$*Tnfα*$^{+/+}$, *Hexb* $^{-/-}$ *Tnfα*$^{+/+}$ and *Hexb* $^{-/-}$ *Tnfα* $^{-/-}$ mice. There are significantly higher numbers of cells undergoing apoptosis in *Hexb* $^{-/-}$ *Tnfα*$^{+/+}$ cerebella and cervical spine tissues, relative to both *Hexb*$^{+/+}$*Tnfα*$^{+/+}$ and *Hexb* $^{-/-}$ *Tnfα* $^{-/-}$ mice. A similar trend is seen in the cerebral cortex and thoracic and lumbar spine regions. (**D**–**F**) Images show examples of TUNEL positive cells in the cerebellum, cerebral cortex and spine, respectively. Apoptotic nuclei are small and stained brown. Scale bars indicate 20 μm. $n = 3$–5 mice per genotype. $^{*}P < 0.05$. Error bars, ± SE.

play a larger role in TNFα secretion relative to than those migrating from the blood.

DISCUSSION

The pathogenesis of neurodegeneration in SD is complex and involves various cellular changes as well as a profound disturbance of neuronal and glial homeostasis (27). Neuronal inflammation, glial activation and cytokine up-regulation are considered among the most prominent convergent points among various neurodegenerative diseases (13). TNFα is up-regulated in various neurodegenerative diseases including SD, suggesting a significant role for this cytokine in modifying the neurodegenerative process (28,29). A critical question has been the extent to which TNFα-mediated neuroinflammation contributes to the neurodegeneration in these disorders. In this study, we have provided direct evidence that TNFα plays a major role in the activation and expansion of the astrocytes populations and that this process accelerates the neuronal cell death. Genetic deletion of TNFα revealed that the *Hexb*$^{-/-}$*Tnfα*$^{-/-}$ mice gained neurological function leading to a delayed neurodegenerative cascade compared with SD mice.

The SD mouse model is considered an ideal prototype of a sphingolipidosis pathology that ultimately leads to neurodegeneration (30,31). In Sandhoff mice, abnormal storage is detectable in multiple CNS locations, including the cerebrum, cerebellum and spinal cord (17,32). Whether a neurological improvement of Sandhoff pathology necessitates a detectable global or localized correction of glycolipid storage in the CNS region has been less clear. In this neurodegenerative model, it is expected that a critical threshold of GM_2 and GA_2 storage is the driving force behind neuronal apoptosis (22,30,32,33). In fact, it was demonstrated that neurological amelioration has been achieved via a reduction in the primary injury of neuronal storage (22,32). However, some therapeutic strategies such as BMT were beneficial to suppress neurological deterioration without the detectable reduction in GM_2 in Sandhoff brain cells (34). While it was demonstrated that TNFα increases GM_2 production via the induction of GM_2 synthase in tumor cells (35), our study did not find differences in the levels of GM_2/GA_2 storage in SD and *Hexb*$^{-/-}$*Tnfα*$^{-/-}$ cerebella, suggesting that the neuroprotective effect of TNFα depletion is not mediated via glycolipid storage.

The early signs of cerebellar dysfunction in SD mice, i.e. ataxia and tremors, were monitored effectively using the behavioral tests conducted in our study. These neurological and behavioral tests made it possible to relate the effects of TNFα deletion in SD mice to cerebellar neuron function, neuronal signaling and motor behavior. Our data pointed to an improvement to the function of the basal ganglia and cerebellum neurons which reflect

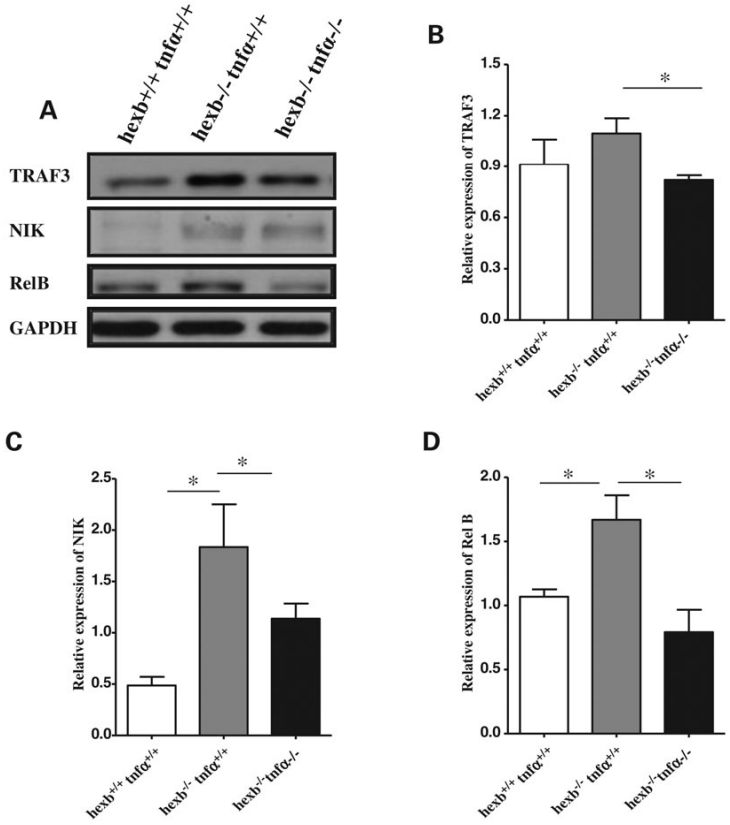

Figure 9. Differential activation of the NF-κB non-canonical pathway in *Hexb* $^{-/-}$ *Tnfα* $^{-/-}$ mice. (**A**) TRAF3, NIK and RelB expression were assessed in the cerebella of 17-week-old *Hexb*$^{+/+}$*Tnfα*$^{+/+}$, *Hexb* $^{-/-}$ *Tnfα*$^{+/+}$ and *Hexb* $^{-/-}$ *Tnfα* $^{-/-}$ mice using western blot analysis. GAPDH was used as a loading control. (**B**) Densitometric quantification of TRAF3 shows a modest trend of up-regulation in SD mice and down-regulation in *Hexb* $^{-/-}$ *Tnfα* $^{-/-}$ mice in comparison with WT mice. TRAF3 expression was significantly reduced in *Hexb* $^{-/-}$ *Tnfα* $^{-/-}$ cerebellum relative to SD cerebellum. (**C**) Densitometric quantification of NIK demonstrates a significant increase in its expression in the cerebella of SD and *Hexb* $^{-/-}$ *Tnfα* $^{-/-}$ mice relative to WT mice. However, NIK expression shows a substantial reduction in the *Hexb* $^{-/-}$ *Tnfα* $^{-/-}$ cerebellum relative to SD cerebellum. (**D**) Densitometric quantification of RelB expression shows a significant reduction in *Hexb* $^{-/-}$ *Tnfα* $^{-/-}$ mice relative to SD mice. RelB expression in SD cerebellum was highly up-regulated compared to WT controls. $n = 3$ mice per group. $^{*}P \leq 0.05$. Error bars, $\pm$SE.

motor function as well as an improvement to muscle strength and coordination, which reflect spinal motor neurons and possible neuromuscular junctions.

The mechanism by which the TNFα signal is translated into a pathophysiological effect remains to be determined. This study provides a new view of neurodegeneration in which TNFα may induce neuronal death indirectly through its effect on astrocytes. We examined the GFAP expression in the spinal cord of $Hexb^{-/-}Tnf\alpha^{+/+}$ and $Hexb^{-/-}Tnf\alpha^{-/-}$ mice. Astrogliosis was significantly reduced in the spinal cord and cerebellum of $Hexb^{-/-}Tnf\alpha^{-/-}$ mice. A similar trend was observed in the cerebral cortex. Our data indicated that the absence of TNFα resulted in a less severe neurodegenerative course that is associated with reduced astrogliosis. Microglia, the main producers of TNFα, have deleterious and/or protective effects on neurons in the course of neurodegenerative disease. Activated microglia have been shown to be involved in the progression of neuronal cell death in GM2 gangliosidosis (18). To investigate the role of activated microglia as a possible pathogenetic mechanism that might be affected by TNFα deletion, we immunostained CNS mouse samples for the microglial marker, MAC3. Our data show a trend toward a reduction in the number of MAC3-immunoreactive macrophages in the cerebellum, cerebral cortex and spine of $Hexb^{-/-}Tnf\alpha^{-/-}$ mice relative to $Hexb^{-/-}Tnf\alpha^{+/+}$ mice, pointing to a reduction in the severity of inflammation in this region due to the absence of TNFα. The lack of statistical significance here may be due to a maximal threshold in microglial numbers reached early on by $Hexb^{-/-}Tnf\alpha^{+/+}$ mice that is approached at 17 weeks by $Hexb^{-/-}Tnf\alpha^{-/-}$ mice, despite a lower overall rate of microglial activation/proliferation over the course of the disease.

SD shares many features with other neurodegenerative disorders such as increased reactive astrocytic pathology and astrogliosis (36). Recent studies have suggested that proinflammatory

Table 1. Effect of CNS-resident and bone marrow-derived TNFα on survival and behavior of $Hexb^{-/-}$ mice

	Bone marrow recipient mice			
	A	B	C	D
Genotype				
Donor	$Hexb^{-/-}$ $Tnf\alpha^{-/-}$	$Hexb^{-/-}$ $Tnf\alpha^{+/+}$	$Hexb^{-/-}$ $Tnf\alpha^{-/-}$	$Hexb^{-/-}$ $Tnf\alpha^{+/+}$
Recipient	$Hexb^{-/-}$ $Tnf\alpha^{-/-}$	$Hexb^{-/-}$ $Tnf\alpha^{-/-}$	$Hexb^{-/-}$ $Tnf\alpha^{+/+}$	$Hexb^{-/-}$ $Tnf\alpha^{+/+}$
Total *n*	12	6	4	6
Survival	145 ± 2.83	139.4 ± 5.96	130.5 ± 0.87[a]	121.7 ± 1.8[a,b]
Behavioral test				
Rotorod	145.4 ± 47.78	62.3 ± 5.56[a]	45.17 ± 4.12[a,b]	35 ± 9.96[a,b,c]
Wire hang	60 ± 0.00	60 ± 0.00	45.8 ± 6.02[a,b]	32.9 ± 13.2[a,b]
Righting reflex	0.5 ± 0.00	0.5 ± 0.00	6 ± 6.41	9 ± 8.93

Tests were performed at 100 days, except for the righting reflex test which was performed at 120 days. $P \leq 0.05$.
[a]Significantly different than group A.
[b]Significantly different than group B.
[c]Significantly different than group C.

cytokines such as TNFα can trigger and modulate astrogliosis (37,38). The impact of TNFα on the induction of astrogliosis has been observed in several studies (38). It was reported that TNFα microinjected into neonatal brain can elicit extensive GFAP immunoreactivity (38). Furthermore, astroglial response to 1-methyl-4-phenyl-1,2,3,6-tetrahydropyridine neuronal injury was almost completely inhibited in mice-deficient in both TNFR1 and TNFR2 (1). Besides these *in vivo* studies, TNFα is reported to increase GFAP expression *in vitro* (39). It is possible that the regulatory JAK2/STAT3 axis of astrogliosis is broadly applicable to other neurodegenerative disorders. STAT3 is a crucial transcription factor involved in several molecular and cellular responses including neuroinflammation, cell proliferation and survival (40). Recent study has reported that cytokine-induced activation of STAT3 is controlled by glycogen synthase kinase-3 (GSK3β) in astrocytes (41). Interestingly, recent work has reported that STAT3 can elicit an atypical cell death mechanism via lysosomal membrane permeabilization that leads to leakage of lysosomal proteases into the cytosol (42). It has been found that STAT3 phosphorylation, accompanied by toxic gliosis, is associated with various neurodegenerative diseases such as spinal cord injury and neuropathic pain (40). It has also been reported that activated JAK2-STAT3 signaling results in the increased expression of IL-6 and IL-10 and that IL-6 is considered an important STAT3 activator (43,44). Thus, it was reasonable to hypothesize that decreased GFAP expression, as well as astrocytic proliferation, in $Hexb^{-/-}$ $Tnf\alpha^{-/-}$ brains is due to the decreased phosphorylation of STAT3. Our data provide a direct clue that inhibition of the JAK-STAT3 signaling pathway may prevent reactive astrogliosis in Sandhoff. Although we found no difference in IL-6 or pJAK2 expression between $Hexb^{-/-}$ $Tnf\alpha^{+/+}$ and $Hexb^{-/-}$ $Tnf\alpha^{-/-}$ mice, other molecules, upstream to STAT3 and downstream of TNFα signaling—such as leukemia inhibitory factor and oncostatin M—could mediate this STAT3 activation (45,46). Recent work has demonstrated that TNFR1 associates with JAK2 constitutively to form a complex and TNF recruits additional molecules of JAK2 (47). Furthermore, the activation of STAT3 can be performed by the TNFR1/JAK2 complex (48). We also observe nuclear localization of STAT3 within astrocytes, which is consistent with activation of STAT3. These findings may explain the increased phosphorylation of STAT3 in Sandhoff brains compared with the reduced levels of pSTAT3 observed in $Hexb^{-/-}$ $Tnf\alpha^{-/-}$ mice.

Unlike the canonical NF-κB pathway, which relies on IκBα activation, the non-canonical pathway relies on inducible processing of p100 (49). We investigated the role of the non-canonical NF-κB pathway in SD mice in the presence or the absence of TNFα. Our results show the down-regulation of TRAF3, NIK and RelB in $Hexb^{-/-}$ $Tnf\alpha^{-/-}$ mice compared with SD mice. It has been reported that TRAF3 degradation is essential to trigger the TNFR2-receptor mediated activation of NIK and the nuclear translocation of p52/RelB heterodimers into the nucleus (50,51). Our results indicate that TNFα utilizes the NIK-mediated NF-κB pathway to elicit an immune response in SD but the stabilization of NIK appears independent of TRAF3 levels. Our results demonstrate that TNFα depletion in SD cerebellum down-modulates non-canonical NF-κB signaling. Whether there is an IKKα-dependent feedback that controls the magnitude and kinetics of the pathway is still an open question.

An intriguing finding was the extensive level of apoptosis occurring in the spinal cord of SD mice which coincided with increased activation of astrocytes. Alongside the reduction in astrogliosis seen in the spinal cord of $Hexb^{-/-}$ $Tnf\alpha^{-/-}$ mice relative to $Hexb^{-/-}$ $Tnf\alpha^{+/+}$ mice, there was a reduction in apoptotic cells. The results indicate that astrocytes residing in the spinal cord may play an important role in the apoptosis-mediated pathogenesis of SD. Our BMT experiments to identify sources of pathological TNFα have demonstrated that both CNS-derived and bone marrow-derived sources of TNFα have similar pathological effects in the progression of SD in our mouse model—though CNS-derived TNFα appears to be of larger influence—and therefore represent important potential targets for treatments in patients. Treatments with TNFα inhibitors should be designed to penetrate the blood-brain barrier for optimal effect. Previous studies involving BMT of wild-type bone marrow into $Hexb^{-/-}$ mice have shown improvements in lifespan and neuromotor function, and reduction in microgliosis, without changes in ganglioside accumulation (30,32,52). That we see an improvement when transplanting $Hexb^{-/-}$ $Tnf\alpha^{-/-}$ bone marrow—which can have no effect on ganglioside accumulations or on possible

alternate functions of hexosaminidase B—speaks to the importance of inflammation in the pathology of this disease and provides further evidence that TNFα is an important detrimental factor in SD.

Our study points to the cytokine, TNFα, as a potential therapeutic target to slow the rapid neurodegenerative process SD. Given that the multifaceted therapeutics to neurodegenerative diseases have gained a growing appreciation and provide a promising avenue to improve prognosis of neurodegeneration, our study also identifies the STAT3 pathway as a target to achieve a better outcome for the disease pathology.

MATERIAL AND METHODS

Mice

The SD model mice (*Hexb* $^{-/-}$) were a generous gift from Dr R. Gravel (University of Calgary, Canada). TNFα-deficient mice were purchased from the Jackson Laboratory (Bar Harbor, MA, USA) and were backcrossed 10 times onto a C57Bl/6 background in house. Since both transgenic strains are on a C57Bl6 genetic background, the *Hexb* $^{-/-}$ mice were crossed with *Tnfα* $^{-/-}$ mice to generate doubly heterozygous (*Hexb*$^{+/-}$*Tnfα*$^{+/-}$) mice. These doubly heterozygous mice were mated with *Tnfα* $^{-/-}$ mice to generate *Hexb*$^{+/-}$*Tnfα* $^{-/-}$ mice. Subsequently, *Hexb*$^{+/-}$ *Tnfα* $^{-/-}$ mice were mated with each other to generate doubly null (*Hexb* $^{-/-}$ *Tnfα* $^{-/-}$) mice. Genotypes were confirmed by PCR using tail DNA.

PCR genotyping

The genotype of the *Tnfα* locus was determined by PCR from tail DNA. A single set of primers was used, 5-GAAAAGCAAG CAGCCAACCAG-3 and 5-GTCCAACCCACGGCTTC-3, yielding a 646 bp product for the wild-type gene and a 1357 bp product for the knockout gene. Primers for detection of *Hexb* wild-type sequence were primer 5′-GGTTTCTACAAGAGA CATCATGGC-3′ and primer yielding 141 bp products for the wild-type gene and primer 5′-CAATCGGTGCTTACAGG TTTCATC-3′ and primer 5′-GATATTGCTGAAGAGCTTGG CGGC-3′ in neo to give 700 bp for the *Hexb* knockout gene.

Behavioral tests

An Animal Utilization Proposal (AUP) was established which is in accordance with the Ontario Animals for Research Act requirements and the standards of the Canadian Council on Animal Care (CCAC). The lifespan, body weight and neurological function of each group of mice were monitored by using modified Irwin (53) and McDaniel and Moser (54) observational test batteries (7). Motor function was evaluated by means of the rotorod, the wire hang, grip strength and righting reflex behavioral tests which were conducted weekly subsequent to weaning.

Rotorod

The rotorod test measured the latency to fall off a rotating rod and infrared photo cells captured exact fall time (7). The Accuscan EZ-Rod and companion computer software EZ rod version 1.20 were used. Predetermined program involved placing the mice on a prespinning rod, which gradually accelerated from 4 rpm to a maximum of 40 rpm over the 6 min test. Each mouse was given three trials, the best of which was included in the data set.

Wire hang

A wire mesh was utilized to conduct the wire hang test. Mice were inverted 20 cm above a padded surface and forced to use their four limbs to hold their body suspended upside down for a maximum of 60 s. The test was conducted in triplicate for each mouse and the highest time was recorded.

Grip strength

A digital force gauge meter (Chatillon Ametek Inc.) was used to measure the peak grip strength (7). This is the amount of force in kilograms exerted by the two front limbs of the mouse grasping a metal rod as the mouse is pulled away from the rod at a constant force.

Righting reflex

The righting reflex was conducted by placing a mouse on its back on a solid surface and recording the amount of time taken for the mouse flip back over to stand on all four limbs. Each mouse was given three reflex trials and the best of these was included in the data. Mice were left on their back to a maximum of 30 s which is indicative of Sandhoff endpoint in our AUP. Data were analyzed using the Student *t*-test to evaluate statistical significance. A P-value of < 0.05 was considered statistically significant.

Brain glycosphingolipid isolation and thin layer chromatography

The *Hexb*$^{+/+}$*Tnfα*$^{+/+}$, *Hexb* $^{-/-}$ *Tnfα*$^{+/+}$, *Hexb* $^{-/-}$ *Tnfα*$^{+/-}$ and *Hexb* $^{-/-}$ *Tnfα* $^{-/-}$ mice were sacrificed at 17 weeks of age. GA2 and GM2 extracts were determined in 430 mg of cerebral cortex and 70 mg of cerebellum, by thin layer chromatography (TLC). Gangliosides from mice brain tissue were extracted and analyzed as described previously (55). Briefly, brain samples were lysed and sonicated (Sonicator XL 2020, Heat systems Inc.) with chloroform/methanol/water (C:M:W, 10:10:1, v/v/v) for 1 h. The upper phase containing the gangliosides was separated from the lower phase after mixing and low-speed centrifugation. The upper phase was applied slowly to a Sephadex G-50 column at a steady rate. The collected eluate was adjusted to C:M:W (30:60:8) and applied slowly to a column of DEAE-Sepharose. The eluted gangliosides and neutral glycolipids were subjected to dry air to evaporate all liquids then adjusted to C:M:0.1M KCl (2:48:47). The mixture was applied to Sep-Pack C-18 reverse phase column and the collected eluate was evaporated and adjusted to C:M:W (10:10:1, 200 μl). Using a Hamilton syringe, glycolipids brain extracts were spotted onto TLC Silica gel 60 F254 plates (EMD Chemicals Inc., Silica Gel 60, 5715-7). TLC plates were air-dried, and developed, using C:M:$CaCl_2$ (60:35:8), for 2.5 h then sprayed with orcinol/sulphuric acid [0.2% (w/v), 1 M] and heat-treated (110°C for 20 min). The digital image of the TLC plate was captured using via flatbed scanner and Photoshop v6.0 (Adobe).

Quantitative RT–PCR

SYBR green assays were performed with SYBR green PCR master mix (Applied Biosystems, #4309155) using cDNA obtained from the cerebella of *Hexb*$^{+/+}$*Tnfα*$^{+/+}$, *Hexb* $^{-/-}$ *Tnfα*$^{+/+}$ and *Hexb* $^{-/-}$ *Tnfα* $^{-/-}$ mice.

Primers were as follows:

Gfap Forward 5′-CACGAACGAGTCCCTAGAGC
Reverse 5′-ATGGTGATGCGGTTTTCTTC
*Mac-1α*Forward 5′-GACTCAGTGAGCCCCATCAT
Reverse 5′-AGATCGTCTTGGCAGATGCT
Mcp-1 Forward 5′-ATGGTCAAGAGTTTGCAGCTT
Reverse 5′-CCTGAATTTTGGGAGAGTGTGAT
Gsr Forward 5′-GACACCTCTTCCTTCGACTACC
Reverse 5′-CACATCCAACATTCACGCAAG
Nxn Forward 5′-GTGGTAGCTTTGTACTTTGCGG
Reverse 5′-CCGTCTGCCGACACGAAAA
Prdx1 Forward 5′-AATGCAAAAATTGGGTATC
Reverse 5′-CGTGGGACACACAAAAGT
Ptgs1 Forward 5′-ATGAGTCGAAGGAGTCTCTCG
Reverse 5′-GCACGGATAGTAACAACAGGGA

Samples, master mix and primers were added to a MicroAmp Optical 96-well Reaction plate (Applied Biosystems, #4316813). The plate was spun down quickly to remove bubbles and placed in a 7900HT Sequence Detection System (Applied Biosystems). Thermocycling conditions were as follows: 50°C, 2 min, 95°C, 10 min, 40 cycles of 95°C, 15 s; 60°C, 1 min. SDSv2.3 (SABiosciences) was used to analyze all gene expression data.

Western blotting

Mice were anesthetized with ketamine/xylazine. Blood was obtained by cardiac puncture. Mice were perfused with phosphate-buffered saline (PBS) through the left ventricle of the heart. The cerebellum was harvested into lysis buffer containing protease inhibitors (Roche, #14791200) and sonicated at 20% pulse for 10 s. Laemmeli sample buffer (2×) was added to the lysate and boiled for 5 min before storage at −20°. Boiled samples were equally loaded into a 10% sodium dodecyl sulfate (SDS)-polyacrylimide (BioRad) gel and transferred at 120 V for 70 min onto a nitrocellulose membrane. Membranes were blocked using 5% non-fat milk (Carnation) in Tris-buffered saline containing 0.5% Tween-20 (TBST) before probing with antibody suspended in 5% milk in TBST and incubated overnight at 4°C. After washing in TBST five times, membranes were blotted with secondary horseradish peroxidase conjugated Immunoglobulin G conjugated antibodies in 5% milk in TBST (1:10000, Santa Cruz Biotechnology, goat anti-rabbit: #sc-2004, goat anti-mouse: #sc-2005, goat anti-rat: #sc-2006, donkey anti-goat: #sc-2020) for 1 h at room temperature, followed by five washes in TBST. Blotted membranes were incubated with Amersham ECL western blotting detection reagents (GE Healthcare, #RPN2106) and exposed on Amersham Hyperfilm ECL film (GE Healthcare, #28906839). Loading was normalized using an anti-glyceraldehyde-3-phosphate dehydrogenase (GAPDH) antibody (1:1000, R+D Systems, #AF5718). Protein levels were analyzed using the Bio Rad DC Protein Assay (#500-0116). Membranes were stripped of secondary antibodies between blotting using a stripping buffer at a pH 2.0 composed of 1.5% glycine, 0.12% SDS and 0.1% Tween-20. The following antibodies were used in this study: antimouse GFAP monoclonal antibody (1:5000, Sigma Aldrich, #G3893), anti-MAC-1α polyclonal antibody (1:300, Sigma Aldrich, #G9269), anti-IL-6 antibody (1:500, Santa Cruz Biotechnology, #sc-7920), anti-pSTAT-3 antibody (1:1000, Cell Signaling, #9145S), anti-STAT-3 antibody (1:1000, Cell Signaling, #4904S), anti-TRAF3 antibody (1:1000, Cell Signaling, #4729), anti-NIK antibody (1:1000, Cell Signaling, #4994P) and anti-RelB antibody (1:1000, Cell Signaling, #4922). For quantification of western blot analysis, X-ray films were scanned and saved as .JPEG files and analyzed using ImageJ (NIH). Image color was inverted and background was subtracted at 50 pixels. Using the free hand tool, bands were outlined, and the area, mean density and integrated density were calculated. The integrated densities of each band were divided by the corresponding value for GAPDH to represent normalized protein levels. Student's *t*-test was used to determine the significant difference of the means at $P < 0.05$.

Immunohistochemistry

Hexb$^{+/+}$*Tnfα*$^{+/+}$, *Hexb* $^{-/-}$ *Tnfα*$^{+/+}$ and *Hexb* $^{-/-}$ *Tnfα* $^{-/-}$ mice were harvested at 17 weeks of age, perfused with PBS, and fixed with 3.7% formaldehyde. The brain and spine were harvested and embedded in paraffin wax. Five-micrometer thick coronal brain sections and cross-sectional spine sections were cut from the blocks and mounted on slides. Samples underwent a xylene/ethanol rehydration series, quenching of endogenous peroxidise activity with 1%H_2O_2, blocked with 10% goat serum for 15 min and were immunolabeled for 1.5 h at 37°C with primary antibodies—mouse monoclonal anti-GFAP (1:150, Sigma, #G3893) for reactive astrocytes and rat monoclonal anti-MAC3 (1:300, BD Pharmingen, #553322) for reactive microglia/macrophages. Biotinylated secondary antibodies were applied, followed by anavidin/HRP-bound biotin solution for signal amplification (Santa Cruz, Mouse ABC Staining System #sc-2017, Rat ABC Staining System #sc-2019). Samples were stained with 3′,3′-diaminobenzadine in the presence of 0.01% H_2O_2, and counterstained with methylene blue. Microwave antigen retrieval in 12 mM citric acid buffer was performed on MAC3 slides prior to the application of the primary antibody. All washes were performed with Tris-buffered saline (0.1% Tween-20). Random field images were captured of the cerebral cortex and cerebellum at 400× magnification, via Zeiss Axiovert 200 microscope, equipped with a Zeiss AxioCamMRc Camera. Areas of images were calculated using AxioVision 4.7 software (Zeiss, Oberkochen, Germany). Positively stained cells were quantified from images. Images of spinal sections were captured, and areas measured with Axiovision 4.7, and positively stained cells were quantified under 400× magnification. All statistical analyses were performed using SPSS v16 (SPSS Inc., Chicago, IL, USA). One-way analysis of variance (ANOVA) performed on sets of data with three or more groups followed by Tukey's *post hoc* were used for all data with high normality and equal variance amongst groups. For groups of unequal variance, Dunnett's T3 test was used to determine the significant difference of the means at $P < 0.05$.

TUNEL analysis

Terminal deoxynucleotidyl transferase dUTP nick end labeling (TUNEL) was performed on the previously described formalin-

fixed, paraffin-embedded CNS samples, according to the manufacturer's instructions using the ApopTag Peroxidase *In Situ* Apoptosis Detection Kit (Millipore, #S7100). Sections were subjected to a xylene/ethanol rehydration series, followed by treatment with proteinase K for 10 min. After blocking for endogenous peroxides activity with 3% hydrogen peroxide, the samples were incubated with terminal deoxynucleotidyl transferase enzyme at 37°C for 1 h. Sections were then treated with anti-digoxigenin-peroxidase and reacted with 3′,3′-diaminobenzadine in the presence of 0.01% H_2O_2. Nuclei were then counterstained with methyl green. All washes were performed with PBS. Areas of the cerebral cortex, and entire cerebella were measured using AxioVision 4.7 and positive cells were quantified at 400× magnification. Images of spinal sections were captured, and areas measured with Axiovision 4.7 (Zeiss), and positively stained cells were quantified under 400× magnification. The number of all astrocytes in a specific spinal tissue type were counted and divided by the total area of all sections of that type, for each mouse. All statistical analyses were performed using SPSS v16 (SPSS Inc. Chicago, IL, USA). One-way ANOVA (performed on sets of data with three or more groups) followed by Tukey's *post hoc* were used for all data with high normality and equal variance amongst groups. For groups of unequal variance, Dunnett's T3 test was used to determine the significant difference of the means at $P < 0.05$.

Immunofluorescence

Brains from $Hexb^{+/+}Tnf\alpha^{+/+}$, $Hexb^{-/-}Tnf\alpha^{+/+}$ and $Hexb^{-/-}Tnf\alpha^{-/-}$ mice were harvested at 17 weeks of age and embedded in paraffin as described above. Samples underwent a xylene/ethanol rehydration series, and microwave antigen retrieval was performed in 12 mM citric acid buffer. Tissues were blocked with 10% goat serum for 15 min and double-labeled with mouse anti-GFAP (1:150, Sigma, #G3893) and rabbit anti-STAT3 (1:150, Cell Signaling, #4904S) antibodies. Slides were then double-labeled with goat anti-mouse Alexa Fluor 594 (1:400, Invitrogen, #A-11005) and Goat anti-rabbit Alexa Fluor 488 (1:400, Invitrogen, #A-11008). Slides were mounted with ProLong Gold antifade reagent (Invitrogen, #P36930). Confocal microscopy optical slices were performed with Argon 488, and HeNe 594 excitation lasers on a Leica TCS SP5 confocal microscope, using Leica Application Suite Advanced Fluorescence software.

Bone marrow transplantation

BMT was performed as described previously (32). Transplantations included $Hexb^{-/-}Tnf\alpha^{+/+}$ bone marrow donors into $Hexb^{-/-}Tnf\alpha^{-/-}$ recipients, $Hexb^{-/-}Tnf\alpha^{+/+}$ bone marrow donors into $Hexb^{-/-}Tnf\alpha^{+/+}$ recipients, $Hexb^{-/-}Tnf\alpha^{-/-}$ bone marrow donors into $Hexb^{-/-}Tnf\alpha^{+/+}$ recipients and $Hexb^{-/-}Tnf\alpha^{-/-}$ bone marrow into $Hexb^{-/-}Tnf\alpha^{-/-}$ recipients ($n = 4–5$). All recipient mice were females at ~2 months of age. Briefly, donor mice were euthanized by cervical dislocation. Humiri, tibia and femurs bones were dissected from each donor mouse under sterile conditions, and bone marrow was flushed with Iscove's medium (Lonza, 12-722F), supplemented with L-glutamine (Gibco, 25030). Cells were passed through a cell strainer (0.45 μm) and red blood cells were lysed with cold ammonium chloride potassium (ACK) lysis buffer. Cells were stored on ice until injection. Bone marrow recipient mice were given sterile chow and Septra water for 1 week prior to irradiation. Irradiation of bone marrow recipient mice was broken into two treatments, with one dose of 7 Gy, followed by a second dose of 4 Gy within 4 h. Under anesthesia, mice were injected intravenously with ~$6–10 \times 10^8$ cells. The recipient mice recovered in autoclaved cages with sterile gel and Septra water.

Conflict of Interest statement. None declared.

FUNDING

H.A. is sponsored by a graduate scholarship from the Egyptian government. E.J.W. is the recipient of a Canadian Institutes of Health Research (CIHR) post-doctoral fellowship. This work was supported by a grant from the Canadian Institute of Health Research (CIHR) to S.A.I.

REFERENCES

1. Hodges, B.L. and Cheng, S.H. (2006) Cell and gene-based therapies for the lysosomal storage diseases. *Curr. Gene Ther.*, **6**, 227–241.
2. Kolter, T. and Sandhoff, K. (2006) Sphingolipid metabolism diseases. *Biochim. Biophys. Acta*, **1758**, 2057–2079.
3. Meier, E.M., Schwarzmann, G., Furst, W. and Sandhoff, K. (1991) The human GM2 activator protein. A substrate specific cofactor of beta-hexosaminidase a. *J. Biol. Chem.*, **266**, 1879–1887.
4. Conzelmann, E., Kytzia, H.J., Navon, R. and Sandhoff, K. (1983) Ganglioside GM2 N-acetyl-beta-D-galactosaminidase activity in cultured fibroblasts of late-infantile and adult GM2 gangliosidosis patients and of healthy probands with low hexosaminidase level. *Am. J. Hum. Genet.*, **35**, 900–913.
5. Sango, K., Yamanaka, S., Hoffmann, A., Okuda, Y., Grinberg, A., Westphal, H., Mcdonald, M.P., Crawley, J.N., Sandhoff, K., Suzuki, K. and Proia, R.L. (1995) Mouse models of Tay-Sachs and Sandhoff diseases differ in neurologic phenotype and ganglioside metabolism. *Nat. Genet.*, **11**, 170–176.
6. Yamanaka, S., Johnson, M.D., Grinberg, A., Westphal, H., Crawley, J.N., Taniike, M., Suzuki, K. and Proia, R.L. (1994) Targeted disruption of the hexa gene results in mice with biochemical and pathologic features of Tay-Sachs disease. *Proc. Natl Acad. Sci. USA*, **91**, 9975–9979.
7. Miklyaeva, E.I., Dong, W., Bureau, A., Fattahie, R., Xu, Y., Su, M., Fick, G.H., Huang, J.Q., Igdoura, S., Hanai, N. and Gravel, R.A. (2004) Late onset Tay-Sachs disease in mice with targeted disruption of the hexa gene: behavioral changes and pathology of the central nervous system. *Brain Res.*, **1001**, 37–50.
8. Wu, Y.P. and Proia, R.L. (2004) Deletion of macrophage-inflammatory protein 1 alpha retards neurodegeneration in Sandhoff disease mice. *Proc. Natl Acad. Sci. USA*, **101**, 8425–8430.
9. Kyrkanides, S., Miller, A.W., Miller, J.N., Tallents, R.H., Brouxhon, S.M., Olschowka, M.E., O'banion, M.K. and Olschowka, J.A. (2008) Peripheral blood mononuclear cell infiltration and neuroinflammation in the hexb-/- mouse model of neurodegeneration. *J. Neuroimmunol.*, **203**, 50–57.
10. Niederkorn, J.Y. (2006) See no evil, hear no evil, do no evil: the lessons of immune privilege. *Nat. Immunol.*, **7**, 354–359.
11. Probert, L., Akassoglou, K., Kassiotis, G., Pasparakis, M., Alexopoulou, L. and Kollias, G. (1997) TNF-Alpha transgenic and knockout models of CNS inflammation and degeneration. *J. Neuroimmunol.*, **72**, 137–141.
12. Mrak, R.E. and Griffin, W.S. (2005) Glia and their cytokines in progression of neurodegeneration. *Neurobiol. Aging*, **26**, 349–354.
13. Mcgeer, P.L. and Mcgeer, E.G. (2001) Inflammation, autotoxicity and Alzheimer's disease. *Neurobiol. Aging*, **22**, 799–809.
14. Mcgeer, P.L. and Mcgeer, E.G. (2004) Inflammation and neurodegeneration in Parkinson's disease. *Parkinsonism. Relat. Disord.*, **10**(Suppl. 1), S3–S7.
15. Shie, F.S. and Woltjer, R.L. (2007) Manipulation of microglial activation as a therapeutic strategy in Alzheimer's disease. *Curr. Med. Chem.*, **14**, 2865–2871.

16. Huang, J.Q., Trasler, J.M., Igdoura, S., Michaud, J., Hanal, N. and Gravel, R.A. (1997) Apoptotic cell death in mouse models of GM2 gangliosidosis and observations on human Tay-Sachs and Sandhoff diseases. *Hum. Mol. Genet.*, **6**, 1879–1885.
17. Wu, Y.P., Mizugishi, K., Bektas, M., Sandhoff, R. and Proia, R.L. (2008) Sphingosine kinase 1/S1P receptor signaling axis controls glial proliferation in mice with Sandhoff disease. *Hum. Mol. Genet.*, **17**, 2257–2264.
18. Myerowitz, R., Lawson, D., Mizukami, H., Mi, Y., Tifft, C.J. and Proia, R.L. (2002) Molecular pathophysiology in Tay-Sachs and Sandhoff diseases as revealed by gene expression profiling. *Hum. Mol. Genet.*, **11**, 1343–1350.
19. Jeyakumar, M., Thomas, R., Elliot-Smith, E., Smith, D.A., Van Der Spoel, A.C., D'azzo, A., Perry, V.H., Butters, T.D., Dwek, R.A. and Platt, F.M. (2003) Central nervous system inflammation is a hallmark of pathogenesis in mouse models of GM1 and GM2 gangliosidosis. *Brain*, **126**, 974–987.
20. Shishodia, S. and Aggarwal, B.B. (2002) Nuclear Factor-kappaB activation: a question of life or death. *J. Biochem. Mol. Biol.*, **35**, 28–40.
21. Ting, A.Y. and Endy, D. (2002) Signal transduction. Decoding NF-kappaB signaling. *Science*, **298**, 1189–1190.
22. Lee, J.P., Jeyakumar, M., Gonzalez, R., Takahashi, H., Lee, P.J., Baek, R.C., Clark, D., Rose, H., Fu, G., Clarke, J. *et al.* (2007) Stem cells act through multiple mechanisms to benefit mice with neurodegenerative metabolic disease. *Nat. Med.*, **13**, 439–447.
23. Sofroniew, M.V. and Vinters, H.V. (2010) Astrocytes: biology and pathology. *Acta Neuropathol.*, **119**, 7–35.
24. Kettenmann, H. (2007) Neuroscience: the Brain's garbage men. *Nature*, **446**, 987–989.
25. Hirota, K., Matsui, M., Murata, M., Takashima, Y., Cheng, F.S., Itoh, T., Fukuda, K. and Yodoi, J. (2000) Nucleoredoxin, glutaredoxin, and thioredoxin differentially regulate NF-kappaB, AP-1, and CREB activation in HEK293 cells. *Biochem. Biophys. Res. Commun.*, **274**, 177–182.
26. Sun, S.C. (2011) Non-canonical NF-kappaB signaling pathway. *Cell Res.*, **21**, 71–85.
27. Wajant, H., Pfizenmaier, K. and Scheurich, P. (2003) Tumor necrosis factor signaling. *Cell Death. Differ.*, **10**, 45–65.
28. Fontaine, V., Mohand-Said, S., Hanoteau, N., Fuchs, C., Pfizenmaier, K. and Eisel, U. (2002) Neurodegenerative and neuroprotective effects of tumor necrosis factor (TNF) in retinal ischemia: opposite roles of tnf receptor 1 and tnf receptor 2. *J. Neurosci.*, **22**, Rc216.
29. Murakami, Y., Saito, K., Hara, A., Zhu, Y., Sudo, K., Niwa, M., Fujii, H., Wada, H., Ishiguro, H., Mori, H. and Seishima, M. (2005) Increases in tumor necrosis factor-alpha following transient global cerebral ischemia do not contribute to neuron death in mouse hippocampus. *J. Neurochem.*, **93**, 1616–1622.
30. Wada, R., Tifft, C.J. and Proia, R.L. (2000) Microglial activation precedes acute neurodegeneration in Sandhoff disease and is suppressed by bone marrow transplantation. *Proc. Natl Acad. Sci. USA*, **97**, 10954–10959.
31. Akiyama, H., Barger, S., Barnum, S., Bradt, B., Bauer, J., Cole, G.M., Cooper, N.R., Eikelenboom, P., Emmerling, M., Fiebich, B.L. *et al.* (2000) Inflammation and Alzheimer's disease. *Neurobiol. Aging*, **21**, 383–421.
32. Norflus, F., Tifft, C.J., Mcdonald, M.P., Goldstein, G., Crawley, J.N., Hoffmann, A., Sandhoff, K., Suzuki, K. and Proia, R.L. (1998) Bone marrow transplantation prolongs life span and ameliorates neurologic manifestations in Sandhoff disease mice. *J. Clin. Invest.*, **101**, 1881–1888.
33. Teng, Y.D., Lavik, E.B., Qu, X., Park, K.I., Ourednik, J., Zurakowski, D., Langer, R. and Snyder, E.Y. (2002) Functional recovery following traumatic spinal cord injury mediated by a unique polymer scaffold seeded with neural stem cells. *Proc. Natl Acad. Sci. USA*, **99**, 3024–3029.
34. Jeyakumar, M., Smith, D.A., Williams, I.M., Borja, M.C., Neville, D.C., Butters, T.D., Dwek, R.A. and Platt, F.M. (2004) NSAIDS increase survival in the Sandhoff disease mouse: synergy with N-butyldeoxynojirimycin. *Ann. Neurol.*, **56**, 642–649.
35. Raval, G., Biswas, S., Rayman, P., Biswas, K., Sa, G., Ghosh, S., Thornton, M., Hilston, C., Das, T., Bukowski, R. *et al.* (2007) TNF-Alpha induction of GM2 expression on renal cell carcinomas promotes t cell dysfunction. *J. Immunol.*, **178**, 6642–6652.
36. Igdoura, S.A., Mertineit, C., Trasler, J.M. and Gravel, R.A. (1999) Sialidase-mediated depletion of GM2 ganglioside in Tay-Sachs neuroglia Cells. *Hum. Mol. Genet.*, **8**, 1111–1116.
37. Jeyakumar, M., Dwek, R.A., Butters, T.D. and Platt, F.M. (2005) Storage solutions: treating lysosomal disorders of the brain. *Nat. Rev. Neurosci.*, **6**, 713–725.
38. Culmsee, C. and Plesnila, N. (2006) Targeting bid to prevent programmed cell death in neurons. *Biochem. Soc. Trans.*, **34**, 1334–1340.
39. Zhang, L., Zhao, W., Li, B., Alkon, D.L., Barker, J.L., Chang, Y.H., Wu, M. and Rubinow, D.R. (2000) TNF-Alpha induced over-expression of GFAP is associated with MAPKs. *Neuroreport*, **11**, 409–412.
40. Tsuda, M., Kohro, Y., Yano, T., Tsujikawa, T., Kitano, J., Tozaki-Saitoh, H., Koyanagi, S., Ohdo, S., Ji, R.R., Salter, M.W. and Inoue, K. (2011) JAK-STAT3 pathway regulates spinal astrocyte proliferation and neuropathic pain maintenance in rats. *Brain*, **134**, 1127–1139.
41. Sakuraba, H., Sawada, M., Matsuzawa, F., Aikawa, S., Chiba, Y., Jigami, Y. and Itoh, K. (2006) Molecular pathologies of an enzyme replacement therapies for lysosomal diseases. *CNS Neurol. Disord. Drug Targets*, **5**, 401–413.
42. Futerman, A.H. and Van, M.G. (2004) The cell biology of lysosomal storage disorders. *Nat. Rev. Mol. Cell Biol.*, **5**, 554–565.
43. Nilsson, C.L., Dillon, R., Devakumar, A., Shi, S.D., Greig, M., Rogers, J.C., Krastins, B., Rosenblatt, M., Kilmer, G., Major, M. *et al.* (2010) Quantitative phosphoproteomic analysis of the STAT3/IL-6/HIF1alpha signaling network: an initial study in GSC11 glioblastoma stem cells. *J. Proteome Res.*, **9**, 430–443.
44. Walkley, S.U. (2009) Pathogenic cascades in lysosomal disease-why so complex? *J. Inherit. Metab. Dis.*, **32**, 181–189.
45. Suzuki, S., Yamashita, T., Tanaka, K., Hattori, H., Sawamoto, K., Okano, H. and Suzuki, N. (2005) Activation of cytokine signaling through leukemia inhibitory factor receptor (LIFR)/gp130 attenuates ischemic brain injury in rats. *J. Cereb. Blood Flow Metab.*, **25**, 685–693.
46. Park, K.W., Nozell, S.E. and Benveniste, E.N. (2012) Protective role of STAT3 in nmda and glutamate-induced neuronal death: negative regulatory effect of SOCS3. *PLoS One*, **7**, E50874.
47. Guo, D., Dunbar, J.D., Yang, C.H., Pfeffer, L.M. and Donner, D.B. (1998) Induction of jak/stat signaling by activation of the type 1 TNF receptor. *J. Immunol.*, **160**, 2742–2750.
48. Pincheira, R., Castro, A.F., Ozes, O.N., Idumalla, P.S. and Donner, D.B. (2008) Type 1 TNF receptor forms a complex with and uses JAK2 and C-SRC to selectively engage signaling pathways that regulate transcription factor activity. *J. Immunol.*, **181**, 1288–1298.
49. Hebert, S.S. and De, S.B. (2009) Alterations of the microrna network cause neurodegenerative disease. *Trends Neurosci.*, **32**, 199–206.
50. Vallabhapurapu, S., Matsuzawa, A., Zhang, W., Tseng, P.H., Keats, J.J., Wang, H., Vignali, D.A., Bergsagel, P.L. and Karin, M. (2008) Nonredundant and complementary functions of TRAF2 and TRAF3 in a ubiquitination cascade that activates NIK-dependent alternative NF-kappaB signaling. *Nat. Immunol.*, **9**, 1364–1370.
51. Rauert, H., Wicovsky, A., Muller, N., Siegmund, D., Spindler, V., Waschke, J., Kneitz, C. and Wajant, H. (2010) Membrane tumor necrosis factor (tnf) induces p100 processing via TNF receptor-2 (TNFR2). *J. Biol. Chem.*, **285**, 7394–7404.
52. Jeyakumar, M., Norflus, F., Tifft, C.J., Cortina-Borja, M., Butters, T.D., Proia, R.L., Perry, V.H., Dwek, R.A. and Platt, F.M. (2001) Enhanced survival in Sandhoff disease mice receiving a combination of substrate deprivation therapy and bone marrow transplantation. *Blood*, **97**, 327–329.
53. Irwin, S. (1968) Comprehensive observational assessment: ia. A systematic, quantitative procedure for assessing the behavioral and physiologic state of the mouse. *Psychopharmacologia*, **13**, 222–257.
54. Mcdaniel, K.L. and Moser, V.C. (1993) Utility of a neurobehavioral screening battery for differentiating the effects of two pyrethroids, permethrin and cypermethrin. *Neurotoxicol. Teratol.*, **15**, 71–83.
55. Irwin, C.C. and Irwin, L.N. (1979) A simple rapid method for ganglioside isolation from small amounts of tissue. *Anal. Biochem.*, **94**, 335–339.

CHAPTER 3: Bi-phasic gliosis drives neuropathology in Sandhoff disease

This paper was accepted for publication in *The Journal of Neuroimmunology* on August 8th, 2016, and is cited as follows:

Hooper, Alexander W.M., Igdoura, Suleiman, Bi-phasic gliosis drives neuropathology in a Sandhoff disease mouse model. *Journal of Neuroimmunology* (2016), doi: 10.1016/j.jneuroim.2016.08.008

Corresponding Author:
Dr. Suleiman Igdoura
McMaster University, 1280 Main St. W.
Hamilton, Ontario, Canada
L8S 4K1
Email: igdoura@Mcmaster.ca
(905) 525-9140 ex. 27729

3.1 Preface

All of the following work was performed by Alexander Hooper.

3.2 Abstract

Microgliosis and astrogliosis are known to be exacerbating factors in the progression of the lysosomal storage disorder Sandhoff disease. We have also found evidence for excitotoxicity via glutamate receptors in Sandhoff disease. To view the interaction of these cascades, we measured cerebellar expression of markers for gliosis, apoptosis, and excitatory synapses over the disease course in a Sandhoff disease mouse model. We observe a 2-stage model, with initial activation of microgliosis as early as 60 days of age, followed by a later onset of astrogliosis, caspase-mediated apoptosis, and reduction in GluR1 at approximately 100 days of age.

3.3 Introduction

Sandhoff disease (SD) is caused by a mutation in the *Hexb* gene, the product of which is a subunit of two lysosomal enzymes- β-hexosaminidase A and β-hexosaminidase B- which leads to accumulations of the gangliosides GM2 and GA2 in neuronal tissues (Itoh et al., 1984; Sandhoff et al., 1971). *Hexb*$^{-/-}$ mice are well studied and are representative of Sandhoff disease and the closely related Tay-Sachs disease (TSD), with mice displaying motorneuronal and behavioural deficits, reaching endpoint at approximately 17-19 weeks (Phaneuf et al., 1996).

The disease is largely viewed as perpetuated through the activation of microglia/central nervous system (CNS) infiltrating peripheral blood mononuclear cells (PBMC) and astrocytes, with many genes related to gliosis upregulated in the disease in both humans and mouse models (Jeyakumar et al., 2003; Myerowitz et al., 2002;

Sargeant et al., 2012). It has been observed that microgliosis occurs before neuronal apoptosis in the brainstem and spinal cord of SD mice, and thus it is suggested that the chronic accumulation of microglia and macrophages- themselves unable to process gangliosides- leads to increased neurotoxicity (Wada et al., 2000). Microglial/macrophage contributions to the disease have been shown to be lessened in double knockouts (DKO) involving inflammatory genes including *Hexb*$^{-/-}$*Ccr2*$^{-/-}$, *Hexb*$^{-/-}$ *Mip1α*$^{-/-}$ and *Hexb*$^{-/-}$*Tnfα*$^{-/-}$, resulting in increased lifespans of SD mouse models (Abo-Ouf et al., 2013; Kyrkanides et al., 2008; Wu and Proia, 2004). Related proteins, macrophage inflammatory protein-1 alpha and beta (MIP-1α, MIP-1β), and tumour necrosis factor receptor 2 (TNFR2) have been identified as strong biomarkers for gangliosidoses in human patients (Utz et al., 2015). Interestingly, ablating *Ccr2*-provoked infiltration of PBMCs (subsequently lowering the number of TNFα expressing cells in the brain) appears to have no effect on apoptotic pathways or astrocyte activation (Kyrkanides et al., 2008). This is surprising since microglial activation can lead to the release of various cytokines, including interleukin-6 (IL6) and tumour-necrosis factor-alpha (TNFα), which may induce an apoptotic pathway in neurons, and since we ourselves have observed a reduction in astrocytes and apoptosis in the cerebellum of *Hexb*$^{-/-}$*Tnfα*$^{-/-}$ mice relative to Hexb$^{-/-}$ mice (Abo-Ouf et al., 2013; Shishodia and Aggarwal, 2002). It is possible that the remaining TNFα in *Hexb*$^{-/-}$*Ccr2*$^{-/-}$ mice is sufficient for the astroglial and apoptotic pathways, or the effect is tissue specific. Astrogliosis appears to be driven by one or more pathways involving Sphk1/S1P receptors, and ERK (but not AKT), and ganglioside

buildup in SD astrocytes is sufficient to activate proliferation (Kawashima et al., 2009; Kyrkanides et al., 2008; Wu et al., 2008). While the importance of microgliosis and astrogliosis in SD are clear, their relationship to each other during their progression in the development of the disease is not, warranting further study.

Because of the importance of gliosis in SD, neuronal aspects of disease progression have been largely ignored in favor of inflammatory mechanisms. However, in Alzheimer's disease, AMPAR dysregulation may lead to neuronal death through excitotoxicity, and Sandhoff patients have been shown to share common traits with Alzheimer's disease, including intraneuronal accumulations of cellular products such as amyloid-beta (Abad et al., 2006; Hynd et al., 2004; Keilani et al., 2012). TNFα has been shown to increase insertion of both calcium-permeable GluR1 in hippocampal pyramidal neurons, and calcium-impermeable GluR2 in motor neurons (Ogoshi et al., 2005; Rainey-Smith et al., 2010). Increased neuronal activity through calcium-permeable AMPARs can cause excitotoxicity, while decreased neuronal activity can lead to caspase-mediated apoptosis in cerebellar granule neurons (Clayton et al., 2012; Van Damme et al., 2007). Due to the involvement of TNFα in SD, and its various roles in AMPAR distribution, AMPARs such as GluR1 make interesting targets for study.

Immunohistochemical time course experiments have been performed in the brainstem and spinal cord of SD mice for glial and apoptotic markers, but did not include measurement of molecular expression levels, and this study seeks to expand on that work (Wada et al., 2000). To identify key developmental time points for various aspects

of SD- including gliosis, neurological markers, and neuronal death- we have analysed expression of disease markers over the progression of the illness in mouse models. We demonstrate a two-stage model of Sandhoff disease, with an early onset of microgliosis followed by a later increase in astrogliosis and apoptosis, and a reduction in GluR1.

3.4 Materials and Methods

3.4.1 Mice

Hexb$^{-/-}$ mice were generated as previously described, on a C57BL/6 background. Control wild-type (WT) mice are C57BL/6 (Phaneuf et al., 1996).

3.4.2 Genotyping

Genotyping of mice was performed via PCR on tail samples, using the following primers at previously described: For *Hexb*- Hexb-R: CAATCGGTGCTTACAGGTTTCATC, HexbWT-F: GGTTTCTACAAGAGACATCATGGC, HexbKO-F: GATATTGCTGAAGAGCTTGGCGGC.

3.4.3 Behaviour testing

Hexb$^{+/+}$ and *Hexb*$^{-/-}$ female mice were tested at 8, 11, 14 and 17 weeks of age, to observe changes in behaviour during the expected major period of decline in the health of *Hexb*$^{-/-}$. Only female mice were used in order to control for effects that natural differences in body mass between sexes would have on physical performance tasks. Measurements were taken of wire hang, rotarod, righting reflex, and body mass. Wire Hang: Mice were placed on top of a wire mesh, which was then inverted, 30 cm above a padded surface. Hang time was measured from the point of inversion, until time to fall-

to a maximum of 5 min. The best time of 3 consecutive trials was used. Rotarod: Mice were placed on a rotating rod (Accuscan EzRod with EzRod v.120 software), and time to fall was measured via photo-sensors. Rotarod rotations were increased from 0 rpm to a maximum of 40 rpm over 360 sec. Mice were placed on the rod at 4 rpm. The best time of 3 consecutive trials was used. Righting Reflex: Mice were positioned on their backs (with a slight tilt to the left and then repeated to the right) on a solid surface, and time for mouse to right itself onto its feet was measured. The average of measurements for the left side and right side righting reflex was used a measurement of cerebellar, pons, and mesencephalon function.

3.4.4 Western blot

The cerebella of female WT and *Hexb*$^{-/-}$ mice at 60, 80, 100, and 120 days were lysed via sonication in proteinase inhibitor-containing RIPA. Laemmli sample buffer (6X) was added to the lysates and the samples were heated at 95°C for 5 min. Samples were resolved on a 10% SDS-PAGE gel, and blotted on nitrocellulose membrane. Membranes were blocked with 5% cow milk in PBS, and stained with the antibodies for the following proteins: MAC3 (BD Pharmingen, 553322), GFAP (Sigma-Adlrich, G3893), GluR1 (Cell Signaling, 8850), Cleaved caspase-9 (Cell Signaling, 9501), PSD-95 (Cell Signaling, 3409S), synaptophysin (Cell Signaling, 5461), neurofilament-L (Cell Signaling, 2837), and GAPDH (R+D Systems, AF5718). Detection was performed via enhanced chemilumescence using Amersham ECL Western Blotting Detection Reagents (GE Healthcare, Cat. No RPN2106).

3.4.5 Immunohistochemistry

Wild-type *and Hexb*$^{-/-}$ mice were processed as previously described (Abo-Ouf et al., 2013). Briefly: mice were harvested at 60, 80, 100, and 120 days, perfused with PBS, and fixed with 3.7% formaldehyde, and embedded in paraffin wax. Five-micrometre thick coronal cerebellar sections were sliced, and mounted on glass slides. The samples were then subjected to a xylene/ethanol/water rehydration series. Endogenous peroxidase was quenched with 1% H_2O_2. Samples to be stained for MAC3 underwent microwave antigen retrieval in 12 mM citric acid buffer. Samples were blocked with 10% goat serum, and immunolabeled with monoclonal antibodies against GFAP (Sigma-Adlrich, G3893), and MAC3 (BD Pharmingen, 553322). Tissues were then incubated with biotinylated secondary antibodies, followed by an avidin/HRP-bound biotin solution (Santa Cruz, Mouse ABC Staining System #sc-2017, Rat ABC Staining System #sc-2019). Samples were then stained with 3,3'- diaminobenzadine in the presence of 0.01% H_2O_2, and counterstained with methylene blue. For each slide, 20 random field images of the cerebellum were captured at 400X magnification, centred on the Perkinje layer. The area of the images was calculated using AxioVision 4.9.1 software (Zeiss, Oberkochen, Germany). For each sample, positively stained cells microglia/macrophages and astrocytes were quantified as (the total count per 20 random fields)/(total area of the 20 fields).

3.4.6 Data Analysis

All statistical analyses were performed using SPSS v16 (SPSS Inc. Chicago, IL). T-tests were used to compare means between data containing 2 groups. One-way ANOVA

(performed on a larger set of data with 3 groups) followed by Tukey's post hoc were used for all data with high normality and equal variance amongst groups. For groups of unequal variance, Dunnett's T3 test was used to determine significant difference of the means at $P<0.05$. Graphs were generated using GraphPad Prism 5 v5.00 (La Jolla, CA, USA).

3.5 Results

3.5.1 Behaviour

As a disease that affects neuromuscular function, Sandhoff disease progression can be measured in mice as a function of the ability to perform several well established behavioural tests (Wu et al., 2008; Wu and Proia, 2004). We sought to observe the stages of critical decline in our *Hexb*$^{-/-}$ mice, generally observed between 11-17 weeks of age (Abo-Ouf et al., 2013).

Significant reductions in peripheral strength and coordination of *Hexb*$^{-/-}$ mice occur between 11 and 14 weeks, as demonstrated by decreases in performance in wire hang and rotarod tests (Fig. 3.1A,B). Righting reflex, on the other hand, declines between 14 and 17 weeks (Fig. 3.1C). The righting reflex requires less peripheral strength and coordination than the wire hang and rotarod tests, and therefore may be less sensitive at earlier stages of the disease, but therefore indicates a period of extreme disease severity (prolonged righting reflex is used as an endpoint for *Hexb*$^{-/-}$ mice). No significant differences were found with respect to body mass between genotypes (Fig. 3.1D). From these data, it appears that there are critical cellular events occurring in

Hexb$^{-/-}$ mice in the time between 11 and 14 weeks of age, which lead to the final stages of the disease. Treatment of these events just prior to their initiation could be an efficient method to delay the ultimate decline of Sandhoff disease sufferers. In order to determine which molecular pathways are activated or altered during this period, we performed Western blots and immunohistochemistry for various glial, neuronal, and apoptotic markers in the cerebellum across these time points.

Figure 3.1. Decline in Sandhoff disease mouse behavioural performance occurs during specific time point.

Hexb$^{-/-}$ mouse deterioration in wire hang (**A**) and rotarod (**B**) performances occur during the same 11-14 week period, and closely precede the loss of the righting reflex (indicating endpoint)(**C**). Body mass is not significantly affected during this time period(**D**). Bars = mean ± SE. T-tests, n = 3 for each group, *P < 0.05.

Figure 3.1

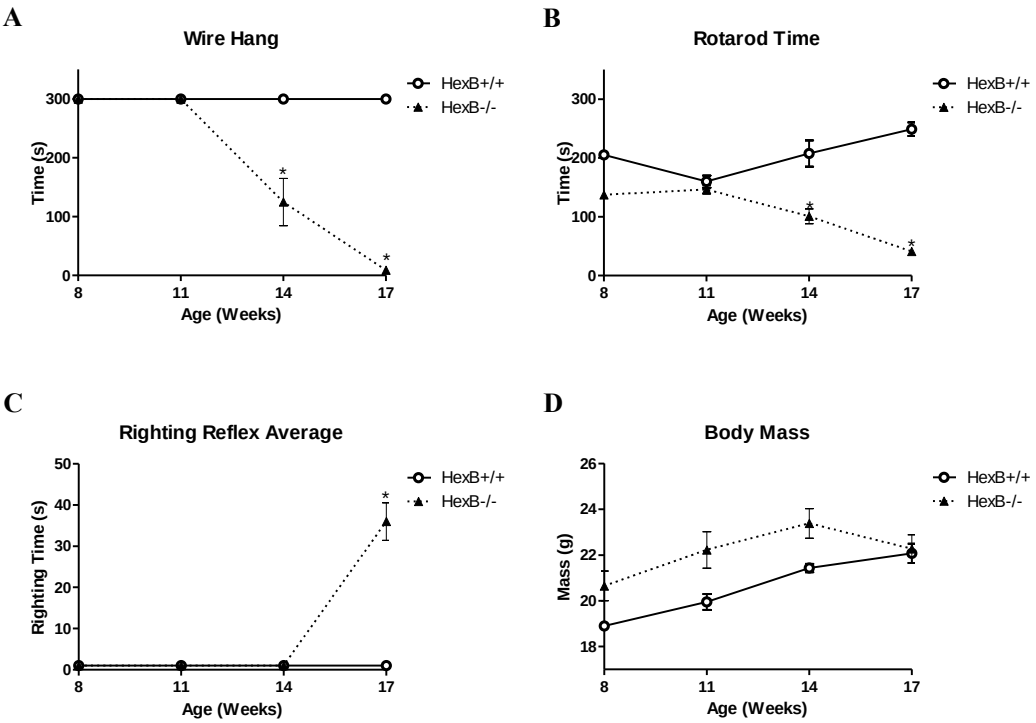
A
Wire Hang
Time (s)
Age (Weeks)
HexB+/+
HexB-/-
B
Rotarod Time
Time (s)
Age (Weeks)
HexB+/+
HexB-/-
C
Righting Reflex Average
Righting Time (s)
Age (Weeks)
HexB+/+
HexB-/-
D
Body Mass
Mass (g)
Age (Weeks)
HexB+/+
HexB-/-

3.5.2 Gliosis/Inflammation

Studies have previously measured the progression of microglial activation in the brains stem and spinal cord of SD mouse models, showing an increase in activation from 1-4 months (Wada et al., 2000). Since the cerebellum is known to be a majorly affected site in the disease, is brain structure involved in the aforementioned affected behaviours, and the precise relationship between microglial activation and astroglial/astrocyte activation in the SD cerebellum is not known, we sought to observe these processes at a higher temporal resolution than previously measured. In order to assess changes in the levels of activated glia over the course of Sandhoff disease, we performed western blots to determine the protein levels of MAC3 (a marker for activated microglia/macrophages) and GFAP (a marker for activated astrocytes) on the cerebella of WT and SD mice at 60, 80, 100, and 120 days of age. The cerebellum was chosen since we have previously found significant increases in MAC3 and GFAP positive cells in the cerebella of 120 SD mice, relative to WT (Abo-Ouf et al., 2013). MAC3 levels do not coincide with GFAP changes, and are significantly higher in SD relative to WT as early as 80 days with a trend to this effect seen at 60 days (Fig. 3.2A).

Figure 3.2. Developmental progression of microgliosis in Sandhoff disease mouse cerebella.

Cerebella from female WT and Sandhoff Disease mice at indicated age-points were blotted for the microglial marker MAC3. MAC3 is significantly higher in SD mice relative to WT mice as early as 80 days, with a trend towards this at 60 days (**A**). Bars = mean ± SE. T-tests, n = 3 for each group, *P < 0.05. Cerebellar sections from C57BL/6 and *Hexb*$^{-/-}$ mice at 60, 80, 100, and 120 days of age were stained for MAC3 (**B**). The total number of MAC3 positively stained cells, from 20 random field images per section, centred on the Perkinje layer, were quantified and normalized to area (**C**). n = 3 for each genotype in each age group. Microgliosis is significantly increased in *Hexb*$^{-/-}$ mice as early as 60 days. *P < 0.05. Scale bar = 50μm. Arrows indicate examples of positively stained microglia.

Figure 3.2

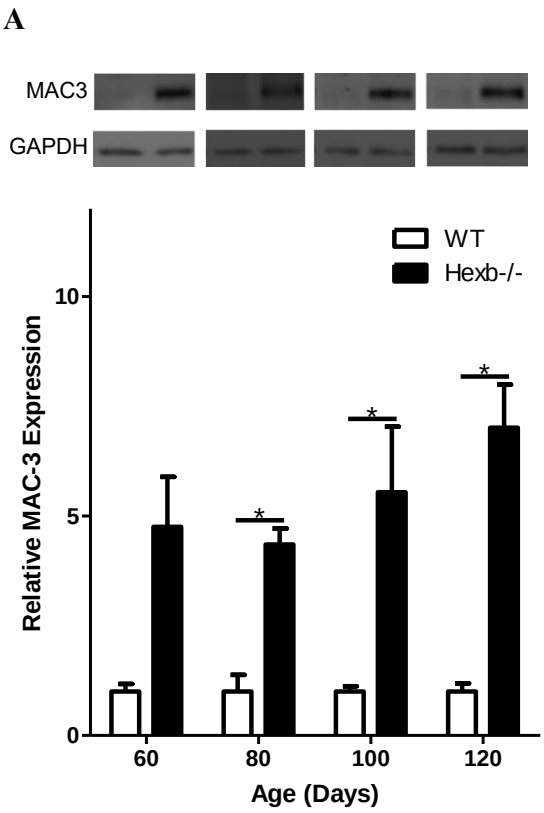
A
MAC3
GAPDH
WT
Hexb-/-
Relative MAC-3 Expression
10
5
0
60
80
100
120
Age (Days)
*
*
*

Figure 3.2 (continued)

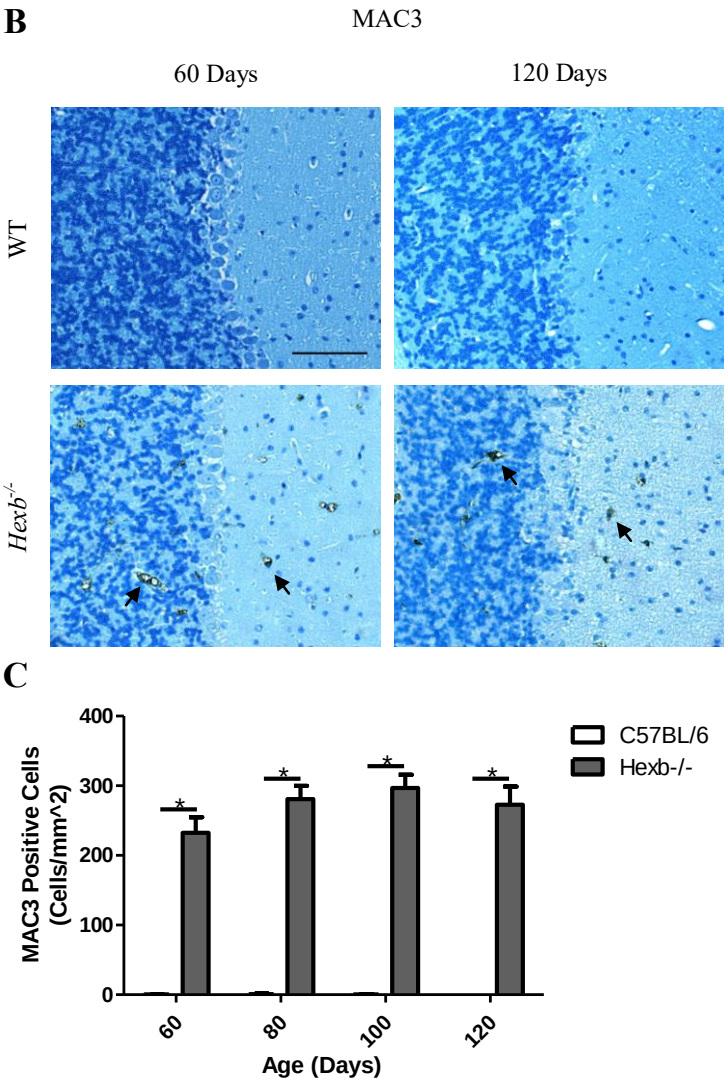

GFAP is not significantly different in SD relative to WT until 100 days, when it increases sharply (Fig. 3.3A). This incongruity between microglial and astroglial regulation suggests the two populations are under unrelated controls, or that astrogliosis is dependent on a threshold not reached until 100 days of age. To further verify this and to determine if there is merely an upregulation of these markers within already activated microglia and astrocytes, or an increase in the number of activate cells, we stained paraffin embedded sections of cerebella from WT and SD mice at 60, 80, 100, and 120 days of age, and quantified the number of positively stained cells from random fields. Consistent with the protein data, microglia are seen to be activated at high numbers in the SD mice, relative to WT mice, as early as 60 days (Fig. 3.2B-C). Activated astrocytes numbers are not significantly higher in SD mice compared to WT mice, until 80 days (Fig. 3.3B-C).

Figure 3.3. Developmental progression of astrogliosis in Sandhoff disease mouse cerebella.

Cerebella from female WT and Sandhoff Disease mice at indicated age-points were blotted for the astroglial marker GFAP. GFAP increases significantly in SD mice at approximately 100 days of age (**A**). Bars = mean ± SE. T-tests, n = 3 for each group, *P < 0.05. Cerebellar sections from C57BL/6 and *Hexb*$^{-/-}$ mice at 60, 80, 100, and 120 days of age were stained for GFAP (**B**). The total number of positively stained cells from 20 random field images per section, centred on the Perkinje layer, were quantified and normalized to area (**C**). n = 3 for each genotype in each age group. Astrogliosis is not significantly increased until 80 days. *P < 0.05. Scale bar = 50µm. Arrows indicate examples of positively stained astroglia.

Figure 3.3

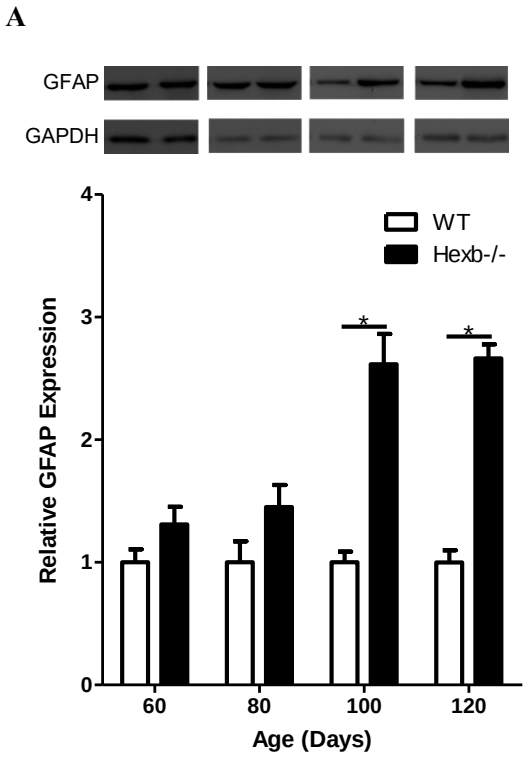
A
GFAP
GAPDH
WT
Hexb-/-
Relative GFAP Expression
0
1
2
3
4
60
80
100
120
Age (Days)
*
*

Figure 3.3 (continued)

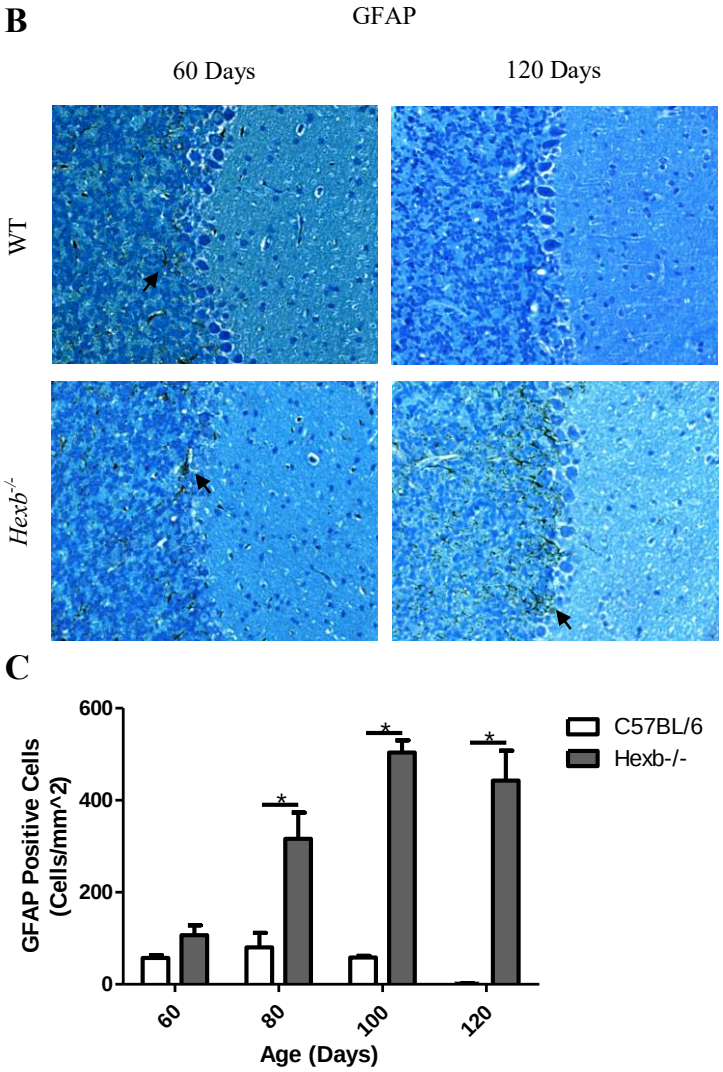

3.5.3 Neuronal Markers

Based on the involvement of AMPA receptors in other neurodegenerative diseases, we observed expression levels of the AMPAR GluR1 in the cerebella of WT and SD mice (Hynd et al., 2004). GluR1 displays a sharp and significant decline at 100 days of age in the cerebellum of SD mice with a similar trend at 120 days, coinciding with the observed increase in GFAP levels (Fig. 3.4A). Since neuronal death is the ultimate result of SD, we felt it important to observe changes in neuronal and synaptic markers- in particular the 75kDa form of neurofilament (NF-L) as a general measure of neurons, synaptophysin as a measure of synapses, and PSD-95 as a marker for excitatory synapses. Despite neuronal death occurring, none of the general synaptic and neuronal markers measured (PSD-95, synaptophysin, or NF-L) appear to change within the cerebellum over the development of the disease (Fig. 3.4B-D).

Figure 3.4. Developmental differences of synaptic and neuronal markers in wild-type and Sandhoff disease mouse cerebella.

Cerebella from female WT and Sandhoff Disease mice at indicated age-points were blotted for GluR1 (**A**), the excitatory synaptic marker PSD-95 (**B**), the general synaptic marker synaptophysin (**C**) and for the neuronal marker neurofilament-L (**D**). Despite a measured increase in cerebellar cell death in SD relative to WT, no changes are seen in PSD-95, synaptophysin, or neurofilament-L. GluR1 drops significantly in SD relative to WT cerebella at a100 days of age, indicating dysregulation and/or specific loss of GluR1 excitatory neurons. Bars = mean ± SE. T-tests, n = 3 for each group, *P < 0.05.

Figure 3.4 (continued)

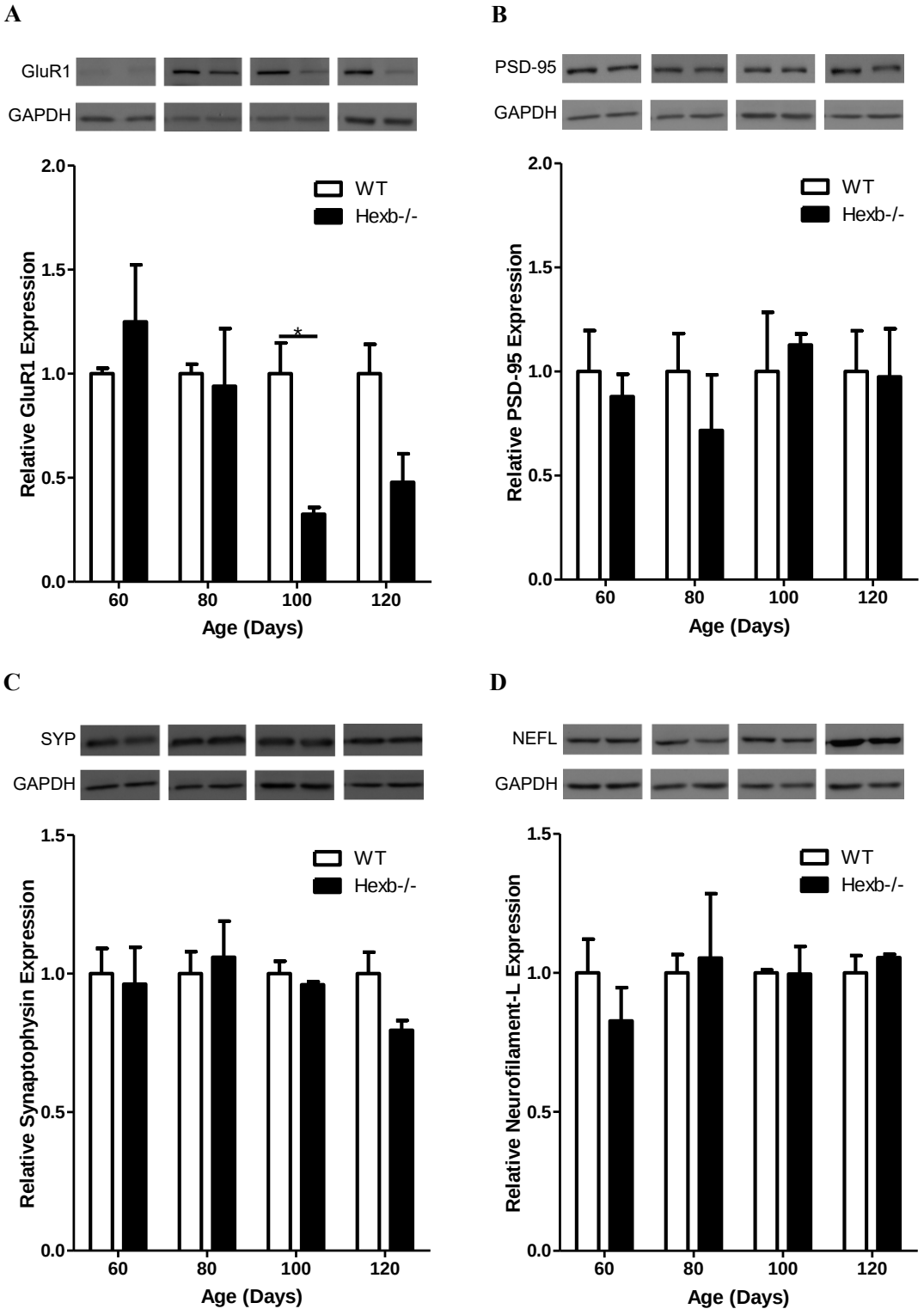

3.5.4 Apoptosis

Despite previous studies showing no increase in apoptosis in the cerebellum of SD mice, our lab has previously found significant increases in TUNEL positive cells in this region of the SD brain at 120 days (Abo-Ouf et al., 2013; Wada et al., 2000). This suggested that we observe protein levels in the cerebellum to determine the onset of apoptotic pathways. Observing classical apoptotic pathways we find that cleaved caspase-9 is significantly higher in SD cerebella relative WT, beginning at 100 days (Fig. 3.5). Activation of the caspase cascade is consistent with models of excitotoxic death, and its onset at 100 days suggests that it may be related to the astrogliosis spike and the decline of GluR1 at the same time point.

Figure 3.5. Apoptosis in Sandhoff disease mouse cerebella.

Cerebella from female WT and Sandhoff disease mice at indicated age-points were blotted cleaved caspase-9. Apoptosis appears to become highly upregulated in SD at 100 days as indicated by a significant increase in cleaved caspase-9 levels relative to WT. Bars = mean ± SE. T-tests, n = 3 for each group, *P < 0.05.

Figure 3.5

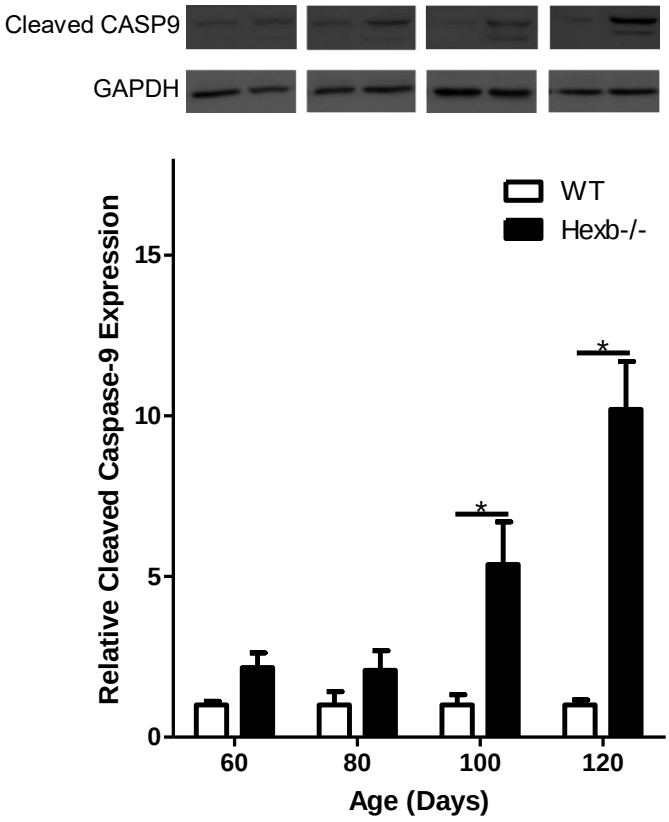
Cleaved CASP9
GAPDH
WT
Hexb-/-
Relative Cleaved Caspase-9 Expression
0
5
10
15
60
80
100
120
Age (Days)
*
*

3.6 Discussion

3.6.1 A Two Stage Model of Sandhoff Disease

The data presented suggests that there are at least 2 stages of disease development. The first involves early activation of microglia, indicated by MAC3 upregulation, and an increase in the density of MAC3 positive cells in the cerebellum. Previous immunohistochemical studies have shown an increase in activated microglia beginning at 2-3 months of age in the brain stem and spinal cord of SD mice relative to controls, with a sharp increase at 3 months (Wada et al., 2000). Our data suggest that this increase begins occurring prior to 2 months in the cerebellum- earlier than implied by the previous research from other tissues, which had fewer time points in this age-range. The second stage begins at approximately 80-100 days- coinciding with the onset of behavioural symptoms in the SD mice- and involves the onset of heavy astroglial activation, a reduction in GluR1, and the invocation of caspase-mediated apoptosis. Similarity in SD and WT GFAP levels demonstrated via western blot in mice at 80 days- when microgliosis has already occurred- suggests that astrocytes are not influenced by the same stimuli activating the microglia, and may be stimulated by an effect of the microglia themselves such as increased TNFα. This is confirmed by the similarity in numbers of activated astrocytes in SD and WT cerebella at 60 days of age (Fig. 3.3D). While this is earlier than the observed upregulation of GFAP in the cerebellum, the number of positively stained cells does not directly reflect the amount of the marker protein within each cell. As well, random fields do not necessarily account for specific

groupings of astrocytes that may be present at specific structures within the cerebellum. The extended lifespan of *Hexb*$^{-/-}$ mice via knockout of *Sphk*, and subsequent downregulation of astrocyte activation relative to *Hexb*$^{-/-}$ mice, suggests that the astrogliosis is not merely a reaction to the end stages of the disease, but rather, one of its causes (Wu et al., 2008). It has been suggested that the abnormal proliferation of astrocytes, due to their internal accumulation of GM2/GA2, may be specifically involved in the damaging of neurons, and these findings support that (Kawashima et al., 2009). Whether playing a supportive role or detrimental role, astrocytes activation is correlative to the severity of the disease progression as indicated by behaviour testing detriments, and serves as a good marker for disease progression. It is recommended that microglia and astroglia- though interconnected- should be treated and studied with their temporal separation in mind.

That GluR1 levels are lower in SD mice at 100 days, despite steady detectable levels of neuronal markers PSD-95, synaptophysin, and neurofilament (70kDa), suggests that AMPARs are somehow specifically involved in the disease. Since PSD-95 not only associates with AMPA receptors, but also N-methyl-D-aspartate receptors (NMDARs), and potassium channels, levels may remain unaltered if the focus of the disease is neurons containing specific receptor subtypes- the same may apply for the ubiquitous synaptophysin. One might expect levels of NF-L and the synaptic markers to drop as neurons undergo apoptosis, however, these are abundant proteins and normalization of protein loading may compensate for this if all the cell types (including glia) in the CNS

face similar declines in number. If excitotoxicity is in fact one of the pathways leading to the apoptosis observed in SD cerebella, then we could expect to see levels of GluR1 drop as internal pools of AMPARs are used up, and/or as GluR1 containing neurons succumb to the disease at a faster rate than other neurons of the cerebellum. We observe caspase-mediated apoptosis and the activation of astrocytes at this stage, coinciding with GluR1 decline. These events may not be trivial, as astrocytes have been shown to be involved with the regulation of AMPAR subunit composition in motor neurons of the spinal cord- a region previously shown to be highly affected by SD (Abo-Ouf et al., 2013; Huang et al., 1997; Van Damme et al., 2007).

In conclusion, we have observed a 2-stage model of Sandhoff disease progression in the cerebella of *Hexb*$^{-/-}$ mice (Fig. 3.6). There is an initial activation of microgliosis, followed by a late onset of astrogliosis, caspase-mediated apoptosis, and a reduction in GluR1. These findings have opened many paths to be examined. The factors that initiate the second stage of the illness require investigation as their manipulation may stay the final declining stages of the disease. Astrogliosis may also be a more sensitive indicator towards signalling the endpoint of the disease, relative to microgliosis. As well, excitotoxicity as a source of neuronal death in SD is possible, as excitotoxicity is observed in other diseases involving the build-up of metabolites, such as Alzheimer's Disease, and this needs to be considered as a mechanism in this disease (Hynd et al., 2004).

Figure 3.6. Schematic of pathological events in the cerebella of Sandhoff disease mice.

Using data from protein markers, approximate levels of glial, apoptotic, and GluR1 receptors are plotted relative to those found in WT mice at the respective ages. There appears to be a threshold or event between 80 and 100 days of age, which initiates an increase in astrogliosis and apoptosis, and a decrease in GluR1 (indicated by vertical dotted-line). Microgliosis may also increase, however it is already demonstrably upregulated by 60 days (indicated by horizontal dotted-line).

Figure 3.6

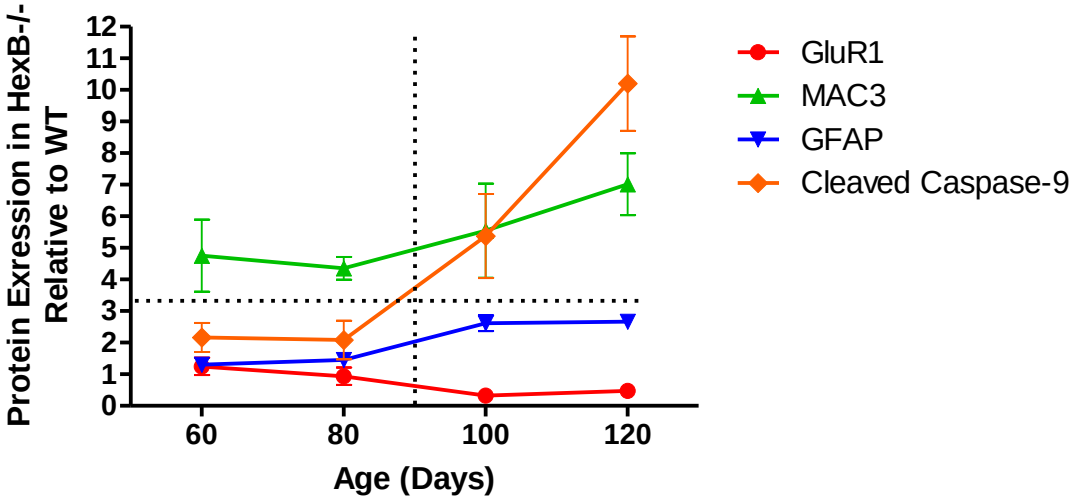
Protein Exression in HexB-/- Relative to WT
12
11
10
9
8
7
6
5
4
3
2
1
0
60
80
100
120
Age (Days)
GluR1
MAC3
GFAP
Cleaved Caspase-9

3.7 Acknowledgement

This work was supported by a grant from the Canadian Institute of Health Research (CIHR) to S.A.I.

CHAPTER 4: Neuronal pentraxin 1 depletion delays neurodegeneration and extends life in Sandhoff disease mice

Alexander W.M. Hooper[1], Javier Alamilla[2,†], Rosemarie E. Venier[1], Deda C. Gillespie[2], Suleiman A. Igdoura[1,3,*]

[1]Department of Biology, McMaster University, Hamilton, Ont., Canada, L8S 4K1, [2]Department of Psychology, Neuroscience & Behaviour, McMaster University, Hamilton, Ont., Canada, L8S 4K1, [3]Department of Pathology and Molecular Medicine, McMaster University, Hamilton, Ont., Canada L8S 4L8

*Corresponding Author
Suleiman A. Igdoura, PhD
McMaster University
1280 Main St. W.
Hamilton, Ontario, L8S4K1
Email: igdoura@Mcmaster.ca

†Present address: CONACYT-Universidad de Colima, Colima Mexico.

4.1 Preface

All work was performed by Alexander Hooper except the following:

Rosemarie Venier performed the qRT-PCR (Figure 4.1A). Javier Alamilla performed the electrophysiology experiments (Figure 4.6).

4.2 Abstract

GM2 gangliosidoses are a group of lysosomal storage disorders which include Sandhoff disease and Tay-Sachs disease. Dysregulation of glutamate receptors has been recently postulated in the pathology of Sandhoff disease. Glutamate receptor association with neuronal pentraxins 1 and 2, and the neuronal pentraxin receptor facilitates receptor potentiation and synaptic shaping. In this study, we have observed an upregulation of a novel form of neuronal pentraxin 1 (NP1-38) in the brains of a mouse model of Sandhoff disease and Tay-Sachs disease. In order to determine the impact of NP1 on the pathophysiology of Sandhoff disease mouse models, we have generated an *Np1*$^{-/-}$*Hexb*$^{-/-}$ double knockout mouse, and observed extended lifespan, improved righting reflex and enhanced body condition relative to *Hexb*$^{-/-}$ mice, with no effect on gliosis or apoptotic markers in the CNS. Sandhoff mouse brain slices reveals a reduction in AMPA receptor-mediated currents, and increased variability in total glutamate currents in the CA1 region of the hippocampus; *Np1*$^{-/-}$*Hexb*$^{-/-}$ mice show a correction of this phenotype, suggesting NP1-38 may be interfering with glutamate receptor function. In fact, some of the psychiatric aspects of Sandhoff and Tay Sachs disease (particularly late onset) are likely due to a dysfunctional hippocampal glutamatergic system. Our work highlights a potential role for synaptic proteins, such as NP1 and glutamate receptors in lysosomal storage diseases.

4.3 Introduction

The GM2 gangliosidoses are a group of lysosomal storage disorders containing Sandhoff disease (SD) and Tay-Sachs disease (TSD). Both diseases present forms that vary in severity and onset of symptoms, depending on the specific mutations involved. Tay-Sachs disease consists of infantile, juvenile, chronic and late-onset Tay-Sachs disease (LOTS) forms (Leinekugel et al., 1992). Sandhoff disease also presents with infantile, juvenile and adult forms of the disease (Mitsuo et al., 1990; Utsumi et al., 2002). These diseases present with a plethora of symptoms including cognitive deficits, muscle weakness and ataxia (Bley et al., 2011; Grunseich et al., 2015). Late-onset Tay-Sachs disease patients can develop psychiatric symptoms, i.e., schizophrenia-like and bipolar disease-like symptoms (Stendel et al., 2015; Zaroff et al., 2004).

Sandhoff disease is caused by accumulation of the gangliosides GM2 and GA2 in the central nervous system. This is due to mutations in the *Hexb* gene, which encodes the beta-subunit of the lysosomal enzymes- β-hexosaminidase A and β-hexosaminidase B. *Hexb*$^{-/-}$ mice are well recognized to represent Sandhoff disease and Tay-Sachs disease. *Hexb*$^{-/-}$ mice display motorneuronal and behavioural deficits, reaching endpoint at approximately 17-19 weeks (Itoh et al., 1984; Sandhoff et al., 1971). Previous studies on Sandhoff disease have focused on gliosis as a phenomenon common with other neurodegenerative disorders such as Alzheimer's and Parkinson's (Teismann and Schulz, 2004; Tuppo and Arias, 2005). Microglial activation appears to precede astroglial activation and is induced via pathways involving C-C chemokine receptor type 2 (CCR2), macrophage-inflammatory protein 1α (MIP-1α), and tumour necrosis factor-α (TNFα)

(Abo-Ouf et al., 2013; Kyrkanides et al., 2008; Wu and Proia, 2004). Astrogliosis, on the other hand, coincides with an increase in caspase-9 activation, suggesting astrocytes may be crucial to the end stages of the disease (Hooper and Igdoura, 2016). Studies have shown that ganglioside accumulation is sufficient to activate astrocytes in SD cells; however, we have also shown a reduction in astrogliosis via knock-out of TNFα in our mouse model, suggesting that cytokine induction is an important factor in astrogliosis at the organismal scale (Kawashima et al., 2009; Wu et al., 2008).

An increase in secreted TNFα has been shown to cause a release of glutamate from microglia, facilitating excitotoxicity- a neurodegenerative process that involves overstimulation of neurons resulting in toxic levels of intracellular calcium ions (Takeuchi et al., 2006). Alterations in glutamate receptors, and an increase in apoptosis, may be indicative of this process as it has been demonstrated that TNFα exposure can stimulate recruitment of the AMPA receptor GluR1 to the cell membrane in dissociated rat hippocampal neurons, as well as inhibit the uptake of synaptic glutamate, enhancing the likelihood of excitotoxicity (Ogoshi et al., 2005; Sama et al., 2012; Wang and Qin, 2010; Zou and Crews, 2005). The mechanism for this TNFα -induced recruitment of GluR1 is currently unknown, and this could potentially occur through regulation by neuronal pentraxins.

Neuronal pentraxin 1 (NP1) has been indicated as directly involved with activation of an apoptotic pathway in rat cerebellar granule cells, and is involved with AMPA induced neuronal death by GluR1 during hypoxic-ischemic injury in neo-natal rats (DeGregorio-

Rocasolano et al., 2001; Hossain, 2008; Yeste-Velasco et al., 2008). Contrarily, neuronal pentraxin complexes, consisting of NP1, neuronal pentraxin 2 (NARP) and the neuronal pentraxin receptor (NPR), could possibly protect from excitotoxicity, via a role in endocytosis of AMPARs. Long term depression in cerebellar Perkinje cell cultures, and in the hippocampus has be shown to be induced via cleavage of the NPR via the matrix metalloprotease (MMP) tumor necrosis factor-α converting enzyme (TACE) (Cho et al., 2008). NP1 has also been suggested to be involved in the elimination of synapses through binding of the complement protein C1q, causing synaptic removal via phagocytosis by glia (Gasque et al., 2000; Kreutzberg et al., 1989; Stevens et al., 2007). Establishing a beneficial or detrimental role for NP1 in Sandhoff disease may open avenues for treatment of neurodegenerative diseases, and point to the study of pathways beyond those established with respect to gliosis.

We observe increased expression of a novel form of NP1 (NP1-38) in our Sandhoff disease mouse model. We also demonstrate increased survival and function of the Sandhoff disease model after knockout of *Np1*, suggesting that NP1 or its alternative form contributes to disease progression.

4.4 Methods and Materials

4.4.1 Mice

Mouse work was conducted under an animal utilization protocol (AUP) in accordance with Ontario Animals for Research Act requirements, and the standards of the Canadian Council on Animal Care (CCAC). *Hexb*$^{-/-}$ mice on a C57BL/6 background

were donated generously by Dr. R. Gravel (University of Calgary, Calgary, AB, Canada), and have been previously characterized and described (Phaneuf et al., 1996). *Np1*$^{-/-}$ mice were generated as previously described, on a C57BL/6 background via a PGK-hprt replacement of the signal peptide-bearing exon 1 (Kirkpatrick et al., 2000). These mice are asymptomatic up until at least the normal *Hexb*$^{-/-}$ endpoint (120-130 days), and so are not expected to contribute to pathology merely by virtue of their knockout). *Np1*$^{-/-}$ mice were crossed with *Hexb*$^{-/-}$ mice to generate *Np1*$^{+/-}$*Hexb*$^{+/-}$ mice. These were then self-crossed to obtain *Np1*$^{-/-}$*Hexb*$^{+/-}$ breeders, which were self-crossed to produce *Np1*$^{-/-}$ *Hexb*$^{+/+}$ and *Np1*$^{-/-}$*Hexb*$^{-/-}$ experimental mice.

4.4.2 Genotyping

Hexb Genotypes were verified with the following primers: WT-Forward, GGTTTCTACAAGAGACATCATGGC; KO-Forward, GATATTGCTGAAGAGCTTGGCGGC; Reverse, CAATCGGTGCTTACAGGTTTCATC. *Np1* Genotypes were verified with the following primers: PGK-hprt Insert Forward, CCTACCGGTGGATGTGGAATGTGT; WT-F, CGTTAGGCGTGCAGCCCGGACCGTGC; Reverse, CGGGCAAGAACACGATGGGCGACCT. Absence of NP1 and NP1-38 protein in *Np1*$^{-/-}$ mice has been verified by western blot.

4.4.3 Cell Culture

Normal and TSD cerebellar cells were obtained from Dr. S Brooks at the Kingsbrook Jewish Medical Centre in New York. Cells were cultured in a 37°C humidified incubator with 21% O_2 and 5% CO_2 and cultured in Dulbecco's modified eagle medium (Invitrogen, #12800017) supplemented with 15% fetal calf serum (Invitrogen,

#12483020), 1% penicillin/streptomycin (Invitrogen, #15140122) and 0.1% fungizone (Invitrogen, #15290018).

4.4.4 RNA Isolation and Reverse Transcription

For cell culture, total RNA from confluent cells was isolated by scraping cells in lysis buffer containing 1% β-mercaptoethanol and passing lysate through an 18½ gauge needle, followed by and purification using the Purelink RNA Isolation Kit (Ambion, #12183018A) or the Total RNA Purification Kit (Norgen, #17200).

RNA was reverse transcribed with oligo-dT or random primers according to the Superscript III protocol (Invitrogen Superscript III, #18080-093). RNA, dNTPs, and primers were incubated at 65°C for 5 min, then on ice for 1 min. First strand buffer, DTT, RNase OUT and Superscript III were added to the mixture and incubated at 25°C for 5 min, if random primers were used. Then, the mixture was incubated at 50°C for 1 hour and inactivated at 70°C for 15 min.

4.4.5 Quantitative RT-PCR

qRT-PCR was performed on normal and TSD cerebellar cell cDNA, using Taqman gene expression master mix (Applied Biosystems, #4370048). cDNA was mixed with master mix and gene specific probes, and added to a MicroAmp Optical 96-well Reaction Plate (Applied Biosystems, #4316813). The plate was spun down quickly to remove bubbles and placed in the 7900HT Sequence Detection System (Applied Biosystems). Thermal cycling conditions were as follows: 50°C for 2 min, 95°C for 10 min, then 40 cycles of 95°C for 15 sec, 60°C for 1 min. A standard curve was used and final values are

expressed as relative gene of interest divided by the endogenous control (*GAPDH*). Primers and probes used were as follows: *NPTX1* Hs00159652_m1, and GAPDH Hs99999905_m1 (Applied Biosystems).

4.4.6 Western Blot

Western blots were performed on cerebellar lysates from *Hexb*$^{+/+}$ and *Hexb*$^{-/-}$ mice at 120 days of age. Mice were perfused via intracardiac injection with PBS, and then cerebella were harvested into microcentifuge tubes, and placed directly into liquid nitrogen. Cerebella were lysed in RIPA buffer (50mM tris, 165mM NaCl, 1% Nonidet P-40, 0.01% sodium dodecyl sulfate, 0.5% Sodium deoxycolate, pH 8.0) containing protease inhibitors, via sonication (Sonicator XL 2020, Heat Systems Inc., Duty 20%, Output 4). Protein was measured using the Bio Rad DC Protein Assay (#500-0116). Samples were diluted to equal protein concentrations with RIPA buffer, and Laemmli sample buffer (6X) was added. Samples were heated at 65C for 20mins, and then placed on ice. Samples were run on a 10% SDS-polyacrylamide gel (90V), and transferred to a nitrocellulose membrane (100V, 1hr). Membranes were blocked with 5% cow milk (Carnation) in Tris-buffered saline containing 0.5% Tween-20 (TBST), before overnight incubation with mouse primary antibody- anti-NP1 (BD Transduction Labs, #610369) suspended in 5% milk in TBST, at 4C. After washing in TBST five times, membranes were blotted with secondary goat anti-mouse (Santa Cruz Biotechnology, sc-2005) IgG-HRP conjugated antibodies in 5% milk in TBST for one hour at room temperature, followed by five washes in TBST. Blotted membranes were incubated with Amersham ECL Western

Blotting Detection Reagents (GE Healthcare, #RPN2106) and exposed on Amersham Hyperfilm ECL film (GE Healthcare, #28906839). Densitometry was measured using the gel analysis feature in ImageJ (v1.46r, NIH, USA), and normalized to respective GAPDH measurements.

4.4.7 Deglycosylation of Np1

Deglycosylation was performed on cerebellar lysates from 120 day-old female wild-type, $Hexb^{-/-}$, and $Np1^{-/-}$ mice, via overnight incubation of samples with recombinant E. coli N-glycosylase F (Roche, Ref. 11365169001) at 38°C. Samples were then resolved by SDS-PAGE, blotted, and stained for NP1 as described (see Western Blot methods).

4.4.8 Immunoprecipitation of Np1

Cerebella from *Hexb-/-* and *Hexb-/-Np1-/-* mice were lysed via sonication on ice, in Triton X-100 buffer (50mM Tris-HCl, 150mM NaCl, pH 7.4, 1% Triton X-100). Samples were spun at 12, 000g for 10min at 4°C, and the pellet was removed. The supernatant was precleared with 100µL of Dynabeads Protein G/1mL sample (Invitrogen, #100.041) and pre-immune mouse IgG (Active Motif, #101226), on a rotator for 1hr at 4°C at 15rpm. Beads were removed with a magnet, and mouse anti-NP1 primary antibody (BD Transduction Labs, #610369) was incubated in the sample overnight at 10ug/uL sample. Dynabeads Protein G were added to the sample at 200uL/mL sample and incubated on a rotator for 1hr at 4°C at 15rpm. The Dynabeads Protein G were isolated via magnet and the supernatant removed. Samples were washed 5 times with 1mL lysis buffer, and then suspended in Laemmli sample buffer. Samples were heated at 65°C for 20min, Dynabeads Protein G were removed and the samples underwent SDS-PAGE and

western blotting on PVDF, followed by staining with a mouse anti-NP1 primary antibody (BD Transduction Labs, #610369) followed by secondary goat anti-mouse (Santa Cruz Biotechnology, sc-2005) IgG-HRP conjugated antibodies (see *Western Blot*).

4.4.9 Behaviour

Hexb$^{+/+}$, *Np1*$^{-/-}$*Hexb*$^{+/+}$, *Hexb*$^{-/-}$, and *Np1*$^{-/-}$*Hexb*$^{-/-}$ female mice were observed at intervals no greater than 7 days, beginning at approximately 7 weeks of age (before the detriments are normally observed in SD mice), until endpoint was reached (i.e. mouse can no longer right self in less than 45s on each side). Measurements were taken of bodyweight, lifespan, righting reflex, wire hang, and rotarod tests. *Righting Reflex:* Mice were positioned on their backs (with a slight tilt to the left and then repeated to the right) on a solid surface, and time for mouse to right itself onto its feet was measured. The average of measurements for the left side and right side righting reflex was used a measurement of cerebellar function/proprioception. Endpoint was reached when mice could not right themselves for 2 consecutive days on both the right and left sides. *Survival:* Lifespan was measured from date of birth until endpoint measured by righting reflex as described above. *Wire Hang:* Mice were placed on top of a wire mesh, which was then inverted, 30 cm above a padded surface. Hang time was measured from the point of inversion, until time to fall- to a maximum of 5 minutes. The best time of 3 consecutive trials was used. *Rotarod:* Mice were placed on a rotating rod (Accuscan EzRod with EzRod v.120 software), and time to fall was measured via photo-sensors.

Rotarod rotations were increased from 0rpm to a maximum of 40 rpm over 360 sec. Mice were placed on the rod at 4rpm. The best time of 3 consecutive trials was used.

Body masses were recorded from another cohort of mice (ages 60-120 days of age for *Hexb*$^{+/+}$, 100-120 days for *Np1*$^{-/-}$*Hexb*$^{+/+}$, *Hexb*$^{-/-}$, and *Np1*$^{-/-}$*Hexb*$^{-/-}$ mice), and their respective brain masses were measured after whole animal intracardiac perfusion with phosphate buffered saline (PBS).

4.4.10 Immunohistochemistry

Hexb$^{+/+}$, *Np1*$^{-/-}$*Hexb*$^{+/+}$, *Hexb*$^{-/-}$, and *Np1*$^{-/-}$*Hexb*$^{-/-}$ mice were processed as previously described (Abo-Ouf et al., 2013). Mice were harvested at 17 weeks of age, perfused with PBS, fixed with 3.7% formaldehyde, and embedded in paraffin wax. Five-micrometre thick coronal cerebellar and cerebral cortex sections were sliced, and mounted on glass slides. The samples were then subjected to a xylene/ethanol/water rehydration series. Endogenous peroxidase was quenched with 1% H2O2. Samples to be stained for MAC3 underwent microwave antigen retrieval in 12 mM citric acid buffer. Samples were blocked with 10% goat serum, and immunolabeled with monoclonal antibodies against GFAP (Sigma-Aldrich, G3893), and MAC3 (BD Pharmingen, 553322). Tissues were then incubated with biotinylated secondary antibodies, followed by an avidin/HRP-bound biotin solution (Santa Cruz, Mouse ABC Staining System #sc-2017, Rat ABC Staining System #sc-2019). Samples were then stained with 3,3'- diaminobenzadine in the presence of 0.01% H2O2, and counterstained with methylene blue. For each slide, 10 random field images of the cerebellum and cerebral cortex were captured at 400X

magnification, centred on the Perkinje layer. The areas of the images were calculated using AxioVision 4.9.1 software (Zeiss, Oberkochen, Germany). For each sample, positively stained cells microglia/macrophages and astrocytes were quantified as the total count per 10 random fields/total area of the 10 fields.

4.4.11 TUNEL

Terminal deoxynucleotidyl transferase dUTP nick end labeling (TUNEL) was performed as previously described on formalin-fixed, paraffin-embedded cerebellar, cerebral cortex and spinal tissues, according to manufacturer's instructions using the ApopTag Peroxidase In Situ Apoptosis Detection Kit (Millipore, #S7100) (Abo-Ouf et al., 2013). Sections were subjected to a xylene/ethanol rehydration series, and then with proteinase K for 10 min. After blocking endogenous peroxides activity with 3% hydrogen peroxide, the samples were incubated with terminal deoxynucleotidyl transferase (TdT) enzyme at 37 °C for 1 h. Sections were incubated with anti-digoxigenin-peroxidase and reacted with 3,3'- diaminobenzadine in presence of 0.01% H_2O_2. Nuclei were counterstained with methyl green. All washes were performed with PBS. Areas of the cerebral cortex, and entire cerebella were measured using AxioVision 4.7 and positively stained cells were quantified at 400X magnification. Images of spinal sections were captured, and areas measured with Axiovision 4.7 (Zeiss, Oberkochen, Germany), and positively stained cells were quantified under 400X magnification. The number of all astrocytes in a specific spinal tissue type were counted and divided by total area of all sections of that type, for each mouse.

4.4.12 Electrophysiology

Ex vivo brain slices were obtained from 24-32 day old *Hexb*$^{+/+}$, *Np1*$^{-/-}$*Hexb*$^{+/+}$, *Hexb*$^{-/-}$, and *Np1*$^{-/-}$*Hexb*$^{-/-}$ mice. Briefly, the mouse was deeply anesthetized and intracardially perfused with artificial cerebro-spinal fluid (aCSF) containing, in mM: NMDG, 93; HCl, 93; KCl, 2.5; NaH_2PO_4, 1.2; $NaHCO_3$, 30; HEPES, 20; glucose, 25; sodium ascorbate, 5; thiourea, 2; sodium pyruvate, 3; $MgSO_4$, 10; $CaCl_2$, 0.5; 300-310 mOsm; pH 7.4 with 10 N HCl. NMDG-aCSF was used for slicing and recovery. Transverse slices containing the hippocampus were obtained at 300 µm using a vibrating microtome. Slices were allowed to recover for 1 hr at 37° C in an oxygenated, humidified interface chamber before being transferred to a recording chamber and continuously perfused with oxygenated recording aCSF solution (32-35° C in bath) containing, in mM: NaCl, 124; KCl, 2.5; NaH_2PO_4, 1.2; $NaHCO_3$, 24; HEPES, 5; Glucose, 12.5; $MgSO_4$, 2; $CaCl_2$, 2; 300-310 mOsm; pH 7.3-7.4 adjusted with 7NaOH or HCl. A borosilicate glass stimulating electrode (1 MΩ) containing aCSF recording solution was placed in the CA3-CA1 pathway. CA1 pyramidal cells were identified, using IR-DIC optics, by morphology and position within the hippocampus. Whole-cell patch recordings were made using borosilicate glass patch pipettes (1.5-2.5 MΩ) filled with internal solution containing, in mM: D-gluconic acid, 64; CsOH, 64; EGTA, 11; CsCl, 56; MgCl, 1; $CaCl_2$, 1; HEPES, 10; GTP-Na, 0.3; ATP-Mg, 4; QX-314, 5. Series resistance was compensated (80 %) and the seal monitored throughout the experiment, and recordings were aborted if input resistance was higher than 150 MΩ or access resistance exceeded 25 MΩ or changed more than 15

%. GABAergic responses were inhibited by addition of the GABA receptor antagonist picrotoxin (50 μM) to the perfusate, and pyramidal neurons of the CA1 region of the hippocampus were voltage-clamped at +40mV to measure total glutamate currents, and at -60mV to measure the contribution of AMPA receptor currents. Specificity of the glutamate currents was confirmed by bath application of the NMDA and AMPA receptor antagonists D-APV (50 μM) and CNQX (5 μM). To guard against possible bias, slice preparation, electrophysiological recording, and analysis were all performed by an experimenter blind to genotype. To account for pseudoreplicates, the measurements for each individual animal were averaged, and then statistics were performed by animal, rather than by neuron (Lazic, 2010; Walcott et al., 2011).

4.4.13 Statistical Software

For data sets with 2 groups, t-tests were used to test for differences between means at $P < 0.05$. For data sets with 3 or more groups, one-way ANOVA was used to test for differences between means at $P < 0.05$. ANOVA was followed by Tukey's post-hoc for all data with high normality and equal variance amongst groups. For groups of unequal variance, Dunnett's T3 test was used for pairwise comparison. For Samples with unequal variance and unequal sample sizes, Kruskal-Wallis test was used for pairwise comparison. Equality of variances was calculated with Levene's test. All statistical analyses were performed using SPSS v16 (SPSS Inc. Chicago, IL).

4.5 Results

4.5.1 Identification of a Novel Form of NP1

GluR1 expression is lowered towards endpoint in our Sandhoff disease mouse model, and is known to be under the control of neuronal pentraxin 1. In order to detect alterations of *NP1* gene expression in lysosomal storage disorders, we measured the expression levels of *NP1* mRNA in human TSD cerebellar cells against those of normal human cerebellar cells (Fig. 4.1A). There is a significant increase in the mRNA for *NP1* in the human TSD cerebellum relative to normal. This suggests an involvement of neuronal pentraxin 1 in these lysosomal storage disorders.

We then performed western blots to determine the temporal expression of NP1 protein in the cerebellum of our WT and *Hexb*$^{-/-}$ mice. No changes in the expression of ~50kDa NP1 were found, relative to controls (Fig. 4.1B). However, we observed a ~38kDa band that was upregulated in the SD mice as early as 60 days of age (currently labeled with the placeholder name NP1-38) (Fig. 4.1C, 4.2A). Inquiry into whether both are forms of NP1 is warranted as discovery of an unexplored regulatory form of neuronal pentraxin 1 could provide great insight into synaptic regulation and disease. To this end, we crossed *Hexb*$^{-/-}$ and *Np1*$^{-/-}$ mice, both on a C57BL/6 background, to obtain *Np1*$^{-/-}$*Hexb*$^{-/-}$ double-knockout (DKO) mice. Indeed, the 38kDa band is absent from the DKO mice, verifying a relationship to NP1 (Fig. 4.2B-C). Immunoprecipitation with an anti-NP1 antibody isolates two bands in *Hexb*$^{-/-}$ mice- at 50kDa and 38kDa- that are absent from *Np1*$^{-/-}$*Hexb*$^{-/-}$ mice (Fig. 4.2B). Since both forms are able to bind the antibody under non-denaturing conditions, it is suggestive of a lack of large conformational changes in the 38kDa protein, at least in the region that the antibody binds towards the centre of the primary

amino-acid sequence (Rat NP1, aa.137-312). NP1 is known to be N-glycosylated, so WT, SD, and DKO cerebellar lysates were treated with N-glycosidase F, and it was found that the both the 50kD and the 38kDa bands are similarly N-glycosylated (Fig. 4.2C). If the 38kDA band is a modified form of NP1, then any alterations in the protein likely do not affect the glycosylation sites.

Figure 4.1. Expression levels of NP1 in Tay-Sachs and Sandhoff cerebella (47kDa and 38kDa).

A. mRNA expression of *NP1* is significantly increased in cerebellar cells of a Tay-Sachs disease patient relative to normal cells. **B.** Cerebellar lysates from WT and *Hexb*$^{-/-}$ mice at varying ages were probed for NP1 by western blotting. The full length NP1 shows no variation in expression between 60-120 days. **C.** Developmental western blots for a smaller form of NP1 (NP1-38) show that it is upregulated as early as 60 days in the cerebella of *Hexb*$^{-/-}$ mice, relative to WT mice (*$P < 0.05$. Data are mean values +/- SE. n = 3 for each group.).

Figure 4.1

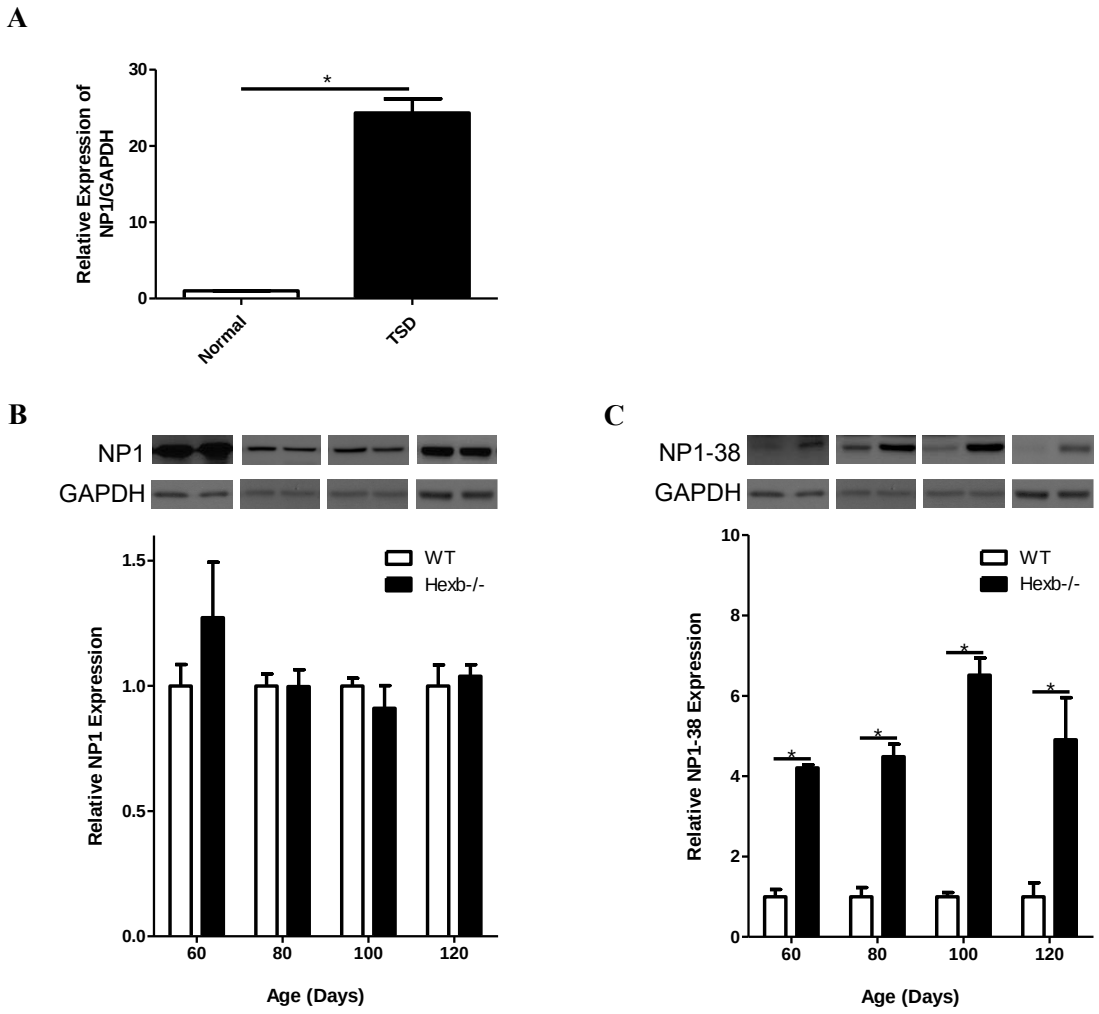
A
Relative Expression of NP1/GAPDH
30
20
10
0
*
Normal
TSD
B
NP1
GAPDH
WT
Hexb-/-
Relative NP1 Expression
1.5
1.0
0.5
0.0
60
80
100
120
Age (Days)
C
NP1-38
GAPDH
WT
Hexb-/-
Relative NP1-38 Expression
10
8
6
4
2
0
*
60
80
100
120
Age (Days)

Figure 4.2. Identification and characterization of a new form of neuronal pentraxin 1.

A. Cerebellar lysates from C57BL/6 and *Hexb*$^{-/-}$ mice at 120 days of age were blotted for NP1. A smaller band, suspected to be a form of NP1, is apparent in the *Hexb*$^{-/-}$ mice, which is barely visible in the WT samples at approximately 38kDa. **B.** Cerebellar lysates from *Hexb*$^{-/-}$ and *Hexb*$^{-/-}$*Np1*$^{-/-}$ mice at 120 days of age were immunoprecipitated with an antibody against NP1, western blotted and the membrane was stained with the same antibody. Both NP1 and NP1-38 are visible in the blot, with both forms absent from the *Hexb*$^{-/-}$*Np1*$^{-/-}$ mouse. NP1 and the smaller form are both able to bind the antibody under non-denaturing conditions, suggesting a lack of large conformational changes in the smaller form. **C.** Cerebellar lysates from C57BL/6, *Hexb*$^{-/-}$ and *Np1*$^{-/-}$ mice were incubated overnight with, or without N-glycosylase F, and then blotted and stained for NP1. A band at approximately 50kDa (expected size of NP1) is absent in the *Np1*$^{-/-}$ mice, and visible in WT and *Hexb*$^{-/-}$ mice. A band at approximately 38kDa is visible in WT and *Hexb*$^{-/-}$ mice that is completely absent from the *Np1*$^{-/-}$ mice, even at the 10min exposure. Upon treatment with N-glycosylase F, there is a downward shift in NP1 from its expected size (50kDa) in WT and *Hexb*$^{-/-}$ samples, indicating N-glycosylation is normally present on the protein. NP1-38, visible in *Hexb*$^{-/-}$ samples, is also deglycosylated and shifts downward in *Hexb*$^{-/-}$ samples treated with N-glycosylase. The smaller form, NP1-38, likely contains the glycosylation sites, and the epitope site for the antibody used to probe it.

Figure 4.2

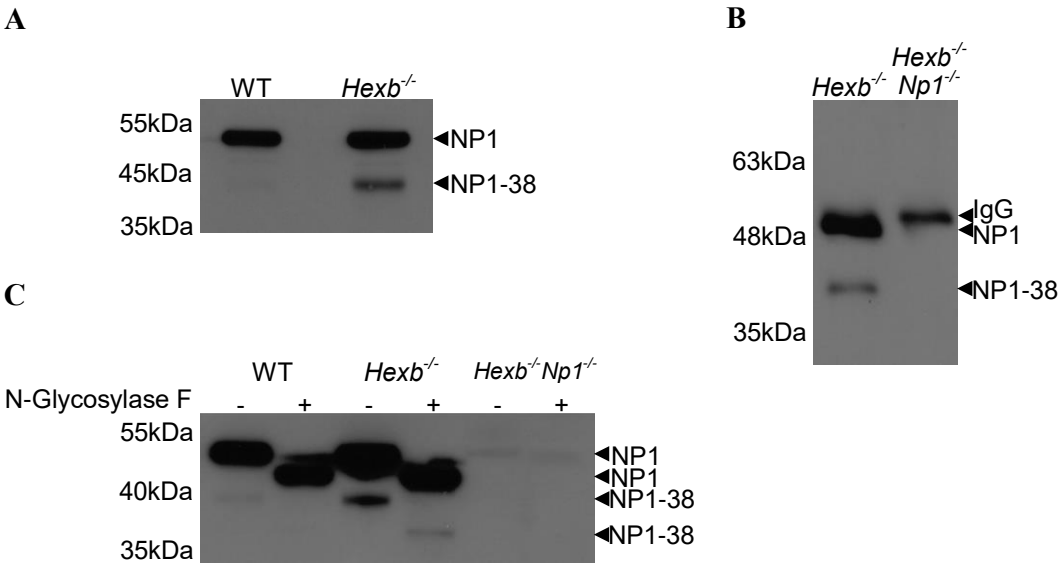
A
WT
Hexb-/-
55kDa
45kDa
35kDa
NP1
NP1-38
B
Hexb-/-
Hexb-/- Np1-/-
63kDa
48kDa
35kDa
IgG
NP1
NP1-38
C
WT
Hexb-/-
Hexb-/- Np1-/-
N-Glycosylase F
- + - + - +
55kDa
40kDa
35kDa
NP1
NP1
NP1-38
NP1-38

4.5.2 Knockout of Np1 Improves Behaviour and Survival of Sandhoff Disease Mice

Since NP1-38 is upregulated early in the disease, indicating potential contribution of NP1 and/or NP1-38 to disease progression, we sought to elucidate the overall effect of NP1 isoforms on the health and behaviour of *Hexb*$^{-/-}$ mice by knocking out the gene for *Np1*.

Np1$^{-/-}$*Hexb*$^{-/-}$ mice show an improvement in some behavioural tests over *Hexb*$^{-/-}$ mice (Fig. 4.3). In particular, the DKO mice show a statistically significant increase in lifespan. DKO mice also have a significantly improved righting reflex at 17 and 18 weeks of age, with a similar trend at 19 weeks. *Np1*$^{-/-}$*Hexb*$^{-/-}$ mice perform similarly to *Hexb*$^{-/-}$ mice in all other tests including rotarod time and wire hang. These findings indicate that the increase in survival and righting reflex in the DKO mice is not due to a universal peripheral neuromuscular mechanism which would affect rotarod and wire hang performance, but perhaps due to an effect exclusive to the cerebellum, pons, and mesencephalon which are responsible for coordinating the righting reflex behaviour. Rear leg stiffness also increases in *Hexb*$^{-/-}$ mice with age, and knocking out Np1 may have some effect on this detriment.

Figure 4.3. Developmental Behaviour in *Hexb*$^{-/-}$ and *Np1*$^{-/-}$*Hexb*$^{-/-}$ Mice.

Hexb$^{+/+}$, *Np1*$^{-/-}$*Hexb*$^{+/+}$, *Np1*$^{-/-}$*Hexb*$^{-/-}$ and *Hexb*$^{-/-}$ mice have undergone behaviour testing as early as 7 weeks of age, to determine degeneration of various cerebellar and peripheral nervous system functions. Measures of survivability, rotarod, body mass, wire hang, and righting reflex (average of left and right sides), were recorded weekly. Measurements suggests that NP1 has a detrimental effect in Sandhoff disease, as *Np1*$^{-/-}$ *Hexb*$^{-/-}$ mice appear to live significantly longer than *Hexb*$^{-/-}$ mice, and display significantly faster righting reflex during later stages of disease. *Np1*$^{-/-}$*Hexb*$^{-/-}$ mice and *Hexb*$^{-/-}$ mice have a similar increase in body mass relative to WT mice, a hallmark of our *Hexb*$^{-/-}$ mice relative to WT. *Np1*$^{-/-}$*Hexb*$^{-/-}$ mice fare similar to *Hexb*$^{-/-}$ mice on the rotarod test and wire hang tests, indicating NP1 has little effect on motor functions. All data is from female mice, with the following sample sizes (n): *Hexb*$^{+/+}$ = 4, *Np1*$^{-/-}$*Hexb*$^{+/+}$ = 3, *Hexb*$^{-/-}$ = 6 and *Np1*$^{-/-}$*Hexb*$^{-/-}$ = 13. Analysis of survival by Mantel-Cox test, $P<0.02$ between *Hexb*$^{-/-}$ and *Np1*$^{-/-}$*Hexb*$^{-/-}$ mice, median survival = 127 days and 134 days respectively. Statistical analysis via ANOVA with Tukey's HSD or Dunnet's T3 post-hoc where appropriate. *$P<0.05$ between *Np1*$^{-/-}$*Hexb*$^{-/-}$ mice and *Np1*$^{+/+}$*Hexb*$^{-/-}$ mice.

Figure 4.3

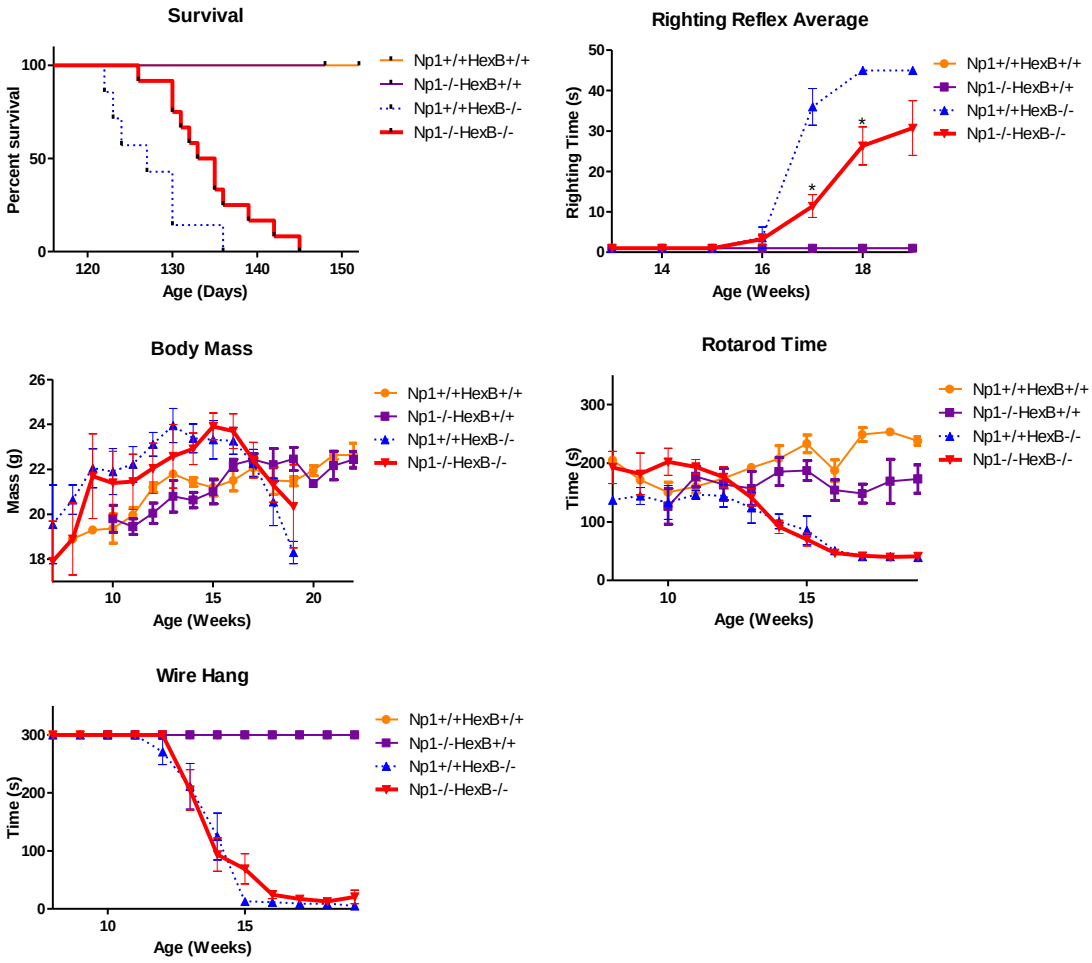
Survival
Percent survival
Age (Days)
Np1+/+HexB+/+
Np1-/-HexB+/+
Np1+/+HexB-/-
Np1-/-HexB-/-
Righting Reflex Average
Righting Time (s)
Age (Weeks)
Body Mass
Mass (g)
Age (Weeks)
Rotarod Time
Time (s)
Age (Weeks)
Wire Hang
Time (s)
Age (Weeks)

Though no significant difference was found between the body masses of *Hexb*$^{-/-}$ and *Np1*$^{-/-}$*Hexb*$^{-/-}$ mice in our behavioural study (likely due to high variation in health of *Np1*$^{-/-}$*Hexb*$^{-/-}$ mice at 19 weeks of age), a larger data set demonstrates that *Hexb*$^{-/-}$ mice have a significant decrease in body mass relative to WT and *Np1*$^{-/-}$ controls (Fig. 4.4A). Once again there appears to be increased variation in the body condition of *Np1*$^{-/-}$*Hexb*$^{-/-}$ mice towards the expected endpoint.

Figure 4.4. Body mass is improved in Sandhoff mouse models by knockout of *Np1*.

The body mass and brain mass of *Hexb*$^{+/+}$, *Np1*$^{-/-}$*Hexb*$^{+/+}$, *Np1*$^{-/-}$*Hexb*$^{-/-}$ and *Hexb*$^{-/-}$ mice were measured at 100 and 120 days of age. **A.** Few differences are seen between genotypes at 100 days, but body mass of *Hexb*$^{-/-}$ mice declines relative to controls at 120 days, while that of *Np1*$^{-/-}$*Hexb*$^{-/-}$ does not. Letters indicate significance between respective groups at a given age ($P < 0.05$). Statistical analysis via ANOVA with Tukey's HSD or Dunnet's T3 post-hoc where appropriate.

Figure 4.4

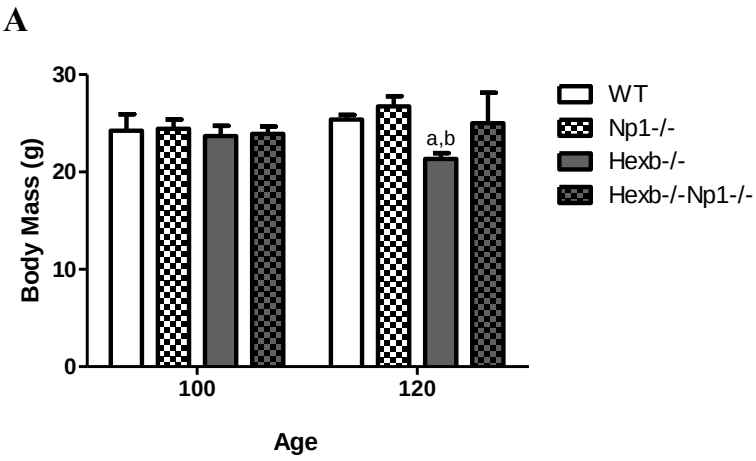

4.5.3 Markers for Gliosis and Apoptosis

Since outcomes of Sandhoff disease are widely known to be negatively influenced by astrogliosis and microgliosis, we sought to observe the effect of *Np1* knockout on these disease processes. Immunohistochemistry of cerebral cortex, cerebellar, and spinal tissues from 120 day *Hexb*$^{+/+}$, *Np1*$^{-/-}$*Hexb*$^{+/+}$, *Hexb*$^{-/-}$, and *Np1*$^{-/-}$ *Hexb*$^{-/-}$ mice reveals little if any difference in either microgliosis or astrogliosis in the CNS between *Hexb*$^{-/-}$ and *Np1*$^{-/-}$*Hexb*$^{-/-}$ mice, suggesting that *Np1* is not a major driving factor in these processes in the disease (Fig. 4.5). There is however, a large (though not significant) effect toward lower levels of TUNEL staining in the cerebellum, and cerebral cortex of *Np1*$^{-/-}$*Hexb*$^{-/-}$ mice, relative to *Hexb*$^{-/-}$. A similar pattern is seen in the cerebellum. These measurements suggest that, between *Hexb*$^{-/-}$ mice, there is high variability in the relative amount of apoptosis in the end-point stages of the disease, though the overall effect size is large.

Figure 4.5. Effect of *Hexb* and *Np1* Knockout on gliosis and apoptosis in the CNS of mice.

A. Representative images of GFAP and MAC3 staining in the anterior horn of thoracic spine sections. Bars = 50µM. **B.** Both *Hexb*$^{-/-}$ and *Np1*$^{-/-}$*Hexb*$^{-/-}$ mice present with higher counts for cells positive for markers for astrogliosis (GFAP) and microgliosis (MAC3) in the cerebellum, cerebral cortex and spine, relative to WT and *Np1*$^{-/-}$ mice. Though non-significant, a large effect size towards lower levels of apoptotic cells in *Np1*$^{-/-}$*Hexb*$^{-/-}$ relative to *Hexb*$^{-/-}$ mice is visible in the cerebral cortex. (a,b,c,d) indicate significance between respective groups, $P < 0.05$. Data are mean values +/- SE. n = 3 for each age, except for TUNEL cerebellar and cerebral cortex measurements; WT = 4, *Np1*$^{-/-}$ = 3, *Hexb*$^{-/-}$ = 7, *Np1*$^{-/-}$*Hexb*$^{-/-}$ = 3.

Figure 4.5

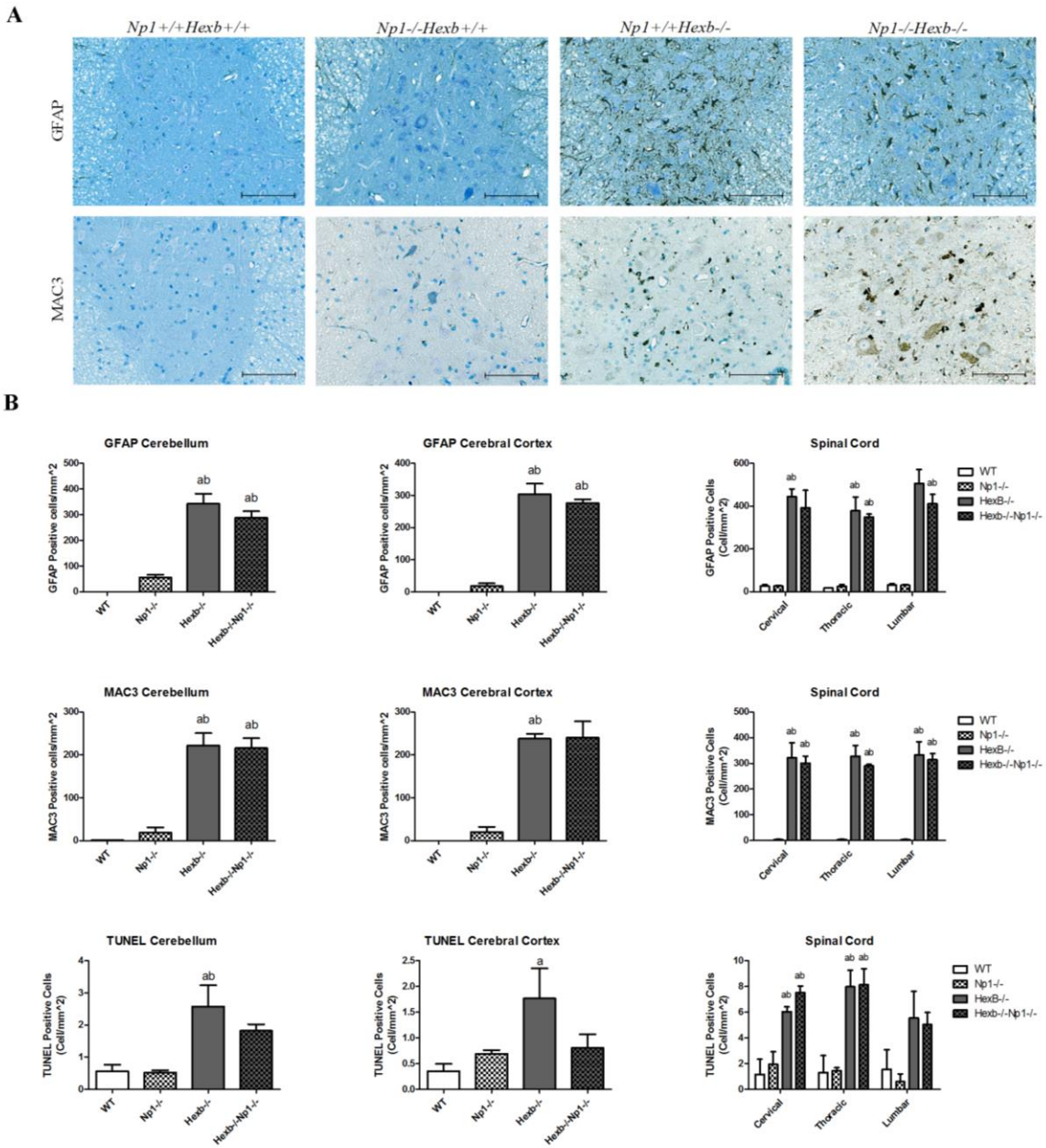
A
Np1+/+Hexb+/+
Np1-/-Hexb+/+
Np1+/+Hexb-/-
Np1-/-Hexb-/-
GFAP
MAC3
B
GFAP Cerebellum
GFAP Cerebral Cortex
Spinal Cord
MAC3 Cerebellum
MAC3 Cerebral Cortex
Spinal Cord
TUNEL Cerebellum
TUNEL Cerebral Cortex
Spinal Cord
GFAP Positive cells/mm^2
MAC3 Positive cells/mm^2
TUNEL Positive Cells (Cell/mm^2)
GFAP Positive Cells (Cell/mm^2)
MAC3 Positive Cells (Cell/mm^2)
WT
Np1-/-
HexB-/-
Hexb-/-Np1-/-
Cervical
Thoracic
Lumbar
ab
a

4.5.4 Knockout of NP1 Reduces Neuronal Dysregulation in Sandhoff Disease

Like the cerebellum, the hippocampus is well known to be pathologically affected in Sandhoff disease, presenting with GM2 accumulations, inflammation, apoptosis, impaired dendritic growth, calcium uptake inhibition, and impaired phospholipid production (Buccoliero et al., 2004; Jeyakumar et al., 1999; Jeyakumar et al., 2003; Kitakaze et al., 2016; Pelled et al., 2003a; Pelled et al., 2003b). Since neuronal pentraxins have been shown to be involved in long term depression through modulation of surface AMPARs in the hippocampus, we sought to observe the effect of NP1 knockout on AMPA and NMDA sensitivity of neurons through patch clamp recording (Cho et al., 2008). GABAergic responses were inhibited with the GABAR antagonist picrotoxin, and pyramidal neurons in of the CA1 region of the hippocampus were voltage-clamped at +40mV to measure combined AMPAR/NMDAR currents, and at -60mV to measure the contribution of AMPAR currents in response to stimulation of the CA3-CA1 pathway. Specificity of the currents was confirmed pharmacologically using the AMPAR and NMDAR antagonists CNQX and D-APV.

Measurements of total currents show a strong trend to differences in variability of current amplitude between groups (Levene's, P=0.068), suggesting glutamatergic currents are less tightly regulated in *Hexb* knockout mice than in controls, and that not all *Hexb*$^{-/-}$ neurons are affected concurrently (Fig. 4.6A). We also observe a trend of reduced amplitude AMPAR-mediated currents in *Hexb*$^{-/-}$ mice relative to controls (Fig. 4.6B). The reduction in AMPAR-mediated currents in *Hexb*$^{-/-}$ mice is consistent with a

reduction in GluR1 expression we have observed in the cerebella of these mice (Hooper and Igdoura, 2016). This may be attributed to either a reduction in the overall number of GluR1 receptors in affected neurons, or perhaps the selective death of GluR1-containing glutamatergic neurons. This reduction in AMPAR-mediated currents may be recovered by knockout of *Np1* (ANOVA, P = 0.135). Since NP1 has a negative effect on the survival of *Hexb*$^{-/-}$ mice, it would seem this loss of AMPARs is detrimental and not a mechanism of protection. AMPRA-mediated currents in *Hexb*$^{-/-}$ neurons were noticeably reduced at physiologically relevant membrane potentials of -60 mV (Fig. 4.6C).

Figure 4.6. Dysregulation of hippocampal excitatory currents in Sandhoff mice.

A. Total currents in hippocampal pyramidal neurons measured at +40mV reveal a trend toward differences in variation of currents strengths (Bars = Mean ± SE, Levene's, P = 0.068). This may be indicative of a dysregulation of currents in the neurons of Sandhoff mice. **B.** AMPA currents measured at –60mV present an interesting trend that indicates a reduction in AMPA currents in *Hexb*$^{-/-}$ mice, which appears to be rescued by knockout of *Np1* (Bars = Mean ± SE, ANOVA, P = 0.135). **C.** Representative current traces from hippocampal pyramidal neurons voltage clamped at +40 mV and –60mV, in the presence of picrotoxin. The *Hexb*$^{-/-}$ trace shows a lack of AMPA current when clamped at -60 mV.

Figure 4.6

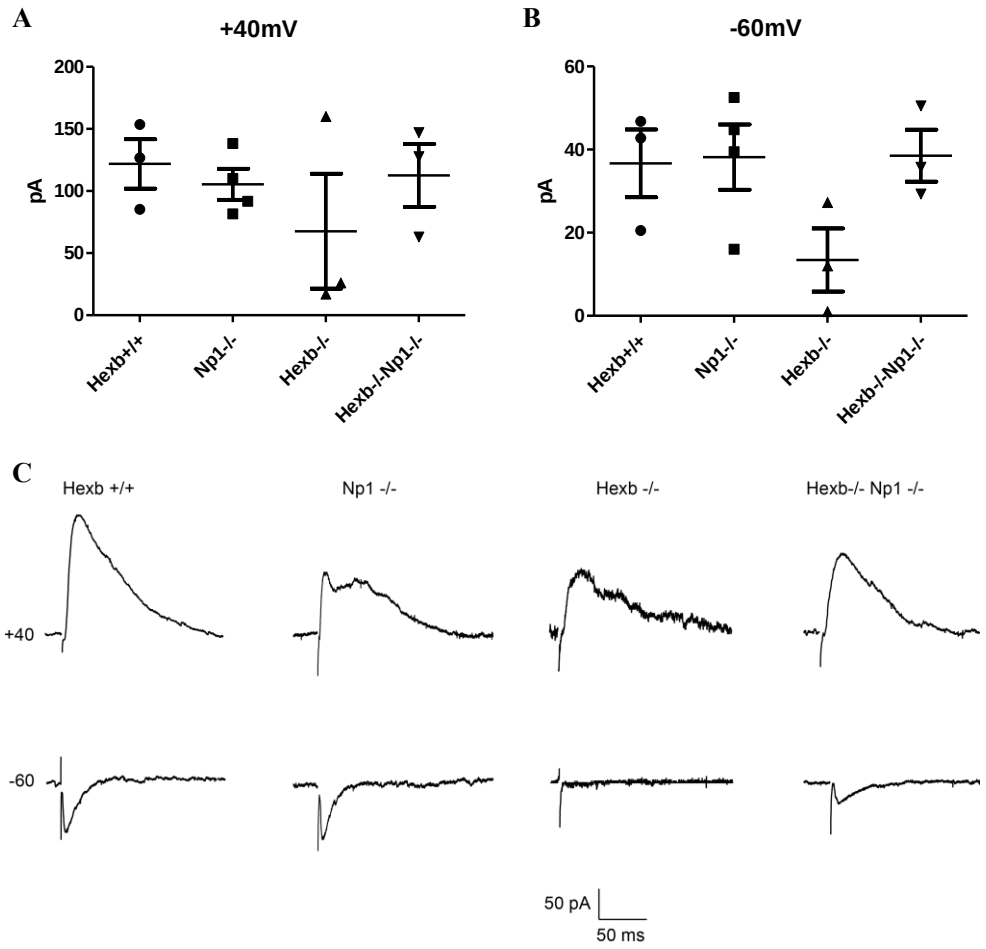
A
+40mV
pA
200
150
100
50
0
Hexb+/+
Np1-/-
Hexb-/-
Hexb-/-Np1-/-
B
-60mV
pA
60
40
20
0
Hexb+/+
Np1-/-
Hexb-/-
Hexb-/-Np1-/-
C
Hexb +/+
Np1 -/-
Hexb -/-
Hexb-/- Np1 -/-
+40
-60
50 pA
50 ms

To test whether the observed effects are due to increases or decreases in excitatory protein levels, western blots were performed on hippocampi and cerebella from 30 day old WT and *Hexb*$^{-/-}$ mice, for NP1-38, GluR1, and GluR2 (Fig. 4.7). An increase is seen in the levels of NP1 in the SD hippocampus, though- due to the small effect size- this difference could be present yet undetectable in the cerebellum, and may require a larger sample size to detect. NP1-38 is significantly upregulated for both tissues in SD mice at 30 days (Fig. 4.7C/G), while the measured glutamate receptors showed no difference between genotypes (Fig. 4.7D-E/H-I). This indicates that differences in neuronal excitability may be due to differences in subcellular receptor trafficking rather than raw protein increases/decreases, and verifies that absolute levels of GluR1 do not drop until late in the disease.

Figure 4.7. Synaptic protein levels in early mouse hippocampi and cerebella.

A. Representative images of Western blots of 30 day mouse hippocampus and cerebella. Western blot analysis reveals an increase in NP1 (**B**) in the hippocampus of *Hexb*$^{-/-}$ mice relative to WT mice, without a similar effect in the cerebellum. A large increase in NP1-38 is observed in the hippocampus (**C**) and cerebellum (**G**) of *Hexb*$^{-/-}$ mice relative to WT mice, but no differences are measured in either tissue for the AMPARs GluR1 (**D/H**) and GluR2 (**E/I**). (Bars = Mean ± SE, *P < 0.05).

Figure 4.7

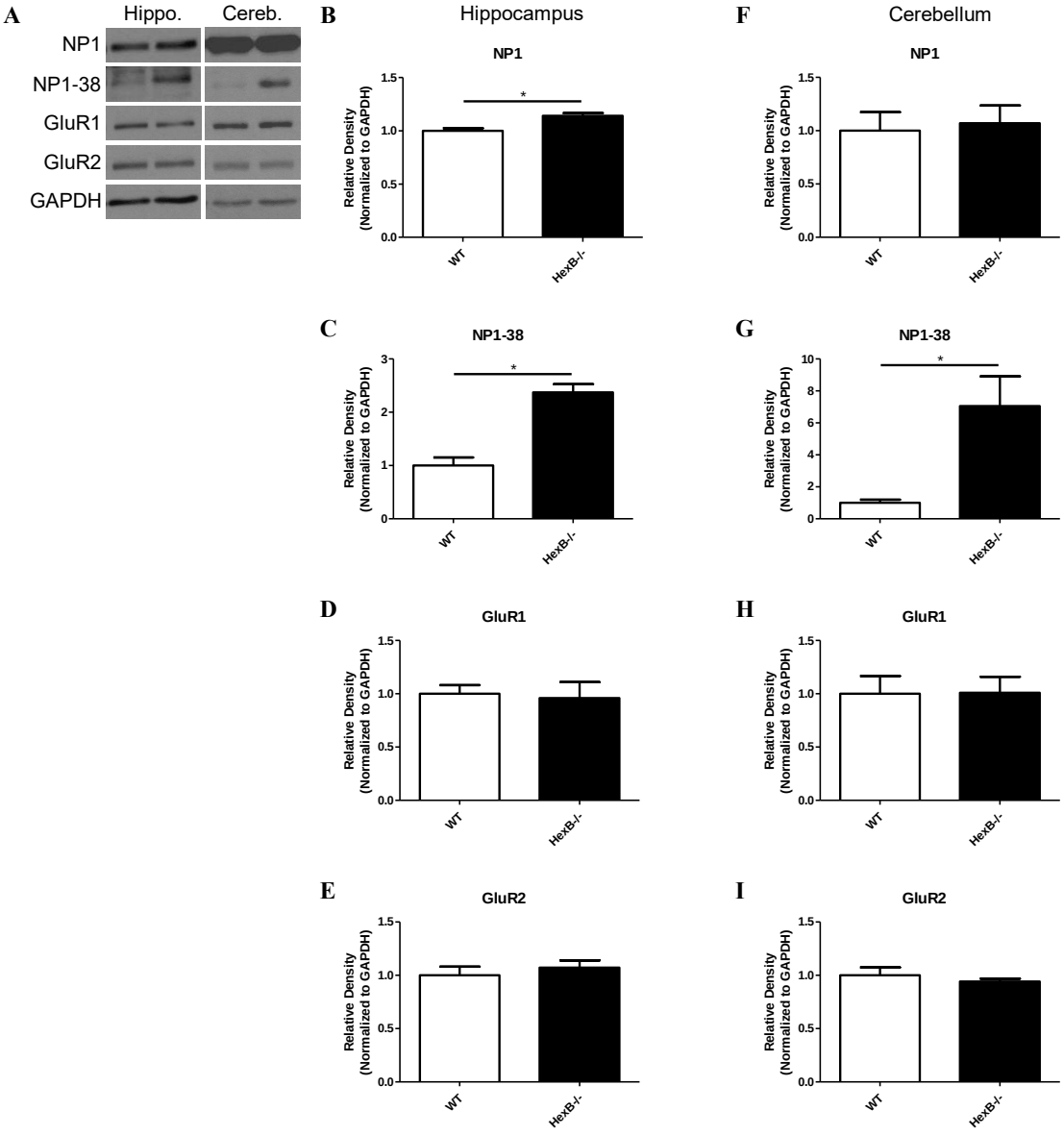
A
Hippo.
Cereb.
NP1
NP1-38
GluR1
GluR2
GAPDH
B
Hippocampus
NP1
C
NP1-38
D
GluR1
E
GluR2
F
Cerebellum
NP1
G
NP1-38
H
GluR1
I
GluR2
Relative Density (Normalized to GAPDH)
WT
HexB-/-
*

4.6 Discussion

4.6.1 A potentially novel isoform of Np1

The increased expression of *NP1* mRNA in Tay-Sachs disease patients, and *Np1* mRNA in Sandhoff disease mice strongly suggests a role for their gene products in lysosomal storage disorders- in both humans and mice. This finding also further validates that our *Hexb*$^{-/-}$ mouse is an accurate representation of human forms of these diseases.

The presence of NP1-38 essentially only in the disease state suggests a specific role in either disease progression or prevention. A separation from the more generalized functions of NP1 would make this an interesting target for manipulation, with limited disruption of normal cellular events. Though the role of this protein is currently unknown, identification of its modifications would give immediate clues to its function. Loss of the N-terminal neuronal pentraxin-neuronal pentraxin binding cysteines would point to a role absent NARP and NPR, since they could no longer bind each other. However, loss of the original N-terminal signal sequence would mean that NP1 does not pass through the ER-Golgi pathway, but maintenance of N-glycosylations suggests the N-terminus is not modified, at least until after passage through the Golgi apparatus. At this stage NP1 would already be bound to NARP and NPR via disulphide bonds near the N-terminus, making modification in this region of the protein difficult or ineffective. On the other hand, loss of the C-terminal AMPAR-binding 'pentraxin domain' would indicate a change in the ability to bind one of its canonical binding partners, including GluR1 or BAX (Al Rahim et al., 2013; Clayton et al., 2012). The ability of the protein to bind anti-

NP1 antibodies in denatured and non-denatured conditions, suggest that no large modifications or conformational changes occur towards the centre of the protein (the epitope for the antibody used). Together these data suggest that NP1-38 is modified at the C-terminus, leading to changes in its AMPAR binding behaviour (Fig. 4.8).

Figure 4.8. A model of neuronal pentraxin 1 interaction in Sandhoff disease.

In normal synapses, NP1 and NARP (anchored to the membrane by NPR) bind and cluster AMPARs at the synapse. In Sandhoff disease, however, NP1 is cleaved at the C-terminus and cannot bind AMPARs. This leads to a decrease in the concentration of AMPARs at the synapse and a reduction in AMPA currents, ultimately leading to neuronal decline. The cleaved portion of NP1-38 may also act as an antagonist for binding of normal neuronal pentraxin multimers, thereby further reducing the clustering of AMPARs.

Figure 4.8

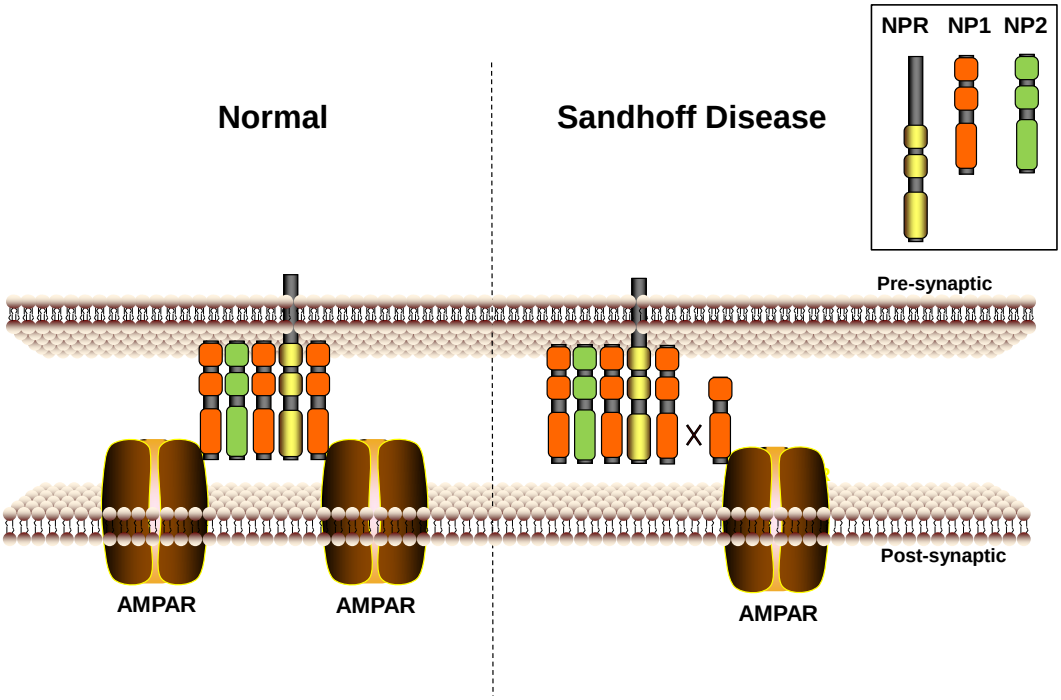
NPR
NP1
NP2
Normal
Sandhoff Disease
Pre-synaptic
X
Post-synaptic
AMPAR
AMPAR
AMPAR

4.6.2 Np1 reduces survival in Sandhoff Disease

Though its precise actions still need to be elucidated, it is clear that Np1 has a negative effect on survivability in Sandhoff disease. As these mice are on the same C57BL/6 background, it is unlikely to be an effect of other genetic differences. This appears to be linked to systems related to the righting reflex, such as the cerebellum, but not to other neuromotor systems. This is surprising, since in many cases of knockout genes improving lifespan, mice improved performance in behaviour testing, including wire hang and rotarod. In these cases, the increases in lifespan were quite large, however; and perhaps any other behavioural improvements in *Np1*$^{-/-}$*Hexb*$^{-/-}$ over *Hexb*$^{-/-}$ mice are too subtle for statistical detection. It is also possible that since the cerebellum is known to be severely affected in the disease, and thus has a high level of cell death, that it is also sensitive/responsive to treatments related to neuronal death (Abo-Ouf et al., 2013; Huang et al., 1997).

4.6.3 Effect of Np1 on Hexb-/- Neuronal Excitation

The observed dysregulation of total currents in the hippocampus of our Sandhoff mice is consistent with reports suggesting an association between dysregulation of the glutamatergic system in the hippocampus and presentation of mood disturbances in patients with bipolar disorder (Chitty et al., 2015; Ng et al., 2009). Since patients with LOTS present with bipolar-like mood disturbances, this may indicative of a common pathophysiology. The apparent recovery of glutamate receptor regulation in our *Np1*$^{-/-}$

Hexb$^{-/-}$ mouse suggests that *Np1* may play a role in mood affect in Tay-Sachs disease, if not in other mood disorders such as bipolar disorder.

The potential reduction in AMPA specific currents in *Hexb*$^{-/-}$ mouse hippocampi appears to be an effect of the presence of NP1. This is consistent with a reduction of GluR1we have observed in the cerebellum of *Hexb*$^{-/-}$ mice towards endpoint (Hooper and Igdoura, 2016). Since NP1 has a negative effect on the survival of *Hexb*$^{-/-}$ mice, it would seem this loss of AMPARs is detrimental and not protective. Though we do not see an increase in NP1 levels aside from a slight increase in the hippocampus of *Hexb*$^{-/-}$ mice at 30 days, we observe a large increase in NP1-38 levels in both the hippocampus and the cerebellum. Both of these brain areas also have similar pathologies involving inflammation, apoptosis, and a late-stage increase in major histocompatibility complex class II molecules (MHC class II), suggesting a common disease mechanism leading to the deterioration of the righting reflex and survival (Jeyakumar et al., 2003). In rats, NP1 has been shown to upregulate and colocalize with GluR1 in response to hypoxic-ischemic brain injury. This association was also shown to be directly responsible for AMPAR-mediated cell death in mouse hippocampal neurons during hypoxic-ischemic conditions, suggesting excitotoxicity as a cause (Al Rahim et al., 2013; Hossain et al., 2004; Thatipamula and Hossain, 2014). On the other hand, in Alzheimer's disease, the build-up of amyloid-β leads to lower synapse activity and ultimately apoptosis of transmitter-specific neurons through a mechanism involving NP1 (Abad et al., 2006; Kamenetz et al., 2003). Similar effects may be causing the death of excitatory neurons in SD after

ganglioside build-up interferes with function of their AMPARs, leading to the decline of glutamate receptors later in life. Other possibilities include that NP1/NP1-38 produced by neurons exposed to TNFα may be recruiting GluR1 to the cell surface, and depleting internal GluR1 stores, or perhaps is regulating GluR1 levels via receptor internalization, or synaptic phagocytosis by microglia- signalled via the complement protein C1q (Cho et al., 2008; Gasque et al., 2000; Kreutzberg et al., 1989; Ogoshi et al., 2005; Stevens et al., 2007). The internalization of AMPARs, and the involvement of C1q seem unlikely, however, since GluR1 and GluR2 levels do not drop directly in correlation with early NP1-38 increases (Hooper and Igdoura, 2016). Regardless of the underlying mechanism, if NP1 or NP1-38 are causing the dysregulation/death of AMPAR containing neurons, then limiting their expression may be a useful treatment to promote the maintenance of functional neurons.

Although we observe changes in glutamate signalling in the hippocampus of our mice at a very early stage, we do not see a decline in glutamate receptor protein or overall health until near the endpoint of the mice (Hooper and Igdoura, 2016). Thus, the effects of the glutamatergic dysregulation are likely to be chronic and develop over a period of time, and will therefore have a larger effect in chronic/late onset forms of Tay-Sachs and Sandhoff disease.

4.6.4 Effect of Np1 knockout on pathological markers

While no significant differences were found between *Np1*$^{-/-}$*Hexb*$^{-/-}$ and *Hexb*$^{-/-}$ mice in measures of markers for gliosis or apoptosis, this is not entirely unexpected at 120 days

of age, where variation in behaviour and protein levels increases, as mice reach endpoint. NP1 has been reported to be present in astrocytes but its level of expression does not change in concordance with a rise in astrogliosis markers, which rise at approximately 100 days (Hooper and Igdoura, 2016; Wang et al., 2012). If NP1-38 was being produced inside activated astrocytes, we would expect similar temporal patterns of expression for the two proteins, but this is not the case. Other mouse studies have shown that a detrimental NP1 response to ischemic brain injury does not colocalize directly with astrocytes, which is consistent with these findings (Thatipamula et al., 2014). Since the effect of NP1 does not appear to be directly linked to levels of CNS inflammation, this may indicate a separate pathway for treatment, alongside inflammation management systems. Macrophages are activated as early as 60 days in *Hexb*$^{-/-}$ mice, consistent with increased levels of NP1-38 (Hooper and Igdoura, 2016). Whether NP1-38 is produced by the activated macrophages, or interacts with them though a mediator such as C1q, remains to be investigated. If NP1 is not acting through microglia or astrocytes, it may be increasing apoptosis by affecting the sensitivity of neurons to excitatory stimuli, or enhancing the direct mechanisms of apoptosis, including mitochondrial function.

4.7 Conclusions

We have identified a novel form of neuronal pentraxin 1, NP1-38, in Sandhoff disease mice, expressed in several brain regions highly affected by the disease. It is evident that NP1 and/or NP1-38 negatively influence health and survival in Sandhoff

disease, apparently through dysregulation of AMPAR function. This dysregulation may play a greater role in chronic and late-onset forms of the disease. Most research into this disease has been focused on inflammation and astrogliosis, but these findings present a new insight and focus on the dysfunction of neurons in Sandhoff disease. The apparent dissociation of this pathway from the inflammatory pathways may allow for concurrent medical interventions alongside those for inflammation, thus increasing potency of treatment.

CHAPTER 5: Discussion and Conclusions

5.1 General Review

Sandhoff disease and Tay-Sachs disease are difficult to treat, complex neurological disorders. They are classically defined by dysfunction of ganglioside metabolism, lysosomal storage, and increased inflammation (Sandhoff et al., 1971; Wada et al., 2000). Identifying novel disease mechanisms and understanding the interplay between these and aforementioned disease processes, will allow for better patient treatment and quality of life.

By manipulation of TNFα through the generation of a *Hexb*$^{-/-}$*Tnfα*$^{-/-}$ mouse, we have shown that TNFα is responsible for neuroinflammation of microglia and astroglia, and its knockout reduces neuronal apoptosis, as well as extends the lifespan of Sandhoff mice. The effect of TNFα removal appears to be greater on astrocytes than on microglia, though this may be due to the timepoint chosen for observation. We have also revealed, through bone-marrow transplantation, that CNS-derived TNFα is more crucial to the disease than that derived from the blood, indicating the importance of treatment delivery beyond the blood-brain barrier.

The focus of studies on microgliosis and astrogliosis have led to many advances in our understanding of the progress of these diseases and methods to treat them, but the interplay between these processes has not been fully explored, nor has the contribution of neurological factors to the disease. Through our work, we have established a timeline for the onset of these factors, highlighting a critical period of

decline and neuronal apoptosis in our mouse model, which involves not only astrogliosis, but a decline in AMPARs as well. This study highlights the observable temporal separation of microgliosis and astrogliosis, and suggests that while microgliosis is certainly a strong initiating factor, astrogliosis is more intimately linked to the ruinous terminal-stages of the disease. The reduction in AMPARs indicates a specific neuronal path that is affected, rather than an overall decline, which likely means a specific, targetable negative process is occurring.

By generation of a *Hexb*$^{-/-}$*Np1*$^{-/-}$ mouse, we have demonstrated that the synaptic protein NP1 plays a detrimental role in the health and behaviour of Sandhoff mice. Mice without Np1 display better performance on behavioural tasks, maintain higher body weights, and live significantly longer than their *Hexb*$^{-/-}$ counterparts. We have also demonstrated a dysregulation of glutamate signalling in the CNS of SD mice, that appears to be rescued by knockout of Np1. We also observe a smaller, novel form of NP1, NP1-38, which is upregulated early in the disease. Due to the difference in expression of this protein between WT and SD mice, it stands to reason that this may be the form of the protein responsible for the detriments observed, though this remains to be investigated.

Our work in mouse models has allowed us to study the disease in its natural and complex state. This work is important in that it identifies new neuronal factors including neuronal pentraxin 1 and GluR1 that should be considered as therapeutic targets, alongside those for inflammatory pathways. It also demonstrates that there are critical

periods for treatments of specific pathways, and highlights that the disease is progressing long before symptoms appear.

5.2 Analysis, Future Directions, and Limitations

In our first study we examined the role of TNFα on the outcome of Sandhoff disease. We identified TNFα as a major factor in the neurodegeneration of our mouse model due to increased lifespan and behaviour testing in our *Hexb*$^{-/-}$*Tnfα*$^{-/-}$ mice.

We also identify that the presence of TNFα increased apoptosis and the presence of activated astrocytes. It is unclear whether the reduction of astrogliosis occurs through TNFα-KO directly, or via a downregulation of other microglial signalling, a matter which requires further investigation. However, TNFα is known to cause the activation of the STAT3 pathway, and the reduced astrogliosis which is seen in the *Hexb*$^{-/-}$*Tnfα*$^{-/-}$ mice, appears to be through reduced STAT3 signaling (Yadav et al., 2005). Unfortunately *Stat3* knockout is lethal at an early embryonic stage of development and so future studies observing the effects of its reduction would need to be based on a conditional reduction, or another stage in this pathway (Takeda et al., 1997).

It is surprising that JAK2 phosphorylation was reduced in the *Hexb*$^{-/-}$ mice, since exposure to TNFα can cause an increase in the activation of STAT3 through TNFR1/JAK2 association (Pincheira et al., 2008). However, after prolonged exposure this association is reduced, so it is possible that constantly high levels of TNFα have an overall effect of lowering cellular JAK2. Measurement of co-immunoprecipitated cerebellar or cultured neuronal TNFα and JAK2 at several time points in the lifetime of WT and *Hexb*$^{-/-}$ mice

could help to explain this. Bone marrow transplantation revealed that our *Hexb*$^{-/-}$*Tnfα*$^{-/-}$ mice receiving bone marrow from *Hexb*$^{-/-}$*Tnfα*$^{+/+}$ mice had better behaviour performance than *Hexb*$^{-/-}$*Tnfα*$^{+/+}$ mice receiving *Hexb*$^{-/-}$*Tnfα*$^{-/-}$ mice receiving bone marrow. Whether this demonstrates that TNF expressed from immune cells within the CNS is of greater importance than that expressed from bone marrow derived cells, or that the age of onset of TNFα exposure is a major predictive prognosis factor, has yet to be completely determined and deserves further investigation. While it is sensible that age of initial treatment would play a large role in treatment outcome, and there are animal studies and patient case studies that suggest age of treatment plays a significant factor, if the targeted system (CNS vs. periphery) plays a role in treatment success, then it would inform decisions on therapeutic tissue transplants, and drug delivery(Sargeant et al., 2012; Tallaksen and Berg, 2009; Wortmann et al., 2009). We have also identified the NIK mediated non-canonical NF-kB pathway as a target for TNFα in SD mice. NIK is normally at low levels in healthy cells, so a downregulation would be expected to be well tolerated (Sheng et al., 2012). Although germline knockout of *Nik* produces metabolic issues, there are several NIK inhibitors already developed, and conditional deletion of *Nik* in adult mice appears to be effective as well (Brightbill et al., 2015; Demchenko et al., 2014; Mortier et al., 2010; Sheng et al., 2012). These tools could allow for treatment more specific than that of treating the upstream TNFα, which likely means fewer side effects.

In our second study we analyzed the interplay between microgliosis, astrogliosis, apoptosis and neuronal dysfunction. We identified a specific and intense period of decline in our Sandhoff mouse model beginning between 80 and 100 days of age. This is consistent with a reduction in behaviour beginning in this time point, and appears to involve an increase in astrogliosis, cleaved capsase-9 induction, and a reduction in GluR1, while microgliosis occurred as early as 60 days, and persists through end-point.

It remains to be seen if this process of failure is initiated by the chronic microgliosis, or if another factor, such as a critical buildup of ganglioside, or general metabolic dysfunction is the catalyzing element. This study can be repeated in a mouse model with a knockout in genes known to increase microgliosis, such as *Tnfα*, *Mip1*, *Ccr2*, to see if a delay in astrogliosis and GluR1 reduction occurs. As has been noted, it has been shown that astrocytes in Sandhoff disease cells appear to be dysfunctional, regardless of ganglioside buildup, but whether this is the same mechanism causing the sharp incline in astrocyte proliferation toward the end of the disease remains to be seen (Kyrkanides et al., 2012).

While neuronal death was expected in the our model, the specific reduction of GluR1, independent of various other associated neuronal proteins, such as PSD-95 is of interest. This is suggestive of the reduction being not due solely to generalized neuronal death. Either GluR1 specific containing neurons are being killed specifically or the protein is being regulated. Cerebellar tissue from near-endpoint *Hexb*$^{-/-}$ and age-matched WT mice could undergo immunofluorescent staining for GluR1 and caspases, to determine if Glur1 containing neurons specifically have an increase in caspase/GluR1 colocalization.

This would also be useful to observe the localization and concentration of GluR1 in the neurons, to give hints at whether it is being regulated spatially or by quantity. It would of therapeutic interest to identify whether the GluR1 reduction is a protective mechanism, detrimental factor, or merely a symptom. While it could prove confounding to regulate GluR1 expression safely due to its knockout mice displaying schizophrenic-related behaviours, it could be possible to control the functions of GluR1 that are causing this change (Wiedholz et al., 2008). GluR1/GluR2 heteromeric AMPARs can be specifically antagonized with philanthotoxin-7,4 (PhTx-74), allowing for a dose-controlled method to test the effect of GluR1 stimulation on *Hexb*$^{-/-}$ neuronal survivability (Nilsen and England, 2007).

Our third study identifies the detrimental role of NP1 in our Sandhoff mouse model, despite little measurable difference from WT in the 50kDA form, and identifies a potentially new isoform of NP1- NP1-38- which is upregulated in the disease.

Though this work outlines the basic size and features of this protein, there is much work to be done to discover its functions, molecular associations, and generation.

Since the 38kDa form is generated from the same gene as the 50kDa form, it is difficult to delineate its role simply from the knockout. If its generation can be determined to be from alternate transcript, then cloning or knock-in studies can be used to identify its roles. If it generated from protein, then the gene could be expressed in an edited form to produce the 38kDa protein, or it could be upregulated and downregulated by manipulation of the enzymes that produce it. Issues may arise in the expression of NP1-

38 if it does, in fact, serve a cytotoxic role, and it may need to be expressed conditionally, or require enzymatic cleaving for activation. The electrophysiology study outlined here adds evidence to the development of dysfunctional AMPARs in Sandhoff disease, which could be the process leading to the observed reduction at endpoint in our SD mice. *Hexb*$^{-/-}$ mice appear to have reduced AMPAR function as well as highly variable NMDAR function, and comparison of calcium imaging from WT and *Hexb*$^{-/-}$ cerebellar or hippocampal neurons would help define this finding. There are technical difficulties involved with clamping of *ex vivo* neurons at the age of mice used in this study, 3-4 weeks of age. As such, variance can be high in unhealthy neurons leaving statistics difficult to perform. With the baseline measurements established here and showing differences between genotypes, it could be of benefit to repeat the experiment on younger mice, to determine if differences can be measured at the very earliest stages of the disease. Clamping of cultured SD neurons may also be useful to delineate the effects of the disease on neuronal receptors, though the effects of chronic ganglioside build-up may be difficult to determine this way if the effects do no onset rapidly. Mixed cultures may be required to simulate the *in vivo* relationships seen between neurons, microglia, and astrocytes, since the cause of the receptor deficit is unknown and could be produced through translational or transcriptional regulation, through neuronal death, through synaptic removal by microglia, or some excitotoxic events involving astrocytes.

5.3 Clinical Implications and Perspectives

The treatments for Sandhoff disease and Tay-Sachs disease are unavailable (e.g. chaperones), or invasive/potentially dangerous (e.g. bone marrow transplants). We have identified several targets that may be possible to treat via administration of drugs. TNFα can be inhibited by thalidomide and bupropion- already available drugs (Brustolim et al., 2006). Inhibitors are under research for STAT3 inhibition, as a target for cancer treatment. While no effective inhibitors have yet been created, cancer research is a large and funded field, so a common target offers hope for discovery of alternative treatments for SD and TSD.

By identifying the timeline for the processes of microgliosis and astrogliosis, we have highlighted the importance of treating microgliosis early in the disease. Though more research is required, it would appear that treating astrogliosis early may not be as important as in the later stages of the disease, but should be treated aggressively towards the end of the disease, since it appears to be involved in the final neurological decline.

We also demonstrate the involvement of several neuronal/synaptic proteins in the disease. Previous work and treatments all involve the treatment of metabolic and inflammatory dysfunction. By ignoring the neuronal components, potential treatments are being put the wayside. By demonstrating a separation/interaction of several disease processes, our work suggests the additive benefits of multiple concurrent treatments for the various cellular pathways. The additive benefit of simultaneous treatments can

already be seen in the co-administration of substrate deprivation and diet restriction (Denny et al., 2010).

5.4 Conclusion

Our works provides further insights into the roles of various inflammatory and pro-apoptotic cytokines, including TNFα, in Sandhoff disease. We show that this readily-treatable molecule plays a role in both astrogliosis and survivability. We have demonstrated that both peripheral and CNS derived-TNFα are of importance in the disease, and may be targets for treatment.

We have teased apart the interconnected cellular pathways of Sandhoff disease and Tay-Sachs disease, and shown that treatment of any one is not a catch all solution to the illness. We emphasize the need for a multi-faceted treatment of disease symptoms.

We have also identified a novel target for study (NP1-38), which is not only of interest in the disease, but as an unrecognized protein. The documented role of NP1 in other neurodegenerative diseases, such as Alzheimer's disease, means this protein could be of great importance to neurology and medicine.

LIST OF REFERENCES

Abad, M.A., Enguita, M., DeGregorio-Rocasolano, N., Ferrer, I., Trullas, R., 2006. Neuronal pentraxin 1 contributes to the neuronal damage evoked by amyloid-beta and is overexpressed in dystrophic neurites in Alzheimer's brain. J Neurosci 26, 12735-12747.

Abo-Ouf, H., Hooper, A.W., White, E.J., van Rensburg, H.J., Trigatti, B.L., Igdoura, S.A., 2013. Deletion of tumor necrosis factor-alpha ameliorates neurodegeneration in Sandhoff disease mice. Hum Mol Genet 22, 3960-3975.

Adamali, H.I., Somani, I.H., Huang, J.Q., Mahuran, D., Gravel, R.A., Trasler, J.M., Hermo, L., 1999. I. Abnormalities in cells of the testis, efferent ducts, and epididymis in juvenile and adult mice with beta-hexosaminidase A and B deficiency. J Androl 20, 779-802.

Akeboshi, H., Chiba, Y., Kasahara, Y., Takashiba, M., Takaoka, Y., Ohsawa, M., Tajima, Y., Kawashima, I., Tsuji, D., Itoh, K., Sakuraba, H., Jigami, Y., 2007. Production of recombinant beta-hexosaminidase A, a potential enzyme for replacement therapy for Tay-Sachs and Sandhoff diseases, in the methylotrophic yeast Ogataea minuta. Appl Environ Microbiol 73, 4805-4812.

Akiyama, H., Barger, S., Barnum, S., Bradt, B., Bauer, J., Cole, G.M., Cooper, N.R., Eikelenboom, P., Emmerling, M., Fiebich, B.L., Finch, C.E., Frautschy, S., Griffin, W.S., Hampel, H., Hull, M., Landreth, G., Lue, L., Mrak, R., Mackenzie, I.R., McGeer, P.L., O'Banion, M.K., Pachter, J., Pasinetti, G., Plata-Salaman, C., Rogers,

J., Rydel, R., Shen, Y., Streit, W., Strohmeyer, R., Tooyoma, I., Van Muiswinkel, F.L., Veerhuis, R., Walker, D., Webster, S., Wegrzyniak, B., Wenk, G., Wyss-Coray, T., 2000. Inflammation and Alzheimer's disease. Neurobiol Aging 21, 383-421.

Al Rahim, M., Thatipamula, S., Hossain, M.A., 2013. Critical role of neuronal pentraxin 1 in mitochondria-mediated hypoxic-ischemic neuronal injury. Neurobiol Dis 50, 59-68.

Andersson, U., Smith, D., Jeyakumar, M., Butters, T.D., Borja, M.C., Dwek, R.A., Platt, F.M., 2004. Improved outcome of N-butyldeoxygalactonojirimycin-mediated substrate reduction therapy in a mouse model of Sandhoff disease. Neurobiol Dis 16, 506-515.

Arthur, J.R., Lee, J.P., Snyder, E.Y., Seyfried, T.N., 2012. Therapeutic effects of stem cells and substrate reduction in juvenile Sandhoff mice. Neurochem Res 37, 1335-1343.

Baek, R.C., Kasperzyk, J.L., Platt, F.M., Seyfried, T.N., 2008. N-butyldeoxygalactonojirimycin reduces brain ganglioside and GM2 content in neonatal Sandhoff disease mice. Neurochem Int 52, 1125-1133.

Bley, A.E., Giannikopoulos, O.A., Hayden, D., Kubilus, K., Tifft, C.J., Eichler, F.S., 2011. Natural history of infantile G(M2) gangliosidosis. Pediatrics 128, e1233-1241.

Boles, D.J., Proia, R.L., 1995. The molecular basis of HEXA mRNA deficiency caused by the most common Tay-Sachs disease mutation. Am J Hum Genet 56, 716-724.

Bovolenta, P., Wandosell, F., Nieto-Sampedro, M., 1993. Neurite outgrowth inhibitors associated with glial cells and glial cell lines. Neuroreport 5, 345-348.

Bradbury, A.M., Cochran, J.N., McCurdy, V.J., Johnson, A.K., Brunson, B.L., Gray-Edwards, H., Leroy, S.G., Hwang, M., Randle, A.N., Jackson, L.S., Morrison, N.E., Baek, R.C., Seyfried, T.N., Cheng, S.H., Cox, N.R., Baker, H.J., Cachon-Gonzalez, M.B., Cox, T.M., Sena-Esteves, M., Martin, D.R., 2013. Therapeutic response in feline sandhoff disease despite immunity to intracranial gene therapy. Mol Ther 21, 1306-1315.

Brightbill, H.D., Jackman, J.K., Suto, E., Kennedy, H., Jones, C., 3rd, Chalasani, S., Lin, Z., Tam, L., Roose-Girma, M., Balazs, M., Austin, C.D., Lee, W.P., Wu, L.C., 2015. Conditional Deletion of NF-kappaB-Inducing Kinase (NIK) in Adult Mice Disrupts Mature B Cell Survival and Activation. J Immunol 195, 953-964.

Brustolim, D., Ribeiro-dos-Santos, R., Kast, R.E., Altschuler, E.L., Soares, M.B., 2006. A new chapter opens in anti-inflammatory treatments: the antidepressant bupropion lowers production of tumor necrosis factor-alpha and interferon-gamma in mice. Int Immunopharmacol 6, 903-907.

Buccoliero, R., Bodennec, J., Van Echten-Deckert, G., Sandhoff, K., Futerman, A.H., 2004. Phospholipid synthesis is decreased in neuronal tissue in a mouse model of Sandhoff disease. J Neurochem 90, 80-88.

Cachon-Gonzalez, M.B., Wang, S.Z., Ziegler, R., Cheng, S.H., Cox, T.M., 2014. Reversibility of neuropathology in Tay-Sachs-related diseases. Hum Mol Genet 23, 730-748.

Chiricozzi, E., Niemir, N., Aureli, M., Magini, A., Loberto, N., Prinetti, A., Bassi, R., Polchi, A., Emiliani, C., Caillaud, C., Sonnino, S., 2014. Chaperone therapy for GM2 gangliosidosis: effects of pyrimethamine on beta-hexosaminidase activity in Sandhoff fibroblasts. Mol Neurobiol 50, 159-167.

Chitty, K.M., Lagopoulos, J., Hickie, I.B., Hermens, D.F., 2015. Investigating the role of glutathione in mismatch negativity: An insight into NMDA receptor disturbances in bipolar disorder. Clin Neurophysiol 126, 1178-1184.

Cho, R.W., Park, J.M., Wolff, S.B., Xu, D., Hopf, C., Kim, J.A., Reddy, R.C., Petralia, R.S., Perin, M.S., Linden, D.J., Worley, P.F., 2008. mGluR1/5-dependent long-term depression requires the regulated ectodomain cleavage of neuronal pentraxin NPR by TACE. Neuron 57, 858-871.

Clarke, J.T., Mahuran, D.J., Sathe, S., Kolodny, E.H., Rigat, B.A., Raiman, J.A., Tropak, M.B., 2011. An open-label Phase I/II clinical trial of pyrimethamine for the treatment of patients affected with chronic GM2 gangliosidosis (Tay-Sachs or Sandhoff variants). Mol Genet Metab 102, 6-12.

Clayton, K.B., Podlesniy, P., Figueiro-Silva, J., Lopez-Domenech, G., Benitez, L., Enguita, M., Abad, M.A., Soriano, E., Trullas, R., 2012. NP1 regulates neuronal activity-dependent accumulation of BAX in mitochondria and mitochondrial dynamics. J Neurosci 32, 1453-1466.

DeGregorio-Rocasolano, N., Gasull, T., Trullas, R., 2001. Overexpression of neuronal pentraxin 1 is involved in neuronal death evoked by low K(+) in cerebellar granule cells. J Biol Chem 276, 796-803.

Demchenko, Y.N., Brents, L.A., Li, Z., Bergsagel, L.P., McGee, L.R., Kuehl, M.W., 2014. Novel inhibitors are cytotoxic for myeloma cells with NFkB inducing kinase-dependent activation of NFkB. Oncotarget 5, 4554-4566.

Denny, C.A., Heinecke, K.A., Kim, Y.P., Baek, R.C., Loh, K.S., Butters, T.D., Bronson, R.T., Platt, F.M., Seyfried, T.N., 2010. Restricted ketogenic diet enhances the therapeutic action of N-butyldeoxynojirimycin towards brain GM2 accumulation in adult Sandhoff disease mice. J Neurochem 113, 1525-1535.

Denny, C.A., Kasperzyk, J.L., Gorham, K.N., Bronson, R.T., Seyfried, T.N., 2006. Influence of caloric restriction on motor behavior, longevity, and brain lipid composition in Sandhoff disease mice. J Neurosci Res 83, 1028-1038.

Dreyfus, J.C., Poenaru, L., Vibert, M., Ravise, N., Boue, J., 1977. Characterization of a variant of beta-hexosaminidase: "hexosaminidase Paris". Am J Hum Genet 29, 287-293.

Fontaine, V., Mohand-Said, S., Hanoteau, N., Fuchs, C., Pfizenmaier, K., Eisel, U., 2002. Neurodegenerative and neuroprotective effects of tumor Necrosis factor (TNF) in retinal ischemia: opposite roles of TNF receptor 1 and TNF receptor 2. J Neurosci 22, RC216.

Gasque, P., Dean, Y.D., McGreal, E.P., VanBeek, J., Morgan, B.P., 2000. Complement components of the innate immune system in health and disease in the CNS. Immunopharmacology 49, 171-186.

Giove, T.J., Sena-Esteves, M., Eldred, W.D., 2010. Transduction of the inner mouse retina using AAVrh8 and AAVrh10 via intravitreal injection. Exp Eye Res 91, 652-659.

Grunseich, C., Schindler, A.B., Chen, K.L., Bakar, D., Mankodi, A., Traslavina, R., Ray-Chaudhury, A., Lehky, T.J., Baker, E.H., Maragakis, N.J., Tifft, C.J., Fischbeck, K.H., 2015. Peripheral neuropathy in a family with Sandhoff disease and SH3TC2 deficiency. J Neurol 262, 1066-1068.

Gulinello, M., Chen, F., Dobrenis, K., 2008. Early deficits in motor coordination and cognitive dysfunction in a mouse model of the neurodegenerative lysosomal storage disorder, Sandhoff disease. Behav Brain Res 193, 315-319.

Hoogerbrugge, P.M., Brouwer, O.F., Bordigoni, P., Ringden, O., Kapaun, P., Ortega, J.J., O'Meara, A., Cornu, G., Souillet, G., Frappaz, D., et al., 1995. Allogeneic bone marrow transplantation for lysosomal storage diseases. The European Group for Bone Marrow Transplantation. Lancet 345, 1398-1402.

Hooper, A.W.M., Igdoura, S.A., 2016. Bi-phasic gliosis drives neuropathology in a Sandhoff disease mouse model. Journal of Neuroimmunology, in press.

Hossain, M.A., 2008. Hypoxic-ischemic injury in neonatal brain: involvement of a novel neuronal molecule in neuronal cell death and potential target for neuroprotection. Int J Dev Neurosci 26, 93-101.

Hossain, M.A., Russell, J.C., O'Brien, R., Laterra, J., 2004. Neuronal pentraxin 1: a novel mediator of hypoxic-ischemic injury in neonatal brain. J Neurosci 24, 4187-4196.

Huang, J.Q., Trasler, J.M., Igdoura, S., Michaud, J., Hanal, N., Gravel, R.A., 1997. Apoptotic cell death in mouse models of GM2 gangliosidosis and observations on human Tay-Sachs and Sandhoff diseases. Hum Mol Genet 6, 1879-1885.

Hynd, M.R., Scott, H.L., Dodd, P.R., 2004. Glutamate-mediated excitotoxicity and neurodegeneration in Alzheimer's disease. Neurochem Int 45, 583-595.

Igdoura, S.A., Mertineit, C., Trasler, J.M., Gravel, R.A., 1999. Sialidase-mediated depletion of GM2 ganglioside in Tay-Sachs neuroglia cells. Hum Mol Genet 8, 1111-1116.

Itoh, H., Tanaka, J., Morihana, Y., Tamaki, T., 1984. The fine structure of cytoplasmic inclusions in brain and other visceral organs in Sandhoff disease. Brain Dev 6, 467-474.

Jeyakumar, M., Butters, T.D., Cortina-Borja, M., Hunnam, V., Proia, R.L., Perry, V.H., Dwek, R.A., Platt, F.M., 1999. Delayed symptom onset and increased life expectancy in Sandhoff disease mice treated with N-butyldeoxynojirimycin. Proc Natl Acad Sci U S A 96, 6388-6393.

Jeyakumar, M., Norflus, F., Tifft, C.J., Cortina-Borja, M., Butters, T.D., Proia, R.L., Perry, V.H., Dwek, R.A., Platt, F.M., 2001. Enhanced survival in Sandhoff disease mice receiving a combination of substrate deprivation therapy and bone marrow transplantation. Blood 97, 327-329.

Jeyakumar, M., Smith, D., Eliott-Smith, E., Cortina-Borja, M., Reinkensmeier, G., Butters, T.D., Lemm, T., Sandhoff, K., Perry, V.H., Dwek, R.A., Platt, F.M., 2002. An inducible mouse model of late onset Tay-Sachs disease. Neurobiol Dis 10, 201-210.

Jeyakumar, M., Smith, D.A., Williams, I.M., Borja, M.C., Neville, D.C., Butters, T.D., Dwek, R.A., Platt, F.M., 2004. NSAIDs increase survival in the Sandhoff disease mouse: synergy with N-butyldeoxynojirimycin. Ann Neurol 56, 642-649.

Jeyakumar, M., Thomas, R., Elliot-Smith, E., Smith, D.A., van der Spoel, A.C., d'Azzo, A., Perry, V.H., Butters, T.D., Dwek, R.A., Platt, F.M., 2003. Central nervous system inflammation is a hallmark of pathogenesis in mouse models of GM1 and GM2 gangliosidosis. Brain 126, 974-987.

Kamenetz, F., Tomita, T., Hsieh, H., Seabrook, G., Borchelt, D., Iwatsubo, T., Sisodia, S., Malinow, R., 2003. APP processing and synaptic function. Neuron 37, 925-937.

Kanzaki, S., Yamaguchi, A., Yamaguchi, K., Kojima, Y., Suzuki, K., Koumitsu, N., Nagashima, Y., Nagahama, K., Ehara, M., Hirayasu, Y., Ryo, A., Aoki, I., Yamanaka, S., 2010. Thymic alterations in GM2 gangliosidoses model mice. PLoS One 5.

Kawashima, N., Tsuji, D., Okuda, T., Itoh, K., Nakayama, K., 2009. Mechanism of abnormal growth in astrocytes derived from a mouse model of GM2 gangliosidosis. J Neurochem 111, 1031-1041.

Keilani, S., Lun, Y., Stevens, A.C., Williams, H.N., Sjoberg, E.R., Khanna, R., Valenzano, K.J., Checler, F., Buxbaum, J.D., Yanagisawa, K., Lockhart, D.J., Wustman, B.A., Gandy,

S., 2012. Lysosomal dysfunction in a mouse model of Sandhoff disease leads to accumulation of ganglioside-bound amyloid-beta peptide. J Neurosci 32, 5223-5236.

Kim, D.Y., Kim, S.H., Choi, H.B., Min, C., Gwag, B.J., 2001. High abundance of GluR1 mRNA and reduced Q/R editing of GluR2 mRNA in individual NADPH-diaphorase neurons. Mol Cell Neurosci 17, 1025-1033.

Kirkpatrick, L.L., Matzuk, M.M., Dodds, D.C., Perin, M.S., 2000. Biochemical interactions of the neuronal pentraxins. Neuronal pentraxin (NP) receptor binds to taipoxin and taipoxin-associated calcium-binding protein 49 via NP1 and NP2. J Biol Chem 275, 17786-17792.

Kitakaze, K., Mizutani, Y., Sugiyama, E., Tasaki, C., Tsuji, D., Maita, N., Hirokawa, T., Asanuma, D., Kamiya, M., Sato, K., Setou, M., Urano, Y., Togawa, T., Otaka, A., Sakuraba, H., Itoh, K., 2016. Protease-resistant modified human beta-hexosaminidase B ameliorates symptoms in GM2 gangliosidosis model. J Clin Invest 126, 1691-1703.

Kolter, T., Sandhoff, K., 2006. Sphingolipid metabolism diseases. Biochim Biophys Acta 1758, 2057-2079.

Kornfeld, S., Mellman, I., 1989. The biogenesis of lysosomes. Annu Rev Cell Biol 5, 483-525.

Kreutzberg, G.W., Graeber, M.B., Streit, W.J., 1989. Neuron-glial relationship during regeneration of motorneurons. Metab Brain Dis 4, 81-85.

Kyrkanides, S., Brouxhon, S.M., Tallents, R.H., Miller, J.N., Olschowka, J.A., O'Banion, M.K., 2012. Conditional expression of human beta-hexosaminidase in the neurons of Sandhoff disease rescues mice from neurodegeneration but not neuroinflammation. J Neuroinflammation 9, 186.

Kyrkanides, S., Miller, A.W., Miller, J.N., Tallents, R.H., Brouxhon, S.M., Olschowka, M.E., O'Banion, M.K., Olschowka, J.A., 2008. Peripheral blood mononuclear cell infiltration and neuroinflammation in the HexB-/- mouse model of neurodegeneration. J Neuroimmunol 203, 50-57.

Lazic, S.E., 2010. The problem of pseudoreplication in neuroscientific studies: is it affecting your analysis? BMC Neurosci 11, 5.

Leinekugel, P., Michel, S., Conzelmann, E., Sandhoff, K., 1992. Quantitative correlation between the residual activity of beta-hexosaminidase A and arylsulfatase A and the severity of the resulting lysosomal storage disease. Hum Genet 88, 513-523.

Liu, Y., Wada, R., Kawai, H., Sango, K., Deng, C., Tai, T., McDonald, M.P., Araujo, K., Crawley, J.N., Bierfreund, U., Sandhoff, K., Suzuki, K., Proia, R.L., 1999. A genetic model of substrate deprivation therapy for a glycosphingolipid storage disorder. J Clin Invest 103, 497-505.

Maegawa, G.H., Tropak, M., Buttner, J., Stockley, T., Kok, F., Clarke, J.T., Mahuran, D.J., 2007. Pyrimethamine as a potential pharmacological chaperone for late-onset forms of GM2 gangliosidosis. J Biol Chem 282, 9150-9161.

Mahuran, D.J., 1999. Biochemical consequences of mutations causing the GM2 gangliosidoses. Biochim Biophys Acta 1455, 105-138.

Martin, L.J., Al-Abdulla, N.A., Brambrink, A.M., Kirsch, J.R., Sieber, F.E., Portera-Cailliau, C., 1998. Neurodegeneration in excitotoxicity, global cerebral ischemia, and target deprivation: A perspective on the contributions of apoptosis and necrosis. Brain Res Bull 46, 281-309.

Matsuoka, K., Tamura, T., Tsuji, D., Dohzono, Y., Kitakaze, K., Ohno, K., Saito, S., Sakuraba, H., Itoh, K., 2011a. Therapeutic potential of intracerebroventricular replacement of modified human beta-hexosaminidase B for GM2 gangliosidosis. Mol Ther 19, 1017-1024.

Matsuoka, K., Tsuji, D., Taki, T., Itoh, K., 2011b. Thymic involution and corticosterone level in Sandhoff disease model mice: new aspects the pathogenesis of GM2 gangliosidosis. J Inherit Metab Dis 34, 1061-1068.

McCurdy, V.J., Rockwell, H.E., Arthur, J.R., Bradbury, A.M., Johnson, A.K., Randle, A.N., Brunson, B.L., Hwang, M., Gray-Edwards, H.L., Morrison, N.E., Johnson, J.A., Baker, H.J., Cox, N.R., Seyfried, T.N., Sena-Esteves, M., Martin, D.R., 2015. Widespread correction of central nervous system disease after intracranial gene therapy in a feline model of Sandhoff disease. Gene Ther 22, 181-189.

Meikle, P.J., Hopwood, J.J., Clague, A.E., Carey, W.F., 1999. Prevalence of lysosomal storage disorders. JAMA 281, 249-254.

Mitsuo, K., Nakano, T., Kobayashi, T., Goto, I., Taniike, M., Suzuki, K., 1990. Juvenile Sandhoff disease: a Japanese patient carrying a mutation identical to that found earlier in a Canadian patient. J Neurol Sci 98, 277-286.

Mortier, J., Masereel, B., Remouchamps, C., Ganeff, C., Piette, J., Frederick, R., 2010. NF-kappaB inducing kinase (NIK) inhibitors: identification of new scaffolds using virtual screening. Bioorg Med Chem Lett 20, 4515-4520.

Myerowitz, R., Hogikyan, N.D., 1986. Different mutations in Ashkenazi Jewish and non-Jewish French Canadians with Tay-Sachs disease. Science 232, 1646-1648.

Myerowitz, R., Lawson, D., Mizukami, H., Mi, Y., Tifft, C.J., Proia, R.L., 2002. Molecular pathophysiology in Tay-Sachs and Sandhoff diseases as revealed by gene expression profiling. Hum Mol Genet 11, 1343-1350.

Narkis, G., Adam, A., Jaber, L., Pennybacker, M., Proia, R.L., Navon, R., 1997. Molecular basis of heat labile hexosaminidase B among Jews and Arabs. Hum Mutat 10, 424-429.

Ng, W.X., Lau, I.Y., Graham, S., Sim, K., 2009. Neurobiological evidence for thalamic, hippocampal and related glutamatergic abnormalities in bipolar disorder: a review and synthesis. Neurosci Biobehav Rev 33, 336-354.

Nilsen, A., England, P.M., 2007. A subtype-selective, use-dependent inhibitor of native AMPA receptors. J Am Chem Soc 129, 4902-4903.

Ogawa, Y., Tanaka, M., Tanabe, M., Suzuki, T., Togawa, T., Fukushige, T., Kanekura, T., Sakuraba, H., Oishi, K., 2013. Impaired neural differentiation of induced

pluripotent stem cells generated from a mouse model of Sandhoff disease. PLoS One 8, e55856.

Ogoshi, F., Yin, H.Z., Kuppumbatti, Y., Song, B., Amindari, S., Weiss, J.H., 2005. Tumor necrosis-factor-alpha (TNF-alpha) induces rapid insertion of Ca2+-permeable alpha-amino-3-hydroxyl-5-methyl-4-isoxazole-propionate (AMPA)/kainate (Ca-A/K) channels in a subset of hippocampal pyramidal neurons. Exp Neurol 193, 384-393.

Omeis, I.A., Hsu, Y.C., Perin, M.S., 1996. Mouse and human neuronal pentraxin 1 (NPTX1): conservation, genomic structure, and chromosomal localization. Genomics 36, 543-545.

Paw, B.H., Tieu, P.T., Kaback, M.M., Lim, J., Neufeld, E.F., 1990. Frequency of three Hex A mutant alleles among Jewish and non-Jewish carriers identified in a Tay-Sachs screening program. Am J Hum Genet 47, 698-705.

Pelled, D., Lloyd-Evans, E., Riebeling, C., Jeyakumar, M., Platt, F.M., Futerman, A.H., 2003a. Inhibition of calcium uptake via the sarco/endoplasmic reticulum Ca2+-ATPase in a mouse model of Sandhoff disease and prevention by treatment with N-butyldeoxynojirimycin. J Biol Chem 278, 29496-29501.

Pelled, D., Riebeling, C., van Echten-Deckert, G., Sandhoff, K., Futerman, A.H., 2003b. Reduced rates of axonal and dendritic growth in embryonic hippocampal neurones cultured from a mouse model of Sandhoff disease. Neuropathol Appl Neurobiol 29, 341-349.

Petersen, G.M., Rotter, J.I., Cantor, R.M., Field, L.L., Greenwald, S., Lim, J.S., Roy, C., Schoenfeld, V., Lowden, J.A., Kaback, M.M., 1983. The Tay-Sachs disease gene in North American Jewish populations: geographic variations and origin. Am J Hum Genet 35, 1258-1269.

Phaneuf, D., Wakamatsu, N., Huang, J.Q., Borowski, A., Peterson, A.C., Fortunato, S.R., Ritter, G., Igdoura, S.A., Morales, C.R., Benoit, G., Akerman, B.R., Leclerc, D., Hanai, N., Marth, J.D., Trasler, J.M., Gravel, R.A., 1996. Dramatically different phenotypes in mouse models of human Tay-Sachs and Sandhoff diseases. Hum Mol Genet 5, 1-14.

Pincheira, R., Castro, A.F., Ozes, O.N., Idumalla, P.S., Donner, D.B., 2008. Type 1 TNF receptor forms a complex with and uses Jak2 and c-Src to selectively engage signaling pathways that regulate transcription factor activity. J Immunol 181, 1288-1298.

Platt, F.M., Reinkensmeier, G., Dwek, R.A., Butters, T.D., 1997. Extensive glycosphingolipid depletion in the liver and lymphoid organs of mice treated with N-butyldeoxynojirimycin. J Biol Chem 272, 19365-19372.

Rainey-Smith, S.R., Andersson, D.A., Williams, R.J., Rattray, M., 2010. Tumour necrosis factor alpha induces rapid reduction in AMPA receptor-mediated calcium entry in motor neurones by increasing cell surface expression of the GluR2 subunit: relevance to neurodegeneration. J Neurochem 113, 692-703.

Reitman, M.L., Kornfeld, S., 1981. Lysosomal enzyme targeting. N-Acetylglucosaminylphosphotransferase selectively phosphorylates native lysosomal enzymes. J Biol Chem 256, 11977-11980.

Rockwell, H.E., McCurdy, V.J., Eaton, S.C., Wilson, D.U., Johnson, A.K., Randle, A.N., Bradbury, A.M., Gray-Edwards, H.L., Baker, H.J., Hudson, J.A., Cox, N.R., Sena-Esteves, M., Seyfried, T.N., Martin, D.R., 2015. AAV-mediated gene delivery in a feline model of Sandhoff disease corrects lysosomal storage in the central nervous system. ASN Neuro 7.

Saftig, P., Klumperman, J., 2009. Lysosome biogenesis and lysosomal membrane proteins: trafficking meets function. Nat Rev Mol Cell Biol 10, 623-635.

Sama, D.M., Mohmmad Abdul, H., Furman, J.L., Artiushin, I.A., Szymkowski, D.E., Scheff, S.W., Norris, C.M., 2012. Inhibition of soluble tumor necrosis factor ameliorates synaptic alterations and Ca2+ dysregulation in aged rats. PLoS One 7, e38170.

Sandhoff, K., Harzer, K., Wassle, W., Jatzkewitz, H., 1971. Enzyme alterations and lipid storage in three variants of Tay-Sachs disease. J Neurochem 18, 2469-2489.

Sango, K., Takano, M., Ajiki, K., Tokashiki, A., Arai, N., Kawano, H., Horie, H., Yamanaka, S., 2005. Impaired neurite outgrowth in the retina of a murine model of Sandhoff disease. Invest Ophthalmol Vis Sci 46, 3420-3425.

Sango, K., Yamanaka, S., Hoffmann, A., Okuda, Y., Grinberg, A., Westphal, H., McDonald, M.P., Crawley, J.N., Sandhoff, K., Suzuki, K., Proia, R.L., 1995. Mouse models of

Tay-Sachs and Sandhoff diseases differ in neurologic phenotype and ganglioside metabolism. Nat Genet 11, 170-176.

Sargeant, T.J., Drage, D.J., Wang, S., Apostolakis, A.A., Cox, T.M., Cachon-Gonzalez, M.B., 2012. Characterization of inducible models of Tay-Sachs and related disease. PLoS Genet 8, e1002943.

Sargeant, T.J., Wang, S., Bradley, J., Smith, N.J., Raha, A.A., McNair, R., Ziegler, R.J., Cheng, S.H., Cox, T.M., Cachon-Gonzalez, M.B., 2011. Adeno-associated virus-mediated expression of beta-hexosaminidase prevents neuronal loss in the Sandhoff mouse brain. Hum Mol Genet 20, 4371-4380.

Shapiro, B.E., Pastores, G.M., Gianutsos, J., Luzy, C., Kolodny, E.H., 2009. Miglustat in late-onset Tay-Sachs disease: a 12-month, randomized, controlled clinical study with 24 months of extended treatment. Genet Med 11, 425-433.

Sheng, L., Zhou, Y., Chen, Z., Ren, D., Cho, K.W., Jiang, L., Shen, H., Sasaki, Y., Rui, L., 2012. NF-kappaB-inducing kinase (NIK) promotes hyperglycemia and glucose intolerance in obesity by augmenting glucagon action. Nat Med 18, 943-949.

Shishodia, S., Aggarwal, B.B., 2002. Nuclear factor-kappaB activation: a question of life or death. J Biochem Mol Biol 35, 28-40.

Simon, P., Dupuis, R., Costentin, J., 1994. Thigmotaxis as an index of anxiety in mice. Influence of dopaminergic transmissions. Behav Brain Res 61, 59-64.

Skaper, S.D., 2007. The brain as a target for inflammatory processes and neuroprotective strategies. Ann N Y Acad Sci 1122, 23-34.

Stanika, R.I., Pivovarova, N.B., Brantner, C.A., Watts, C.A., Winters, C.A., Andrews, S.B., 2009. Coupling diverse routes of calcium entry to mitochondrial dysfunction and glutamate excitotoxicity. Proc Natl Acad Sci U S A 106, 9854-9859.

Stendel, C., Gallenmuller, C., Peters, K., Burger, F., Gramer, G., Biskup, S., Klopstock, T., 2015. Paranoid delusion as lead symptom in two siblings with late-onset Tay-Sachs disease and a novel mutation in the HEXA gene. J Neurol 262, 1072-1073.

Stevens, B., Allen, N.J., Vazquez, L.E., Howell, G.R., Christopherson, K.S., Nouri, N., Micheva, K.D., Mehalow, A.K., Huberman, A.D., Stafford, B., Sher, A., Litke, A.M., Lambris, J.D., Smith, S.J., John, S.W., Barres, B.A., 2007. The classical complement cascade mediates CNS synapse elimination. Cell 131, 1164-1178.

Suzuki, K., Iseki, E., Katsuse, O., Yamaguchi, A., Katsuyama, K., Aoki, I., Yamanaka, S., Kosaka, K., 2003. Neuronal accumulation of alpha- and beta-synucleins in the brain of a GM2 gangliosidosis mouse model. Neuroreport 14, 551-554.

Takeda, K., Noguchi, K., Shi, W., Tanaka, T., Matsumoto, M., Yoshida, N., Kishimoto, T., Akira, S., 1997. Targeted disruption of the mouse Stat3 gene leads to early embryonic lethality. Proc Natl Acad Sci U S A 94, 3801-3804.

Takeuchi, H., Jin, S., Wang, J., Zhang, G., Kawanokuchi, J., Kuno, R., Sonobe, Y., Mizuno, T., Suzumura, A., 2006. Tumor necrosis factor-alpha induces neurotoxicity via glutamate release from hemichannels of activated microglia in an autocrine manner. J Biol Chem 281, 21362-21368.

Tallaksen, C.M., Berg, J.E., 2009. Miglustat therapy in juvenile Sandhoff disease. J Inherit Metab Dis 32 Suppl 1, S289-293.

Teismann, P., Schulz, J.B., 2004. Cellular pathology of Parkinson's disease: astrocytes, microglia and inflammation. Cell Tissue Res 318, 149-161.

Thatipamula, S., Hossain, M., 2014. Critical role of extracellularly secreted neuronal pentraxin 1 in ischemic neuronal death. BMC Neurosci 15, 133.

Thatipamula, S., Rahim, M.A., Zhang, J., Hossain, M.A., 2014. Genetic deletion of neuronal pentraxin 1 expression prevents brain injury in a neonatal mouse model of cerebral hypoxia-ischemia. Neurobiol Dis 75C, 15-30.

The Government of Canada, Neurological Health Charities Canada, 2011. Mapping Connections: an Understanding of Neurological Conditions in Canada, Public Health Agency of Canada.

The World Health Organization, 2004. The Global Burden of Disease: 2004 Update, WHO Press.

Triggs-Raine, B.L., Feigenbaum, A.S., Natowicz, M., Skomorowski, M.A., Schuster, S.M., Clarke, J.T., Mahuran, D.J., Kolodny, E.H., Gravel, R.A., 1990. Screening for carriers of Tay-Sachs disease among Ashkenazi Jews. A comparison of DNA-based and enzyme-based tests. N Engl J Med 323, 6-12.

Tuppo, E.E., Arias, H.R., 2005. The role of inflammation in Alzheimer's disease. Int J Biochem Cell Biol 37, 289-305.

Utsumi, K., Tsuji, A., Kase, R., Tanaka, A., Tanaka, T., Uyama, E., Ozawa, T., Sakuraba, H., Komaba, Y., Kawabe, M., Iino, Y., Katayama, Y., 2002. Western blotting analysis of the beta-hexosaminidase alpha- and beta-subunits in cultured fibroblasts from cases of various forms of GM2 gangliosidosis. Acta Neurol Scand 105, 427-430.

Utz, J.R., Crutcher, T., Schneider, J., Sorgen, P., Whitley, C.B., 2015. Biomarkers of central nervous system inflammation in infantile and juvenile gangliosidoses. Mol Genet Metab 114, 274-280.

Van Damme, P., Bogaert, E., Dewil, M., Hersmus, N., Kiraly, D., Scheveneels, W., Bockx, I., Braeken, D., Verpoorten, N., Verhoeven, K., Timmerman, V., Herijgers, P., Callewaert, G., Carmeliet, P., Van Den Bosch, L., Robberecht, W., 2007. Astrocytes regulate GluR2 expression in motor neurons and their vulnerability to excitotoxicity. Proc Natl Acad Sci U S A 104, 14825-14830.

Wada, R., Tifft, C.J., Proia, R.L., 2000. Microglial activation precedes acute neurodegeneration in Sandhoff disease and is suppressed by bone marrow transplantation. Proc Natl Acad Sci U S A 97, 10954-10959.

Walcott, E.C., Higgins, E.A., Desai, N.S., 2011. Synaptic and intrinsic balancing during postnatal development in rat pups exposed to valproic acid in utero. J Neurosci 31, 13097-13109.

Walia, J.S., Altaleb, N., Bello, A., Kruck, C., LaFave, M.C., Varshney, G.K., Burgess, S.M., Chowdhury, B., Hurlbut, D., Hemming, R., Kobinger, G.P., Triggs-Raine, B., 2015.

Long-term correction of Sandhoff disease following intravenous delivery of rAAV9 to mouse neonates. Mol Ther 23, 414-422.

Wang, C.C., Chen, P.S., Hsu, C.W., Wu, S.J., Lin, C.T., Gean, P.W., 2012. Valproic acid mediates the synaptic excitatory/inhibitory balance through astrocytes - A preliminary study. Prog Neuropsychopharmacol Biol Psychiatry 37, 111-120.

Wang, J., Lozier, J., Johnson, G., Kirshner, S., Verthelyi, D., Pariser, A., Shores, E., Rosenberg, A., 2008. Neutralizing antibodies to therapeutic enzymes: considerations for testing, prevention and treatment. Nat Biotechnol 26, 901-908.

Wang, Y., Qin, Z.H., 2010. Molecular and cellular mechanisms of excitotoxic neuronal death. Apoptosis.

Weiss, L.M., Harris, C., Berger, M., Tanowitz, H.B., Wittner, M., 1988. Pyrimethamine concentrations in serum and cerebrospinal fluid during treatment of acute Toxoplasma encephalitis in patients with AIDS. J Infect Dis 157, 580-583.

Wiedholz, L.M., Owens, W.A., Horton, R.E., Feyder, M., Karlsson, R.M., Hefner, K., Sprengel, R., Celikel, T., Daws, L.C., Holmes, A., 2008. Mice lacking the AMPA GluR1 receptor exhibit striatal hyperdopaminergia and 'schizophrenia-related' behaviors. Mol Psychiatry 13, 631-640.

Wortmann, S.B., Lefeber, D.J., Dekomien, G., Willemsen, M.A., Wevers, R.A., Morava, E., 2009. Substrate deprivation therapy in juvenile Sandhoff disease. J Inherit Metab Dis 32 Suppl 1, S307-311.

Wu, Y.P., Mizugishi, K., Bektas, M., Sandhoff, R., Proia, R.L., 2008. Sphingosine kinase 1/S1P receptor signaling axis controls glial proliferation in mice with Sandhoff disease. Hum Mol Genet 17, 2257-2264.

Wu, Y.P., Proia, R.L., 2004. Deletion of macrophage-inflammatory protein 1 alpha retards neurodegeneration in Sandhoff disease mice. Proc Natl Acad Sci U S A 101, 8425-8430.

Xu, D., Hopf, C., Reddy, R., Cho, R.W., Guo, L., Lanahan, A., Petralia, R.S., Wenthold, R.J., O'Brien, R.J., Worley, P., 2003. Narp and NP1 form heterocomplexes that function in developmental and activity-dependent synaptic plasticity. Neuron 39, 513-528.

Yadav, A., Kalita, A., Dhillon, S., Banerjee, K., 2005. JAK/STAT3 pathway is involved in survival of neurons in response to insulin-like growth factor and negatively regulated by suppressor of cytokine signaling-3. J Biol Chem 280, 31830-31840.

Yamaguchi, A., Katsuyama, K., Nagahama, K., Takai, T., Aoki, I., Yamanaka, S., 2004. Possible role of autoantibodies in the pathophysiology of GM2 gangliosidoses. J Clin Invest 113, 200-208.

Yanagisawa, K., Odaka, A., Suzuki, N., Ihara, Y., 1995. GM1 ganglioside-bound amyloid beta-protein (A beta): a possible form of preamyloid in Alzheimer's disease. Nat Med 1, 1062-1066.

Yang, B., Li, S., Wang, H., Guo, Y., Gessler, D.J., Cao, C., Su, Q., Kramer, J., Zhong, L., Ahmed, S.S., Zhang, H., He, R., Desrosiers, R.C., Brown, R., Xu, Z., Gao, G., 2014.

Global CNS transduction of adult mice by intravenously delivered rAAVrh.8 and rAAVrh.10 and nonhuman primates by rAAVrh.10. Mol Ther 22, 1299-1309.

Yeste-Velasco, M., Alvira, D., Sureda, F.X., Rimbau, V., Forsby, A., Pallas, M., Camins, A., Folch, J., 2008. DNA low-density array analysis of colchicine neurotoxicity in rat cerebellar granular neurons. Neurotoxicology 29, 309-317.

Zaroff, C.M., Neudorfer, O., Morrison, C., Pastores, G.M., Rubin, H., Kolodny, E.H., 2004. Neuropsychological assessment of patients with late onset GM2 gangliosidosis. Neurology 62, 2283-2286.

Zou, J.Y., Crews, F.T., 2005. TNF alpha potentiates glutamate neurotoxicity by inhibiting glutamate uptake in organotypic brain slice cultures: neuroprotection by NF kappa B inhibition. Brain Res 1034, 11-24.